

**DOKUZ EYLUL UNIVERSITY
GRADUATE SCHOOL OF NATURAL AND APPLIED
SCIENCES**

**INVESTIGATION OF EARTHQUAKE HAZARD
AND SEISMIC SITE CHARACTERISTIC
IN THE EXAMPLES OF BURSA AND IZMIR**

by
Elçin GÖK

**July, 2011
IZMIR**

**INVESTIGATION OF EARTHQUAKE HAZARD
AND SEISMIC SITE CHARACTERISTIC
IN THE EXAMPLES OF BURSA AND IZMIR**

**A Thesis Submitted to the
Graduate School of Natural and Applied Sciences of Dokuz Eylül University
In Partial Fulfillment of the Requirements for the Degree of Doctor of
Philosophy in Geophysical Engineering, Geophysical Engineering Program**


**by
Elçin GÖK**

**July, 2011
IZMIR**

Ph. D. THESIS EXAMINATION RESULT FORM

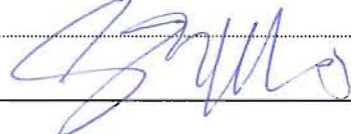
We have read the thesis entitled “**INVESTIGATION OF EARTHQUAKE HAZARD AND SEISMIC SITE CHARACTERISTIC IN THE EXAMPLES OF BURSA AND IZMIR**” completed by **ELÇİN GÖK** under supervision of **ASSC.PROF.DR. ORHAN POLAT** and we certify that in our opinion it is fully adequate, in scope and in quality, as a thesis for the degree of Doctor of Philosophy.

ASSC. PROF.DR. ORHAN POLAT



Supervisor

PROF.DR. GUNAY ÇİFÇİ



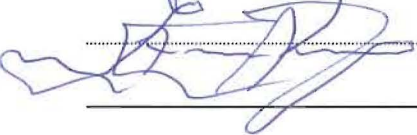
Thesis Committee Member

PROF.DR. RAHMİ PINAR



Examining Committee Member

PROF.DR. ZAFER AKÇİĞ



Examining Committee Member

PROF.DR. FRANCISCO

J. CHAYEZ-GARCIA



Examining Committee Member

Prof.Dr. Mustafa SABUNCU

Director

Graduate School of Natural and Applied Sciences

ACKNOWLEDGMENTS

I would like to thank my supervisor Orhan Polat for offering me, supervision and support, for the enlightening discussions and for his help throughout the process of writing scientific articles.

I am grateful to my colleagues at Department of Geophysical Engineering in Dokuz Eylul University who have supported during my whole education time.

I would like to thank Zafer Akçıĝ who is the manager of the Earthquake Research and Implementation Center for his all supports.

Special mention to Murat Keçecioĝlu who is my colleague always helped me during my thesis duration.

In my thesis, there are two different project; firstly TUBITAK-JULICH-102Y156 (DEU+METU Turkey and GFZ-Germany) scientific cooperation for Bursa city, and second one has been performed for Izmir city by using the dataset obtained from the TUBITAK-KAMAG (106G159) national collaboration between the Earthquake Research Directorate (ERD) of the Disaster Emergency Management (AFAD) of the Turkish Prime Ministry and the Dokuz Eylul University. I would like to thank all project staff for their efforts.

Finally, I thank my parents Seyyide and Sadi Geçim and my brothers Sami and Ersin Geçim for encouraging me and always being there and caring for me in every possible way in these difficult years. Also thanks to my husband Hakan Gök who has always been a great inspiration for me.

At the end, my loving son; Atakan thanks for being my sunshine.

ELÇİN GÖK

INVESTIGATION OF EARTHQUAKE HAZARD AND SEISMIC SITE CHARACTERISTIC IN THE EXAMPLES OF BURSA AND IZMIR

ABSTRACT

The principal objectives of this thesis are to investigate the earthquakes are recorded by the local networks installed in Bursa and Izmir cities which belong to the Marmara and Aegean regions of Turkey respectively, and to make a contribution to study, engineering seismology in those cities. These cities are important since they are the most developed and populated settlements of Western Anatolia. The results in this thesis were obtained in the framework of two different TUBITAK projects, formulated to contribute to the understanding of the seismotectonics and engineering seismology in Bursa and Izmir.

A temporary seismic network was installed in Bursa as a part of a bi-lateral TUBITAK-JULICH collaboration, and operated during six months. Its main purpose was to determine the seismic activity. 384 well located events were mapped, and 10 focal mechanism solutions were obtained. The principal stress tensor axes were calculated by using fault planes, and a North-South directed extension was determined as a stress regime around Bursa. In addition to this study, microtremor records together with H/V method were used in the north of the city, the most densely populated area of Metropolitan Bursa. Fundamental site frequencies and amplifications at different geological sites were obtained. The results coincide well with the underlying geology.

In August, 2008 a strong-motion local network was installed as part of a bi-lateral TUBITAK cooperation between the Disaster and Emergency Management Presidency (AFAD) of the Turkish Republic and the Dokuz Eylul University. This local array samples the different geologic units in Izmir. Similar investigations as those performed for Bursa were also carried out in Izmir.

Keywords: Izmir, Bursa, Seismotectonics, Engineering seismology, Microtremor.

DEPREM TEHLİKESİ VE ZEMİN SİSMİK DAVRANIŞLARININ İZMİR VE BURSA ÖRNEĞİNDE İNCELENMESİ

ÖZ

Bu tezin temel hedefi; Marmara ve Ege bölgesinde yer alan Bursa ve İzmir illerinde meydana gelen ve iki farklı işbirliği kapsamında kurulan istasyonlar tarafından kaydedilen depremleri incelemek ve yapılan mühendislik sismolojisi çalışmalarını değerlendirmektir. Bu şehirler Batı Anadolu'nun en gelişmiş ve yoğun nüfusa sahip yerleşim bölgeleri olmalarından dolayı, ayrıca önem arz etmektedir. Dolayısıyla bu tez çalışmasında, Bursa ve İzmir İl'lerinde, biri uluslararası iki ayrı TÜBİTAK projesi kapsamında yürütülen sismotektonik ve mühendislik sismolojine yönelik bilimsel araştırmalardan elde edilen bulgular irdelenmiştir.

Bursa'da sismik etkinliğin ortaya konmasına yönelik olarak, TÜBİTAK-JÜLICH ortak ikili işbirliği projesi kapsamında geçici deprem istasyon ağı kurulmuş ve 6 ay süreyle işletilmiştir. Bu süreçte, en iyi lokasyon kalitesine sahip 384 adet depremin çözümü yapılmış ve 10 adet odak mekanizması çözümü elde edilmiştir. Fay düzlemi çözümleri kullanılarak gerilme tensörü (stress tensor) eksenleri elde edilmiş ve Bursa ve çevresinde kuzey güney yönlü açılma rejiminin hakim olduğu ortaya konmuştur. Bu çalışmaya ek olarak, yoğun yerleşime sahip Bursa'nın kuzeyinde yapılan mikrotremor ve deprem çalışmalarında HVSR (yatay- düşey spektral oran) yöntemi kullanılmıştır. Bu yöntemle farklı jeolojik birimlerin hakim frekansı ve spektral oranları hesaplanmıştır. Elde edilen sonuçların, jeolojik birimlerle uyumlu olduğu anlaşılmıştır.

2008 yılı Ağustos ayında, T.C. Başbakanlık Afet ve Acil Durumu Yönetimi Deprem Dairesi Başkanlığı ile Dokuz Eylül Üniversitesi işbirliğindeki bir başka TÜBİTAK projesi kapsamında, İzmir İl'ine 16 adet kuvvetli yer hareketi deprem istasyon ağı kurulmuştur. Bu yerel ağ, İzmir'in farklı jeolojik birimlerini temsil edecek şekilde yerleştirilmiştir. Bursa'da yapılan araştırmalara benzer çalışmalar (sismolojik-sismotektonik çalışmalar, deprem kayıtlarının analizi, mikrotremor

ölçümleri, yerel zemin etkileri), Ege Bölgesinin kültürel başkenti konumundaki İzmir İl'inde de ayrıntılı olarak irdelenmiştir.

Anahtar sözcükler: İzmir, Bursa, Sismotektonik, Mühendislik sismolojisi, Mikrotremor.

CONTENTS

	Page
THESIS EXAMINATION RESULT FORM	ii
ACKNOWLEDGEMENTS	iii
ABSTRACT	iv
ÖZ	v
CHAPTER ONE - INTRODUCTION	1
1.1. Preface.....	1
1.2. Outline of Thesis.....	2
1.2.1 First Theme: Seismic activity and Site Properties of Bursa.....	2
1.2.2 Second Theme: Seismic activity and Site Effects of Izmir.....	3
CHAPTER TWO - AN ASSESSMENT OF THE SEISMICITY OF THE BURSA REGION FROM A TEMPORARY SEISMIC NETWORK	5
2.1. Introduction.....	7
2.2. Geology and Tectonic Setting.....	8
2.3. Background Seismicity	9
2.4. Temporary Network and Data Analysis.....	13
2.4.1. Seismic Activity of the Bursa Area.....	16
2.4.2. Focal Mechanisms and Stress Tensor Inversion	18
2.5. Discussions and Conclusions	26
2.6 Acknowledgements.....	32
CHAPTER THREE - MICROTREMOR HVSr STUDY OF SITE EFFECTS IN BURSA CITY (NORTHERN MARMARA REGION, TURKEY).....	33

3.1 Preface.....	33
3.2 Introduction.....	34
3.3 Tectonic and Geological Setting.....	36
3.4 Method.....	38
3.5 Microtremor Measurements and Analyses.....	39
3.5.1 Instruments and Data.....	39
3.5.2 HVSR Analyses.....	39
3.5.3 Time-dependent HVSR.....	42
3.6 HVSR Results Using Earthquake Data.....	45
3.7 Conclusion and Discussion.....	46

CHAPTER FOUR - IZMIRNET: A STRONG-MOTION NETWORK IN METROPOLITAN IZMIR, WESTERN ANATOLIA, TURKEY 49

4.1 Introduction.....	50
4.2 Seismotectonic Setting.....	51
4.3 Description of IzmirNET.....	53
4.3.1 Station Hardware.....	54
4.3.2 Site Characterization.....	56
4.4 Sample Data.....	58
4.5 Future Plans.....	59
4.6 Conclusions.....	60
4.7 Acknowledgements.....	63

CHAPTER FIVE - SEISMIC ACTIVITY OF IZMIR AND SURROUNDINGS 64

5.1 Regional Tectonics in the Western Anatolia.....	64
5.2 The seismicity of Western Anatolia.....	67
5.3. Local tectonics of Izmir and surroundings.....	72
5.3.1 Major Tectonic Structures around Izmir.....	72
5.3.1.1 The Izmir Bay.....	73
5.3.1.2 Faults.....	74
5.4 Seismic Activity around Izmir.....	76
CHAPTER SIX - LOCAL SITE EFFECTS IN IZMIR, AEGEAN REGION OF TURKEY.....	82
6.1 Introduction.....	84
6.2 Geological Setting and Instruments.....	85
6.3 Method and Data Analysis.....	87
6.4 Results.....	94
6.5 Discussions.....	101
6.6 Acknowledgements.....	104
CHAPTER SEVEN - CONCLUSIONS.....	105
REFERENCES.....	110

CHAPTER ONE

INTRODUCTION

1.1 Preface

Engineering seismology is the link between earth sciences and engineering and aims at earthquake mitigation. Earthquake hazard varies significantly around the world. In places like Japan, Turkey...etc., earthquakes are part of people's everyday life. In areas of high seismicity, disastrous events remind us of the importance of earthquake hazard and force the local authorities to take precautions in earthquake preparedness and risk mitigation. Turkey is one of the most seismically active countries in the world. Particularly, Marmara Region and Aegean Region play an essential role in the tectonics of Turkey.

In the Marmara Region the 1999 Kocaeli earthquake, which resulted in more than 17,000 fatalities and huge damage, was a major disaster for the most industrial and urbanized region of Turkey. Bursa is one of the most industrialized and populated cities of the Marmara Region. The 1999 Kocaeli earthquake was also felt in Bursa, but did not cause serious structural damage in this city. However, during the history of Bursa City, many earthquakes from the southwestern branch of the North Anatolian Fault Zone (NAFZ) have caused devastating damage.

The Aegean Region shows extension regime (McKenzie, 1972, 1978) due to the relative motion between Anatolia and Aegean plate. The result is a significant deformation and seismicity problem for Izmir City and surrounding areas. Izmir is the 3rd largest city after Istanbul and Ankara in terms of population, industrial density and contribution to the national economy. It is located very close to active faults and grows rapidly on thick Quaternary-Neogene sediments. Unconsolidated soil deposits in the city may significantly affect the propagation of earthquake motion close to the ground surface.

1.2 Outline of Thesis

This thesis has two main themes: seismicity and site properties, both in Bursa and Izmir which are important cities of the Marmara and Aegean regions, respectively. These two themes are presented as follows.

- *Studies performed in Bursa city (Marmara region, Turkey)*
Chapter 2: Seismic activity in Bursa
Chapter 3: Microtremor HVSR study of site effects in Bursa city
(Northern Marmara Region, Turkey)
- *Studies performed in Izmir city (Aegean region, Turkey)*
Chapter 4: IzmirNet: A Strong-motion Network in Metropolitan
Izmir, Western Anatolia, Turkey
Chapter 5: Seismic Activity around Izmir
Chapter 6: IzmirNET Strong Motion Analysis

1.2.1 First Theme: Seismic activity and Site Properties of Bursa

The first theme has two parts. In the first part (Chapter 2), we discuss and evaluate the seismicity of Bursa using data from a temporary seismic network. It operated during six months and was the result of a scientific collaboration between Dokuz Eylul University (DEU, Turkey) and GeoForschung Zentrum Potsdam (GFZ, Germany). Earthquake recordings of local events have been analyzed using the SEISAN software in order to quantify the seismic activity which has great importance for earthquake hazard assessment in the vicinity of Bursa. *Paper 1*, published by Pure and Applied Geophysics (PAAG) in 2011 contains the results of this cooperation, and deals with the seismic activity of Bursa, focal mechanisms and inversion of focal mechanism.

In the second part (Chapter 3), expected local site effects in Bursa City were evaluated, and encouraging results have been obtained by using both microtremor measurements and earthquake data with regard to microzonation and first-order evaluation of site response. The microtremor data were collected in many different sites during a 10-day field survey in Bursa. A small number of accelerometric earthquake data was also used to compare obtained results and to better understand site properties of the studied area. The horizontal to vertical spectral ratio (HVSR), Nakamura method, was applied to compute local site response. My main contribution to this study has been in data collection, processing of microtremor and earthquake data, and interpretation of the results.

1.2.2 Second Theme: Seismic activity and Site Effects of Izmir

This theme deals with the seismic activity and site characteristics of Izmir using data from a new local strong motion network (IzmirNET), installed towards to the end of 2008. The project “MODELLING OF SEISMIC SITE RESPONSE FOR EARTHQUAKE RESISTANT STRUCTURAL DESIGN IN IZMIR METROPOLITAN AREA AND ALIAGA-MENEMEN DISTRICTS” was the basis for theme. The project resulted from another scientific cooperation of the Dokuz Eylul University (DEU) in Izmir with the Earthquake Department of the Presidency of Disaster and Emergency Management Directorate (AFAD-ERD) in Ankara. Details of the accelerometric monitoring system are given in Chapter four.

The objective of IzmirNET is primarily engineering seismology research, emphasizing soil characteristics and site response at station locations. However, during the project duration (for 3 years), it also served to record seismic activity around Izmir city. This information was used to understand the seismogenic behaviour of geologic structures. IzmirNET contributes precise location parameters for local earthquakes with good quality records. Chapter five deal with the seismic activity recorded by IzmirNET. A set of strong-motion records from local earthquakes and microtremors at station locations were collected for this study and interpreted for soil characteristics at station sites. IzmirNET was deployed on

different geological formations and most of them are on sediments with different surface geology, so that local site effects on ground motions have been studied at these sites by analyzing both earthquake data and microtremor measurements (Polat et al, 2009).

Site effects and amplification of strong ground motion at IzmirNET locations were estimated using two different approaches: Standard Spectral Ratio (SSR) and HVSR methods. *More details are given in Chapter six.*

CHAPTER TWO

AN ASSESSMENT OF THE SEISMICITY OF THE BURSA REGION FROM A TEMPORARY SEISMIC NETWORK

(PAPER 1)

Elcin Gok^{1,*} and Orhan Polat²

¹ Dokuz Eylul University, Earthquake Research and Implementation Center, Izmir
Turkey

² Dokuz Eylul University, Engineering Faculty, Department of Geophysics, Izmir
Turkey

Published in Pure and Applied Geophysics

DOI 10.1007/s00024-011-0347-6

Abstract

A temporary earthquake station network of 11 seismological recorders was operated in the Bursa region, south of the Marmara Sea in the northwest of Turkey, which is located at the southern strand of the North Anatolian Fault Zone (NAFZ). We located 384 earthquakes out of a total of 582 recorded events that span the study area between 28.50-30.00°E longitudes and 39.75-40.75°N latitudes. The depth of most events was found to be less than 29 km, and the magnitude interval ranges were between $0.3 \leq M_L \leq 5.4$, with RMS less than or equal to 0.2. Seismic activities were concentrated southeast of the Uludag Mountain (UM), in the Kestel-Igdir area and along the Gemlik Fault (GF). In the study, we computed 10 focal mechanisms from temporary and permanent networks. The predominant feature of the computed focal mechanisms is the relatively widespread near horizontal northwest-southeast (NW-SE) *T*-axis orientation. These fault planes have been used to obtain the orientation and shape factor (*R*, magnitude stress ratio) of the principal stress tensors (σ_1 , σ_2 , σ_3). The resulting stress tensors reveal σ_1 closer to the vertical (oriented NE-SW) and σ_2 , σ_3 horizontal with $R=0.5$. These results confirm that Bursa and its vicinity could be defined by an extensional regime showing a primarily normal to oblique-slip motion character. It differs from what might be expected from the stress tensor inversion for the NAFZ. Different fault patterns related to structural heterogeneity from the north to the south in the study area caused a change in the stress regime from strike-slip to normal faulting.

Keywords: Bursa region, seismicity, focal mechanism, stress tensor

2.1 Introduction

Many studies have concluded that Western Anatolia is dominantly characterized by mainly E-W trending graben forming high-angle normal faults that have developed since the Upper Miocene-Pliocene (Bozkurt & Sozbilir 2004; Uzel & Sozbilir 2008). The Bursa region (Figure 2.3) is located south of the Marmara Region and the Middle Strand of the North Anatolian Fault (NAFMS) Zone. Iznik Lake has subsided under the control of the NAFMS, located near its southern shoreline, and that created step-wise normal faults to the north. It is separated from Gemlik Gulf (GG) by a narrow valley. The Bursa region is seismically active and cut by many active faults forming some distinct tectonic features such as Gemlik Fault (GF), Geyve-Iznik Fault Zone (GIFZ), Yenisehir Fault (YNF), Bursa Fault (BF), and the Inonu-Eskisehir Fault Zone (IEFZ; Figure 2.3a, b).

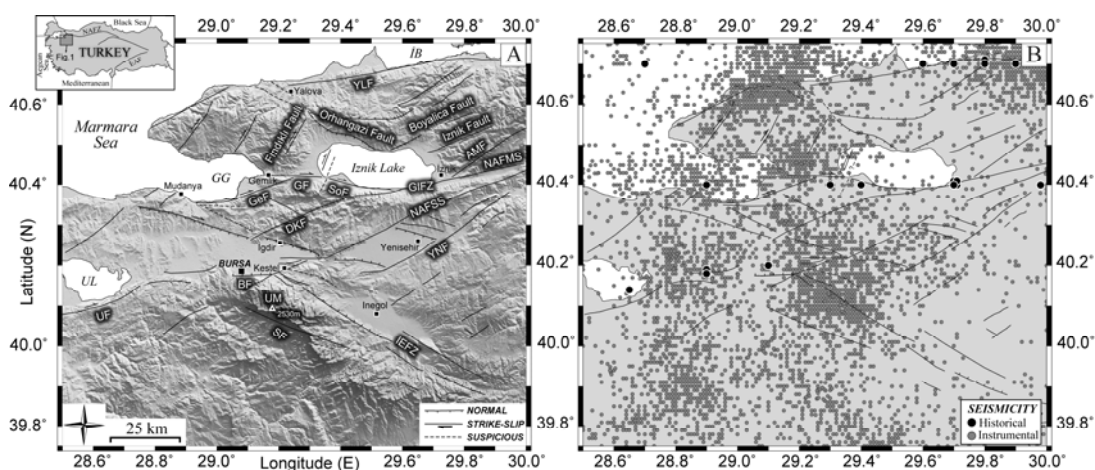


Figure 2.3 Regional framework showing: (a) main tectonic element, (b) seismicity and seismotectonics of Bursa and the surrounding area (KOERI, 2010). Shaded topographic (3sec-90m SRTM) view was used to illustrate the geomorphology of the study area. Tectonic features were modified after Adatepe et al. (2002), Alpar & Yaltirak (2002), Imbach (1997); Kuscu et al. (2009), Schindler & Pfister (1997), Ozturk et al. (2009); Saroglu et al. (1992), Topal et al. (2003), Yaltirak (2002), Yaltirak & Alpar (2002). AMF- Adliye Mesruriye Fault, BF- Bursa Fault, DKF- Demirtas-Kiblepinar Fault, GeF- Gencali Fault, GF- Gemlik Fault, GG- Gemlik Gulf, GIFZ- Geyve-Iznik Fault Zone, IEFZ- Inonu-Eskisehir Fault Zone, NAFMS- North Anatolian Fault Middle Strand, NAFSS- North Anatolian Fault Southern Strand, SF- Sogukpinar Fault, SoF- Soloz Fault, UF- Uluabat Fault, UL- Uluabat Lake, UM- UM, YLF- Yalova Fault, YNF- Yenisehir Fault.

In the south of the study area, earthquakes are associated with the IEFZ and the Southern Strand of the North Anatolian Fault (NAFSS). The NAF extends from NW Turkey near Bolu to the North Aegean Sea (Barka & Kadinsky-Cade, 1988). The surface trace of the NAFSS is clearly evident in the morphology from the southern shore of Lake Iznik to the town of Gemlik (Kuscu et al., 2009). The NAFSS extends from Bursa to the west, bending southwest from the southern part of the Uluabat Lake (UL; Yaltirak, 2002). The UF is a right lateral strike-slip fault with a normal component and the BF is a normal fault. The city of Bursa is rapidly growing on thick Quaternary sediments, and is the fourth biggest city of Turkey. Its population is 2.5 million and grows at a rate of more than 27% per census (TUIK, 2009). Therefore, seismological researches are crucial for earthquake hazard studies.

The August 17, 1999 Izmit earthquake ($M_s=7.4$; Polat et al., 2002a), which caused extensive structural damage and the loss of almost 18.000 lives in the Marmara Region, was also felt strongly by the residents of Bursa. The earthquake produced no serious structural damage but caused significant ground vibrations and created panic among the people. This paper aims to describe the results of a microseismic survey carried out from October 2003 to April 2004 with a dense local network in Bursa and surrounding regions, and to use the earthquake locations and focal mechanisms to investigate seismic activity and fault kinematics. Finally, we discuss the significance of the mean stress regime related to the seismotectonic feature.

2.2 Geology and Tectonic Setting

The main lithological units in the vicinity of Bursa are Quaternary and Neogene deposits. The thickness of the Quaternary deposits exceeds 300 m in the Bursa basin (Imbach, 1997). Neogene deposits are essentially detrital and consist mostly of sandstone and claystone. The thickness of the units varies from 50 m to 200 m near the Yenisehir basin (Topal et al., 2003). The GIFZ zone corresponds to the NAFSS and has the potential to generate a strong earthquake (Gulkan et al., 1993; Cisternas et al., 2004). It extends from the east of Iznik Lake to the northern slopes of the UM

along the Yenisehir plain (Ozturk et al., 2009). The BF extends in an E-W direction for a distance of 45km between the UF and the city of Bursa, showing a right-lateral strike-slip character with a normal component (Adatepe et al., 2002; Alpar & Yaltirak 2002; Kuscu et al., 2009; Yaltirak & Alpar 2002). The IEFZ follows a NW-SE direction for a distance of 380km up to the city of Bursa. The BF and GIFZ are seismically less active than the IEFZ, GF and Yalova Fault (YLF) through GG and Izmit Bay (IB) in the Marmara Sea (Ucer et al., 1997).

2.3 Background Seismicity

Several earthquakes prior to 1900 have been included in the study area (Ambraseys, 2000, 2002; Ocal, 1968; Sellami et al., 1997). Among these the February 28, 1855 earthquake with an intensity of $I_0=IX$ ($M_s=7.1$) caused extensive damage and loss of lives in Bursa and its vicinity. This is one of the well-documented earthquakes in the region. Destruction extended within a narrow zone between the UM south of Bursa, and the south coast of Uluabat Lake (Ambraseys, 2000). Instrumental seismicity from 1900 to 2005 (Kalafat et al., 2007) recorded several major earthquakes. The April 15, 1905 and November 13, 1948 earthquakes, which occurred 7-10km away from Bursa, had $M_s=5.6$. Other major earthquakes in 1939 and 1964 ($M_s=5.5, 6.7$ and 6.8) also affected Bursa and its vicinity. Table 1 shows significant events that occurred during historical and instrumental periods in the Bursa area. It should be noted that epicenter locations of events before 1900 are not expected to be accurate.

Table 2.1 Historical (until 1894) and instrumental earthquakes in Bursa and surrounding regions limited to an area between 39.75 – 40.75°N latitudes and 28.5 – 30.0°E longitudes (Intensity \geq VI, Ms \geq 5.5). Data compiled after Ambraseys (2000 and 2002), Sellami et al. (1997) & Kalafat et al. (2007).

Day	Month	Year	Lat (°)	Lon (°)	Intensity	Ms	Remarks
24	11	0029	40.41	29.70	IX		Iznik
-	-	0033	40.40	29.71	VIII	-	Iznik, Bursa
02	01	0069	40.41	29.71	VII	-	Iznik
-	-	0120	40.40	29.70	VIII	-	Iznik
-	-	0129	40.40	29.40	VIII		Iznik
-	-	0268	40.70	29.90	-	7.3	Iznik
11	10	0368	40.40	29.70	VII	-	Iznik
-	-	0378	40.40	29.70	VI	-	Iznik
25	09	0478	40.70	29.80	-	7.3	Yalova
16	08	0554	40.71	29.80	-	6.9	Iznik
-	-	0715	40.40	28.90	VIII	-	Iznik
26	10	0740	40.70	28.70	-	7.1	Yalova
-	09	1065	40.40	30.00	VIII	6.8	Iznik
-	-	1417	40.20	29.10	VII	-	Bursa
15	03	1419	40.40	29.30		7.2	Bursa
-	-	1674	40.20	29.10	VII	-	Bursa
25	05	1719	40.70	29.80	-	7.4	Izmit
12	09	1844	40.70	29.70	-	5.5	Izmit
19	04	1850	40.10	28.30	-	6.1	Bursa
28	02	1855	40.14	28.65	X	7.1	Bursa

11	04	1855	40.19	28.90	VII	6.3	Bursa
29	04	1855	40.18	28.90	-	6.7	Bursa (*)
10	07	1894	40.70	29.60	-	7.3	Izmit
15	04	1905	40.20	29.00	-	5.6	Bursa
03	08	1939	39.75	29.68	-	5.5	Bursa
15	09	1939	39.76	29.56	-	6.7	Bursa
13	11	1948	40.23	29.02	-	5.6	Bursa
							Manyas
06	10	1964	40.10	28.20	-	6.8	(East of the UL)

(*): In the catalogues of Ambraseys (2000 & 2002) and Sellami *et al.* (1997), we could not find no evidence that an aftershock (*of 1855 event*) on 29 April 1855 ($M_s=6.7$) listed in the catalogues of Ocal (1968) and Karnik (1971).

Swarm type seismic activity can clearly be observed along the IEFZ, the northern part of the GF and YLF, and east of the IB. There is also some diffuse activity in the eastern and southern part of the UL (Figure 2.3b). The morphology of Bursa suggests a long-term seismicity that accounts for an average shear velocity of about 0.3 cm/yr, which is compatible with GPS measurements (Straub, 1996). However, we must admit that the long-term activity of the inland part of Bursa is not well known.

We examined the overall characteristics of the instrumental seismicity by means of the cumulative number of events as a function of time for the period 1900-2005. The cumulative number of events in the catalogue was analyzed by using the ZMAP (Wiemer, 2001). We found that a total of 6.637 events had $M_s \leq 6.8$ (Figure 2.4a).

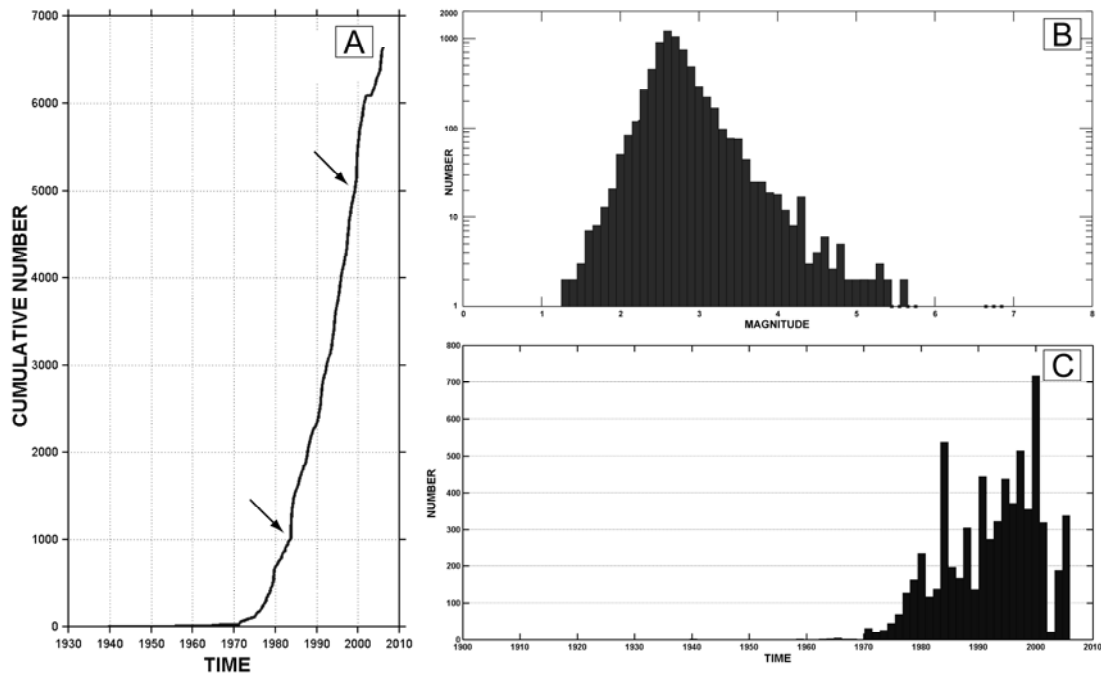


Figure 2.4 (a) Cumulative numbers of the events as a function of time for the city of Bursa and its vicinity, a time change in reporting seismicity rate occurred between 1970 and 1975. The arrow indicates a sharp change in the seismic rate, (b) the magnitude histogram of the earthquakes ($M_s \leq 6.8$) in logarithmic scale, (c) and a time histogram of the events (during 1900-2005).

A time dependency near 1970-1975 was observed and interpreted as a result of man-made effects or tectonic stress changes in the region. Starting from the period 1970-1975, the Kandilli Observatory and Earthquake Research Institute (KOERI) began to install permanent seismic stations and to collect data with local networks in the study area. After 1978, the regional radio-link (seismic telemetry) seismic network (MARNET) became operational. More than 6.300 earthquakes were collected within the following 27-year period (1978-2005). Important earthquakes in this period occurred on December 26, 1981 (near UF) and October 21, 1983 (on IEFZ), both of which had a magnitude $M_s=4.9$ (Kalafat et al., 2007). These events, as illustrated in Figure 2.4a, determined an increase in the cumulative number of earthquakes. There were several small to medium-sized earthquakes between 1983 and 1984. These earthquakes can be assumed to be aftershocks of the two previously mentioned earthquakes (Sellami et al., 1997). Another seismic rate change, less sharp than the 1983 quake, was observed in 2000. This increase could probably be associated with the improvement of the station coverage following the devastating

Izmit and Duzce earthquakes in 1999 and the aftershocks of the Izmit earthquake. Figure 2.4b defines the spread of the cumulative number of the earthquakes' magnitudes in logarithmic scale. Most of the earthquakes were below 3.0. It is immediately apparent that the majority of the earthquakes show a magnitude interval between 1.9 and 3.6. A time histogram for the period from 1900 to 2005 indicates an increase in the number of recorded events after 1970 (Figure 2.4c). There are remarkable increases in 1983 and 2000. But the earthquakes with $M_s \leq 4.0$ have been accepted as homogeneous (Kalafat et al., 2007).

The seismicity of Western Anatolia is high and reveals swarm-type activity with remarkable clustering of low magnitude earthquakes in time and space (Ucer et al., 1997; Gulkan et al., 2007; Polat et al., 2009). The epicenters and fault mechanisms are closely associated with major structures (McKenzie, 1972, 1978). The focal depths range from 0km to 40km according to various bulletins and sources, but these have low reliability. The accurate determination of focal depths and modeling of the long period body waves indicate that at least the hypocenters of the larger earthquakes in the region are not deeper than 20-25 km (Eyidogan, 1988; Eyidogan & Jackson, 1985).

2.4 Temporary Network and Data Analysis

The goal of this study was to install a seismic network for monitoring earthquake activity in and around Bursa. For this purpose, nine short-period (Mark Products L4-3D) and two broadband (Guralp 40T) sensors with 24-bit digitizers were deployed to an area between 40.0-40.6°N and 28.8-29.3°E (Figure 2.5) in a cooperative study conducted by Dokuz Eylul University (DEU) in Izmir, Turkey and GeoForschung Zentrum (GFZ) in Potsdam, Germany. The temporary network was operated during six months between October 2003 and April 2004. KOERI's permanent regional stations were also used to improve the precision of all available results along the middle and southern strands of the NAFZ, and assure a good azimuthal coverage of the recorded events. Each station was equipped with a GPS time receiver, and data was recorded continuously during the project duration.

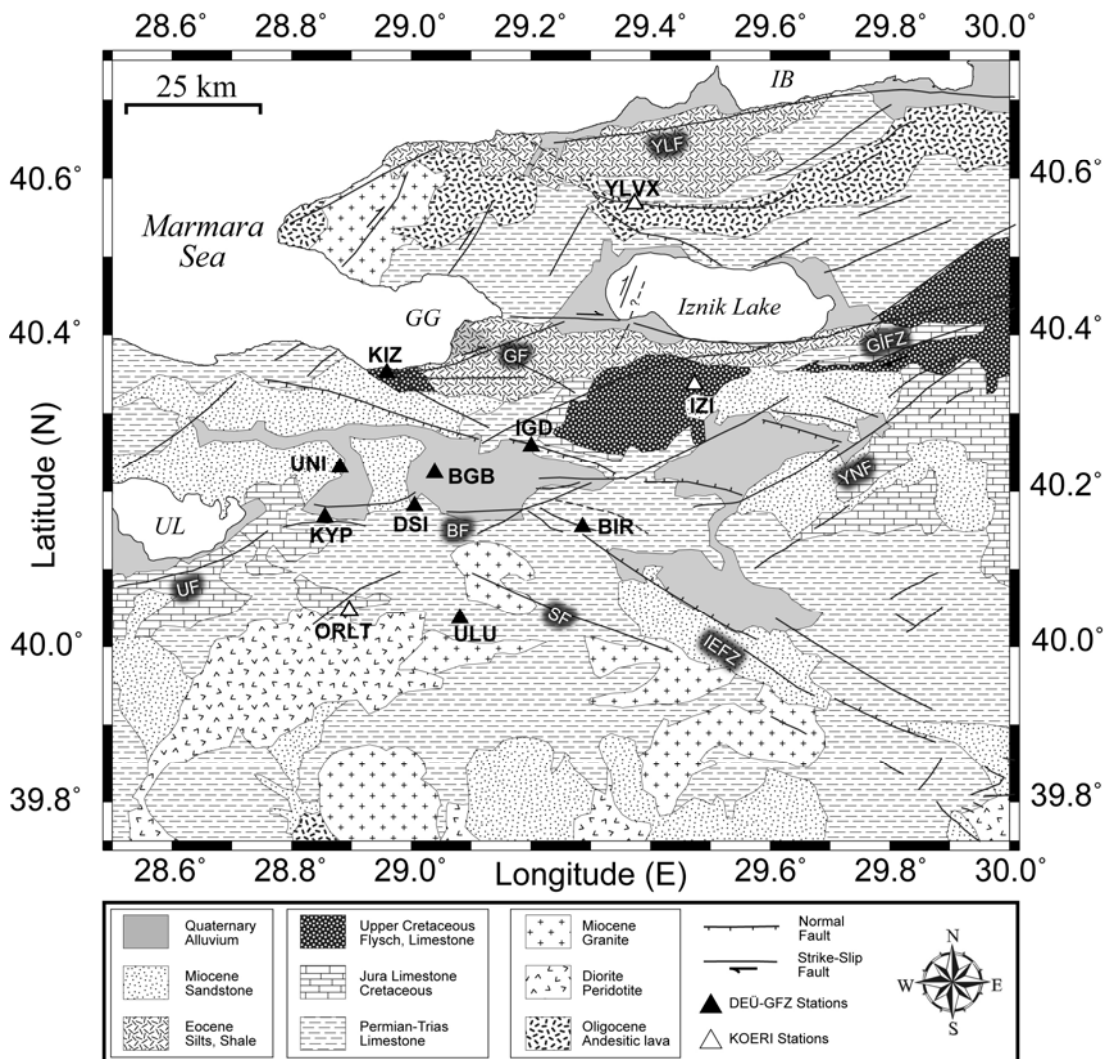


Figure 2.5 Distribution of the present seismic stations on the simplified geological map of the Bursa region. Tectonic and geological framework was reproduced from Adatepe et al. (2002) and references therein; Imbach (1997); Ozturk et al. (2009); Topal et al. (2003); Yaltirak & Alpar (2002), and 1:500,000 scale geologic map. Filled triangles represent the DEU-GFZ temporary network, and open triangles indicate the KOERI permanent network.

Approximately 1.000 events were registered, and more than 11.000 P+S phases allowed us to locate 582 events in the study area, 28.50-30.00°E and 39.75-40.75°N. The one-dimensional crustal velocity model was obtained using the VELEST inversion code (Kissling et al., 1994). It solves nonlinear inversion problems and obtains a velocity model iteratively via damped least-squares. An initial velocity model was chosen from previous studies and refraction profiles available for the region (Sellami et al., 1997; Gurbuz et al., 1998). At the beginning, events with a good azimuthal coverage were used to derive a velocity model. The procedure was

repeated until the overall RMS value remained almost constant and resulted in minimum one dimensional P-wave, together with derived S-wave velocity models (V_P/V_S ratio assumed to be 1.74).

Phase picking, computing magnitude and the location of the earthquakes were obtained by careful inspection with SEISAN software (Havskov & Ottemoller, 1999). For the initial locations of the events, we used the HYPO71 routine (Lee & Lahr, 1972) integrated in SEISAN. Both P- and S-arrivals from stations were used in determining the locations.

In the present study, five layers were defined within the upper 33 km of the earth's crust. Low P-wave velocities (2.90 km/sec) were observed in the uppermost layer (up to 2 km below the surface). The P-wave velocity increases to 5.40 km/sec from a depth of 2 km to 7 km. The third layer was defined with a P-wave velocity of 6.16 km/sec at a depth range of 7-17 km. A thick layer occurs at a depth between 17 km and 33 km with a 6.63 km/sec P-wave velocity. And finally, the last layer has an 8.16 km/sec P-wave velocity and occurs at depths deeper than 33 km (Table 2.2).

Table 2.2 Crustal structure in the region obtained by using VELEST algorithm (Kissling et al., 1994)

Layer (km)	V_P (km/s)
0-2	2.90
2-7	5.40
7-17	6.16
17-33	6.63
>33	8.16

After several iteration tests, 384 events out of a total of 582 were characterized by a RMS of less than 0.2 seconds. The mean residuals at stations ULU and BIR are very small (0.002 and 0.003 seconds, respectively), and quite stable. For the UNI and

IGD stations, they were larger (up to 0.03 seconds). The threshold level for standard deviation in time residuals was below 0.20 seconds and indicated 0.078 seconds for the BGB and 0.192 seconds for the UNI stations (Figure 2.6a). Standard errors in azimuths at recording stations are shown in Fig 2.6b, revealing a deviation around 33° for the BGB and 119° for the IGD stations, respectively. The mean azimuths were detected to be 67° for the KIZ and 302° for the BGB stations. A total of 1.023 residual and azimuth records were observed in the selected 384 events (Fig 2.6c, 2.6d). Their distributions with distance confirm the improved location characteristics. These results better describe the location properties and show less oscillation for distances larger than 45 km.

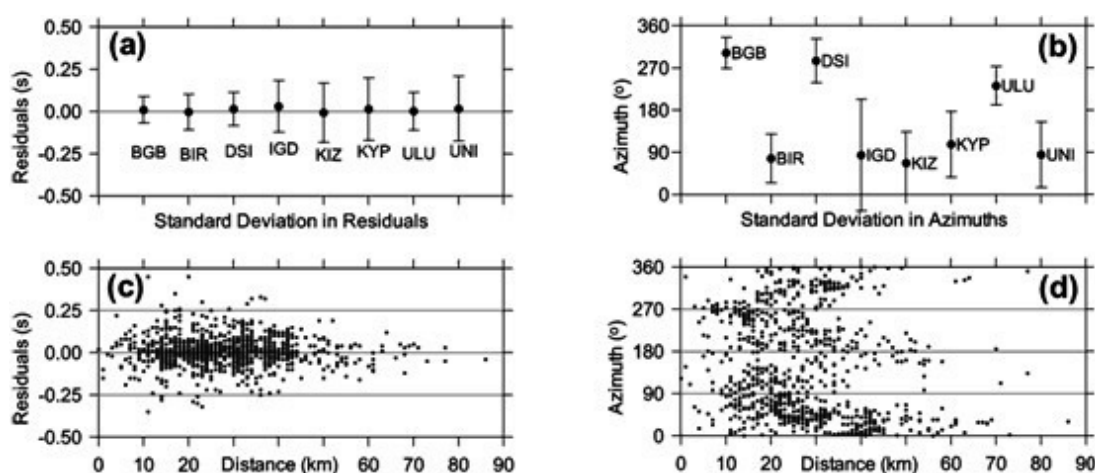


Figure 2.6 Time residuals of the selected 384 events. a) Standard deviation curve in residuals at the stations, b) Residuals (for $RMS \leq 0.20$ sec) versus distance, c) a) Standard deviations in azimuths, d) Azimuth versus distance curve.

2.4.1. Seismic Activity of the Bursa Area

The final epicenter and hypocenter locations obtained from the one-dimensional P - and S -wave velocity model reveal three clusters (Figure 2.7). The depth of the majority of the events was found to be less than 29 km, and the magnitude interval ranges were between $0.3 \leq M_L \leq 5.4$. The swarms were: 1) UM activity (40.05°N - 29.30°E), 2) Kestel-Igdir activity (40.20°N - 29.25°E), and 3) cluster at the south of GF. There were also some clusters at the south (39.80°N , 29.35°E) and north

(40.50°N, 29.25°E) of the study area. However, these swarms could not be interpreted due to the weak station coverage in those areas.

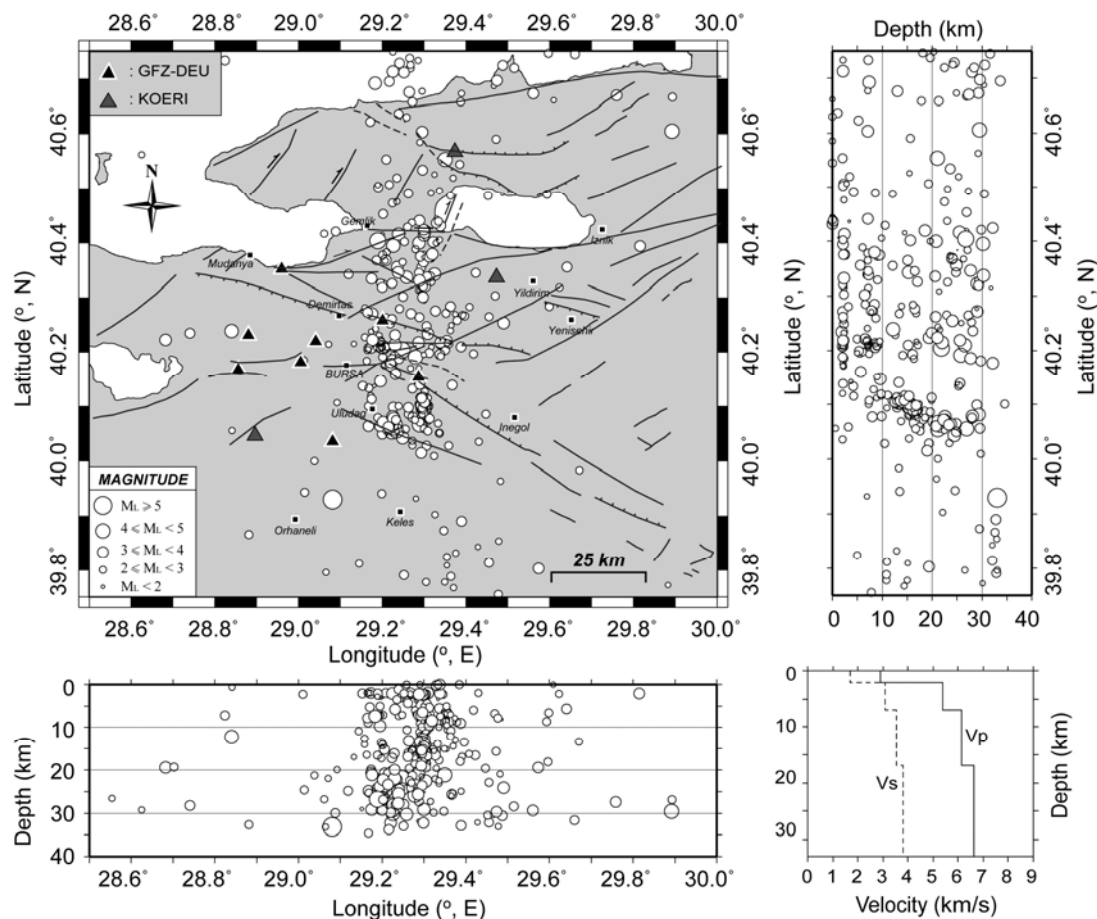


Figure 2.7 Earthquake locations for 384 events in the study area recorded by a detailed temporary microseismic survey between October 2003 and April 2004. Only those earthquakes having $M_L \leq 5.4$ and $RMS \leq 0.20$ sec are included. Two depth sections covering an area between Gemlik Fault (GF) and Sogukpinar Fault (SF) are shown at the below and right panels. Seismic activity is concentrated between 29.15-29.30°E longitudes and 40.05-40.40°N latitudes, revealing $h \leq 29$ km depths. The crustal velocity structure used in the study is also shown at the lower-right corner.

The UM activity takes place at the southeast of the seismic network. We observed two separate clusters here. The southwest swarm could most probably be associated with the Sogukpinar Fault (SF) (in a NW-SE direction) and is traceable through geomorphologic features at the surface (Imbach, 1997). The northeast cluster, which separates gradually from the southwestern swarm, concentrates on Uludag uplift. The hypocenters of these two swarms were located at depths between 12 km and 29 km.

The Kestel-Igdir activity concentrates at the eastern end of the Bursa plain. This cluster is surrounded by the intersection of the IEFZ and BF at the south, and Igdir village at the north. It should be noted that epicenters and hypocenters of this cluster are diffused compared to the Uludag swarm. Earthquakes concentrate in the shallow crust, at a focal depth of between 2 km and 25 km.

The swarm at the south of GF is located between Igdir village, Iznik Lake and GG. The events show a linear distribution and could be related to the GIFZ. Focal depths of the earthquake were located mainly between 2 km and 27 km.

In general, seismic activity is distributed along the north-south direction in the study area. We also observed diffused seismicity at the northwest of Iznik Lake, and surprisingly no remarkable seismic events around Bursa city (40.20°N-29.00°E) in spite of the adequate coverage of seismic stations. The resulting seismicity map confirms that seismic activity is mainly concentrated in the area between SF and GF. The hypocentral distribution of the events indicates that peak seismicity for the region occurs at depths of about 29 km. During the project duration, only 8 earthquakes with magnitudes greater than or equal to 4.0 occurred in the study area. An event with a magnitude of $M_L=5.4$ occurred towards the south of the region near 29.08°E and 39.93°N. The magnitude interval of most earthquakes (226 over 384 events) was between $2.0 \leq M_L < 3.0$.

2.4.2 Focal Mechanisms and Stress Tensor Inversion

The relationship between seismicity and local tectonics was investigated by looking at fault-plane solutions of selected earthquakes that occurred in the Bursa region. We determined the individual focal mechanisms for 2 events by using both P-wave first motion polarities and S/P amplitude ratio (Snoke, 2003) as done by many authors (i.e. Mohamed et al., 2001; Kang & Baag, 2004; Kang & Shin, 2006; Plenefisch & Klinge, 2003; Badawy et al., 2009; Ritter et al., 2009). Unfortunately, it was not possible to obtain well-constrained fault plane solutions for all the events

because in many cases the azimuthal distribution of the DEU-GFZ stations was inadequate. For this reason, we improved the number of focal mechanisms solutions by adding KOERI digital broadband data running under zSacWin software (Yilmazer, 2003; Altuncu et al., 2008; Kalafat et al., 2009). Additionally, 8 fault plane solutions were analyzed for earthquakes occurred between 2003 and 2004 based on the regional moment tensor inversion method (Dreger 2003) integrated in zSacWin. In total, we could determine well constrained (azimuthal GAP <math>< 150^\circ</math> and location horizontal error ≤ 1.0 km) fault plane solutions for 10 events. The results are summarized in Figure 2.8 and Table 2.3.

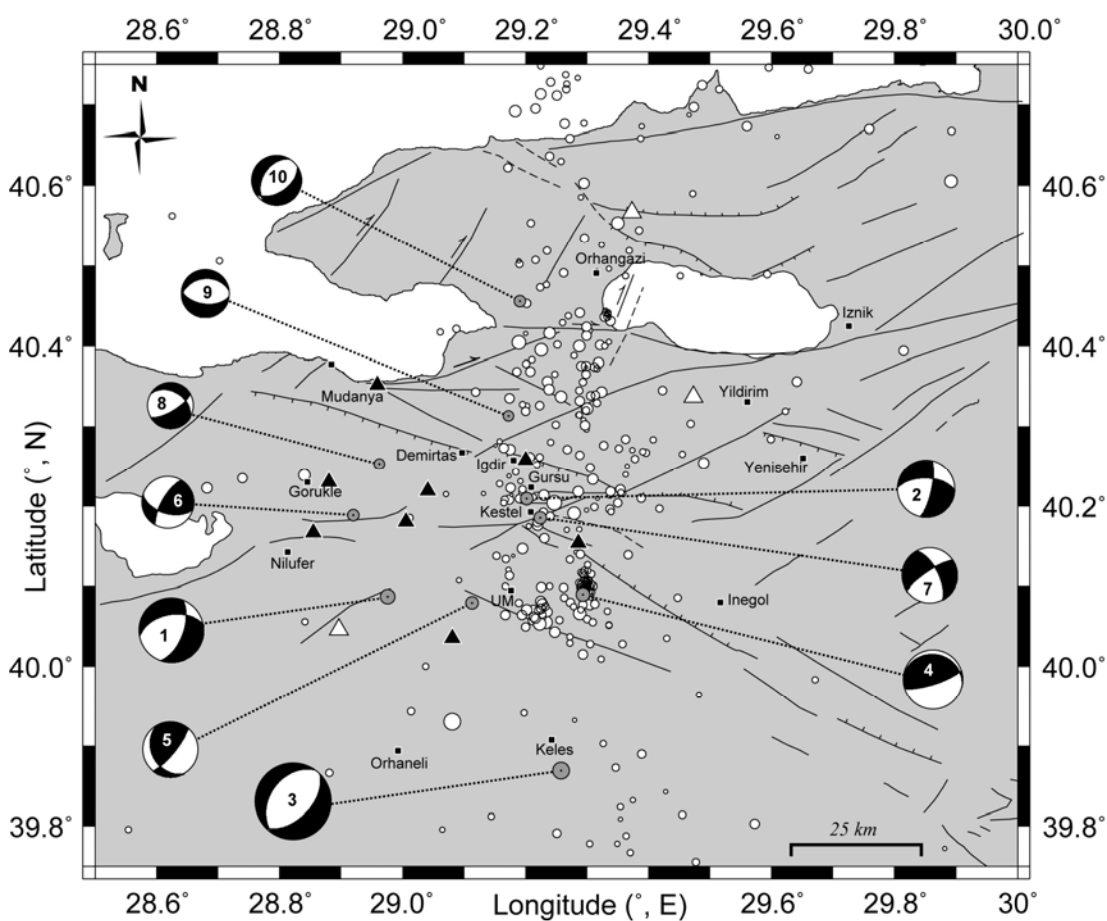


Figure 2.8 Seismic activity and 10 fault plane solutions obtained through the 2003-2004 DEU-GFZ temporary microseismic experiment and the KOERI permanent network. Focal mechanisms constrained at least six reliable *P*-wave first motion polarities.

Table 2.3 Focal mechanisms of Bursa earthquakes. CG– Gurbuz et al. (2000); HRV– Harvard CMT ; SS– Sellami et al. (1997); OP–Polat et al. (2002a,b)

No	Year	Time	Lon. E	Lat. N	Depth	Mag	Az.	Dip	Strike	RMS	GAP	Ref
1*	20031112	00:54	28.976	40.087	6.1	3.5	20	60	-131	0.38	48	this study
2*	20031115	20:49	29.202	40.209	9.0	3.1	12	75	-147	0.41	78	
3*	20031223	15:07	29.258	39.869	8.3	4.1	45	52	-84	0.56	63	
4*	20031227	09:51	29.294	40.090	13.8	3.2	72	77	82	0.39	53	
5	20031231	10:20	29.113	40.079	20.3	3.1	150	33	24	0.05	124	
6*	20040104	10:31	28.920	40.188	26.8	2.8	210	71	38	-	118	
7	20040202	19:27	29.224	40.185	27.6	3.0	236	76	-26	0.10	142	
8*	20040311	23:31	28.962	40.253	7.4	2.5	59	70	-124	0.27	53	
9*	20040330	13:22	29.172	40.313	13.3	2.6	97	54	-82	0.39	82	
10*	20040425	22:52	29.191	40.456	3.8	2.7	56	50	-73	0.21	83	
11	19990819	15:17	29.100	40.680	15.0	5.1	273	45	-120		HRV	
12	19990929	00:13	29.690	40.550	15.0	5.2	66	48	-171			
13	20061024	00:23	28.980	40.460	14.3	5.0	133	57	-32			
14	19930824	15:11	29.290	40.210	5.0	2.5	299	42	-133		SS	

Table 2.3 Continue...

15	19930826	00:42	29.270	40.230	6.0	2.5	302	56	-119
16	19930922	08:53	29.280	40.190	14.0	3.1	55	49	-103
17	19940221	04:36	29.320	40.220	6.0	3.5	64	46	-174
18	19990821	23:34	29.060	40.670	10.5	4.0	88	56	-110
29	19990830	09:00	29.170	40.490	16.1	3.0	215	54	-156
20	19990904	01:45	29.400	40.710	8.4	3.3	277	87	158
21	19990904	23:49	29.390	40.700	20.3	3.2	111	85	-116
22	19990905	05:29	28.900	40.590	9.6	3.2	107	59	-96
23	19990905	22:45	29.250	40.450	17.0	3.1	215	71	-120
24	19990906	14:08	29.400	40.690	10.1	3.3	103	62	-103
25	19990911	07:26	29.360	40.710	12.4	3.5	193	38	-4
26	19990922	17:44	29.180	40.640	8.4	3.1	83	64	-127
27	19990924	00:01	29.160	40.460	20.0	3.2	226	67	-155
28	19990927	21:44	29.060	40.410	7.5	3.1	52	59	-111
29	19990930	07:55	29.880	40.710	8.4	3.4	12	45	-14
30	19991006	14:16	28.700	40.430	8.4	3.0	257	59	-164
31	19991021	08:20	28.580	40.350	6.3	3.0	183	33	17

OP

Table 2.3 Continue...

32	19951030	16:09	28.650	40.410	10.0	2.1	300	45	-90
33	19951102	08:40	29.650	40.150	2.5	2.1	210	80	-170
34	19951102	20:28	29.360	40.530	16.6	1.5	30	65	170
35	19951103	17:01	29.280	40.280	5.0	2.1	305	50	-115
36	19951104	00:06	28.950	40.450	8.7	2.2	165	50	-50
37	19951113	08:36	28.840	40.140	5.0	2.2	131	41	-54
38	19951114	20:03	29.020	40.380	11.6	1.9	100	20	-20
39	19951119	07:47	29.390	40.240	7.3	1.9	80	80	170
40	19951123	08:40	29.460	40.500	8.4	2.1	325	45	-90
41	19951123	08:43	29.560	40.470	6.1	1.9	270	70	-105
42	19951124	22:12	29.030	40.730	12.5	2.0	355	15	60
43	19951126	02:49	29.920	40.210	14.1	2.4	275	45	-110
44	19951130	23:32	28.710	40.330	8.3	1.8	290	55	-135
45	19951207	21:57	29.140	40.700	7.9	2.3	170	50	-50

* : Solution was provided by using KOERI digital broadband data running under zSacWin

CG

These are events for which a minimum of six reliable polarities were obtained, and stations covered an azimuthal range of 142° . We attempted to calculate fault-plane solutions for all local (epicenters within 10km of the Bursa city center) and regional (epicenters 10-70km from the city center) earthquakes occurred between October 2003 and April 2004 that had clear P-wave polarities recorded at a minimum of six stations. Focal mechanisms mainly show normal or normal-to-strike-slip characters. Good polarity prediction and preferred solutions have been performed for all focal mechanisms.

Inversion of stress tensors involves the following three basic elements: fault planes, slip vectors on the fault planes, and stress tensors (Gephart & Forsyth, 1984; Michael, 1984; Rivera & Cisternas, 1990). A fault plane is specified by three angles: the fault strike ϕ is defined as the azimuth of the strike direction, the dip δ is defined as the angle between a horizontal plane and the fault plane, and the direction of a slip on a fault plane is conveniently described by the rake, which is the angle λ , between the slip and strike directions.

The state of stress within the Earth's crust is of particular interest for geologists and geophysicists as it can provide a better understanding of geodynamic processes. Microseismic events represent shear or mixed-mode failure of rocks along pre-existing planes of weakness that is accompanied by significant seismic energy release at relatively high frequencies. The slip direction of failure is controlled by the direction of the plane of weakness and the stress regime. Thus, if the focal mechanisms of microseismic events are known, the inverse problem can be solved to yield information about the state of stress. The use of focal mechanisms to estimate the nature of the stress tensor in the seismogenic zone has been frequently used in the past (i.e; Gephart and Forsyth, 1984; Michael, 1984; Angelier, 1990). The fault plane solution of a microseismic event usually provides two possible fault planes which are orthogonal to each other. Consequently it is necessary to identify which one is the true failure plane. In addition to these methods, Rivera and Cisternas (1990) developed a stress inversion method that a unique stress could explain the whole set of data (polarities with their respective positions on the focal sphere), that is the

entire region is under the same stress regime. This hypothesis is not as strong as the hypothesis implicitly assumed to construct composite focal mechanisms and the method has the advantage that the orientation and shape factor (R) of the stress tensor is determined together with the individual fault plane solutions (Polat et al., 2002b). In a recent study, Angelier (2002) proposed a new inversion technique which does not require distinguishing between two nodal planes.

In the last two decades, two inversion methods proposed by Gephart & Forsyth (1990) & Michael (1987) have been widely used for the stress tensor inversions. In fact, these two methods typically obtain similar stress orientations for similar focal mechanism data sets, revealing some differences in error (misfit) estimates (Hardebeck & Hauksson, 2001). The size of the average misfit provides a guide to how well the assumption of stress homogeneity is fulfilled in relation to the seismic sample submitted to the inversion algorithm. In the present study, we adapt the inversion technique of Michael (1987) and Gephart & Forsyth (1990) to our purpose and estimate the principle stress directions by using slip data recorded on fracture surfaces assuming that the slip striations are created by a frictional slip between two fracture surfaces. These techniques define the confidence regions on the quantities obtained through a statistical tool and attempts to choose the correct fault plane while determining the stress tensor. Applying both techniques to a set of focal mechanisms, we obtain the scalar which describes the relative magnitudes of the principal stresses and hence constrains the shape of the deviatoric stress ellipsoid, known as stress magnitude ratio (shape factor, R) parameter. This parameter is expressed as:

$$R = \frac{\sigma_1 - \sigma_2}{\sigma_1 - \sigma_3} \quad (1)$$

where σ_1 , σ_2 , and σ_3 are the maximum, the intermediate, and the minimum compressive principal stress axis, respectively. In addition to the geometrical illustration of fault planes; interpretations of focal mechanisms and stress tensor results are presented as the structural diagram of the fault-striate orientation for the

strike, normal, thrust and oblique faults with minor horizontal or vertical slip components.

We have analyzed the seismicity in the Bursa region to determine the stress field (Figure 2.9). Ten focal mechanisms obtained from 2003 to 2004, microseismic experiments and four fault plane solutions from Sellami et al. (1997) were used to invert for the stress tensor. Orientation of the σ_1 , σ_2 , and σ_3 were computed for the study area, and an estimation of the principal stress orientations were projected onto a lower hemi-sphere Wulff net. Figure 2.9a shows the results by using Michael's (1987) algorithm. The well-defined maximum principal stress (σ_1 dips 67.9° to $N111.4^\circ E$) is vertical, and the intermediate (σ_2) and minimum (σ_3) axis are nearly horizontal with $N64.6^\circ W$ (22° dip) and $N155.1^\circ W$ (1.3° dip), respectively. Similar results approaching to vertical for maximum principal stress axis (σ_1 , dips 81° to $N182^\circ E$) were also observed by using Gephart & Forsyth (1990) method (Figure 2.9b). The magnitude stress ratio is $R=0.5$ defining an extension regime.

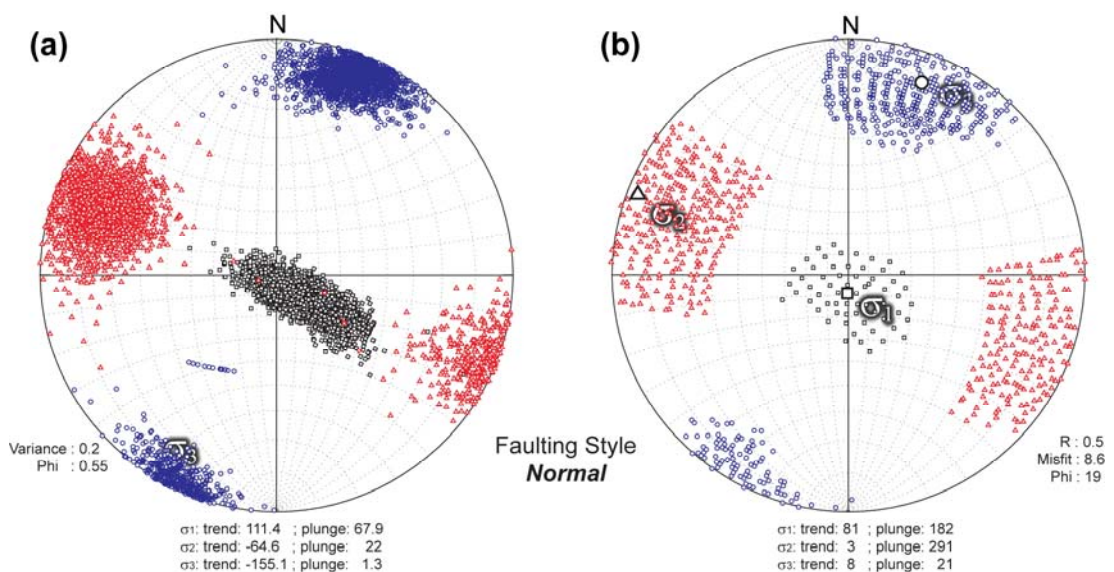


Figure 2.9 Shape and orientation of the stress tensor calculated from 14 sets of fault planes and slip directions obtained 10 fault plane solutions in the frame of this study and four focal mechanisms from Sellami et al. (1997) for the city of Bursa. The principal stress directions are projected onto a lower hemisphere Wulff net. The maximum principal stress direction (σ_1) is close to vertical and the minimum principal stress (σ_3) is on the NW-SE direction. The stress regime reveals normal faulting of $R=0.5$. Square, triangle and circle symbols represent σ_1 , σ_2 and σ_3 , respectively.

2.5 Discussions and Conclusions

We have used earthquake recordings of local events in the distance range of 90 km in order to quantify the seismicity in the vicinity of Bursa. The hypocentral distribution of the events indicates that peak seismicity occurs at depths of about 29 km. Only few earthquakes with a magnitude greater than 4.0 have occurred in the study area, and the magnitudes of the majority of the recorded events were below $M_L \leq 3.0$.

Fault plane solutions of 10 earthquakes obtained in the present study are compatible with normal or oblique mechanisms (Figure 2.10). All events located at the northern part of the study area reveal normal or oblique mechanisms with a dominant normal component with the exception of Nr.6, which exhibits a reverse faulting mechanism. Its azimuthal gap (118°) is rather reasonable; however, it was only determined by six stations. Therefore it may not be adequate to observe the preferential orientation of fault planes with the limited number of polarities.

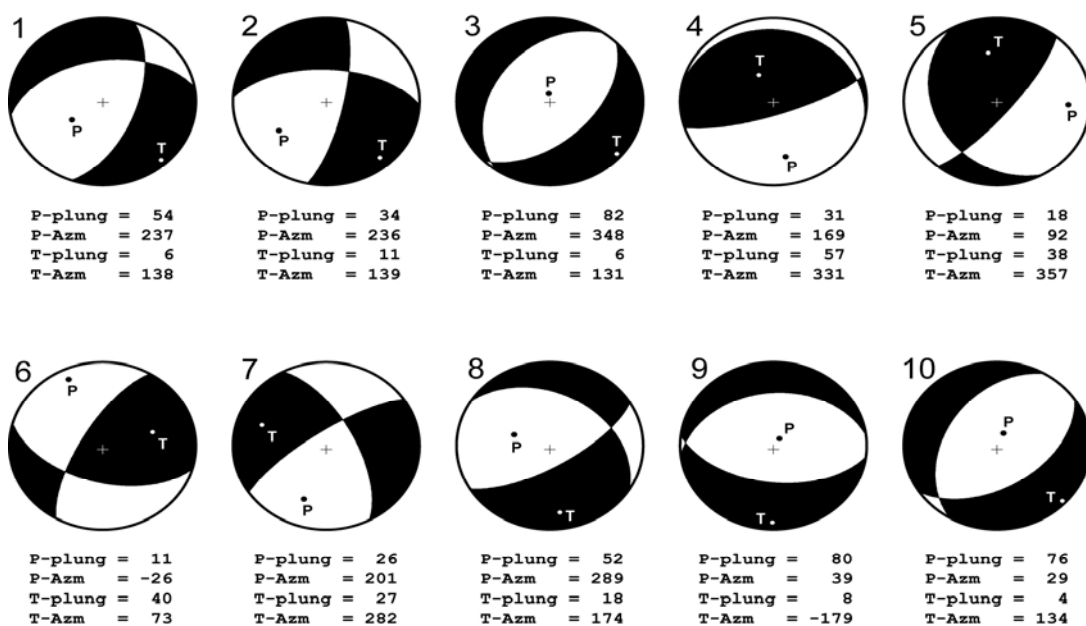


Figure 2.10 Individual focal mechanisms (lower hemisphere projection) obtained both from the inversion of *P*-wave polarities (Snoko 2003) and regional moment tensor inversion methods (Dreger, 2003). A total of 10 selected events were investigated through the 2003-2004 microseismic experiment (Nr.5 and Nr.7 by using FOCMEC) and digital broad-band data provided by KOERI permanent network. Each mechanism shows the best fitting solution. Compression and dilatation are marked by P and T, respectively.

Fault planes of two earthquakes (Nr.9, Nr.10) at the north, near GF and the Demirtas-Kiblepinar Fault (DKF), are aligned on the NE-SW and E-W directions. Both focal mechanisms reveal normal faulting. At the middle of the study area (between Igridir and Kestel), fault planes for the events Nr.2 and Nr.7 are compatible with the morphology of faults near Kestel. They show strike-slip faultings with minor normal slip exhibiting E-W (for Nr.2) and NE-SW (for Nr.7) orientations. Focal mechanisms of the earthquakes (events 4 and 5) located to the east and west of the Uludag uplift (near the UM area) reveal reverse faultings. Towards the south of the study area (near Keles), we calculated one focal mechanism (Nr.3) showing normal faulting character along the NE-SW direction. Three other events (Nr.1, 6, 8) were determined in the area to the east of the seismic swarms aligned in the north-south direction in the study area. They also show dominant normal faulting with minor strike-slip components (as in Nr.1 and Nr.8) with the exception of Nr.6. All fault plane solutions (except Nr.5 and 7) were determined by using the regional moment tensor inversion method (Dreger, 2003) unified to the program code zSacWin (Yilmazer, 2003).

The S/P amplitude ratios significantly improved the determination of focal mechanism solutions in many ways as seen in two examples in Bursa (Figure 2.11). First, they allow more events to have acceptably constrained solutions when polarity data are only used. Hence, if the number of polarity errors is within a prespecified number of allowable errors, then the difference between theoretical amplitude ratios and the corresponding observed S/P amplitude ratios is compared to the preset error allowance. Second, the S/P ratios restrict, at least to some extent, the strike, dip, and rake angles determined by polarities, thereby producing better constrained results. The amplitude ratio was important to distinguish the fault planes of the events. And finally, the RMS errors and other statistics generated from the amplitude ratio data provide an objective method to select a favored solution from the family of solutions obtained. If the number of acceptable ratio differences (within the preset error allowance) is less than a specified number of allowed ratio errors, then a valid solution is declared and its parameters are output. The fault plane solutions for the

events Nr.5 and Nr.7 were calculated with the program code FOCMEC (Snoke, 2003) and used the S/P ratio added to P -polarities. This method puts considerable constraints on focal mechanisms (Figure 2.11). Both events comprise minor strike-slip components with reverse (Nr.5) and normal (Nr.7) faultings near UM at the south, and Kestel at the middle of the study area, respectively. For event Nr.5, we found that fault planes had a strike of 150° , 33° dip and 24° rake angles, while event Nr.7 was characterized by a 236° strike, 76° dip and -26° rake angles. The estimated uncertainty is about 5° . The variations of all possible solutions are given in Figure 2.11a and 2.11d. The solutions are performed not only from the P -polarities but also from the S/P amplitude ratios. The scatter of solutions for two events (Figure 2.11b, e) is smaller than all solutions. Figure 2.11c and 2.11f show the results of best-fit fault plane solutions after P -polarities and S/P amplitude ratios. There are 11 acceptable solutions for event Nr.5 and five for event Nr.7. Errors for acceptable solutions are between 0.02 seconds and 0.18 seconds for Nr.5, and 0.08 and 0.13 seconds for Nr.7. The RMS log amplitude ratio error for all solutions varies between 0.2 and 1.0 seconds in event Nr.5, while it varies from 0.2 to 0.9 for Nr.7 (Figure 2.11). All suggested errors in the polarity data were checked and reviewed. If more than one group of mechanisms gave a good fit to the first S/P amplitude ratios, we ruled out the competing solutions by synthetic waveform modeling of the total wave train. We then proceeded by tightening the error limits until the output includes the best-fitting type of mechanisms only. Hence we believe that error statistics for focal mechanisms are favorable for the investigated events.

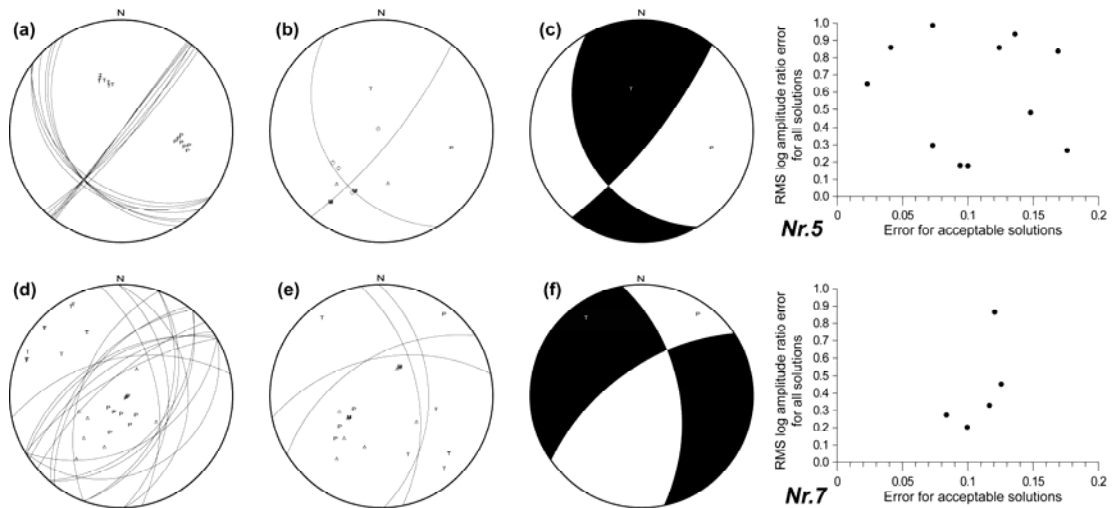


Figure 2.11 Details on the fault plane solutions of the two analyzed events. The December 31, 2003 and February 2, 2004 (Nr.5) events corresponding all possible solutions using P -arrival polarities, were observed as shown in (a) and (d). The results of amplitude ratios S/P , indicating possible focal mechanisms, are in (b) and (e) showing the preferred solutions (minimum error statistics). Finally, the best-fit fault plane solutions from P -polarities and S/P ratios are given in (c) and (f), respectively. All plots are on the lower hemisphere and are equal-area projections. Location RMS errors are 0.05 sec for Nr.5 and 0.10 sec for Nr.7.

On the other hand, it is true that we could not observe sufficient numbers of fault plane solutions within the temporary network area despite the good coverage of the Bursa. This result may arise from the lack of seismicity near the city; we also detected swarm type activities towards to the east of the network.

Stress tensor inversion for the overall study shows a nearly pure extensional regime (Figure 2.9) with σ_1 along the vertical and σ_2, σ_3 closer to horizontal. Shape factor (R) of the investigated area is 0.5, indicating a heterogeneous stress regime and complex deformation pattern since we included 10 focal mechanisms obtained from the present study. However, we found that the stress regime was poorly defined because many focal mechanisms were rejected as incompatible. Hence, we decided to divide the study into the three subsets (Figure 2.12; Z1, Z2, Z3) based on earthquake locations and tectonic regimes. As performed in the single-stress state for the whole region, the 95% confidence region was also computed by the same bootstrap re-sampling technique of Michael (1987) which is adequate to produce stable confidence regions up to the 95% level for the subset zones. In order to

include the effects of mispicked fault planes on the confidence region, each nodal plane has the same probability of being chosen during the resampling.

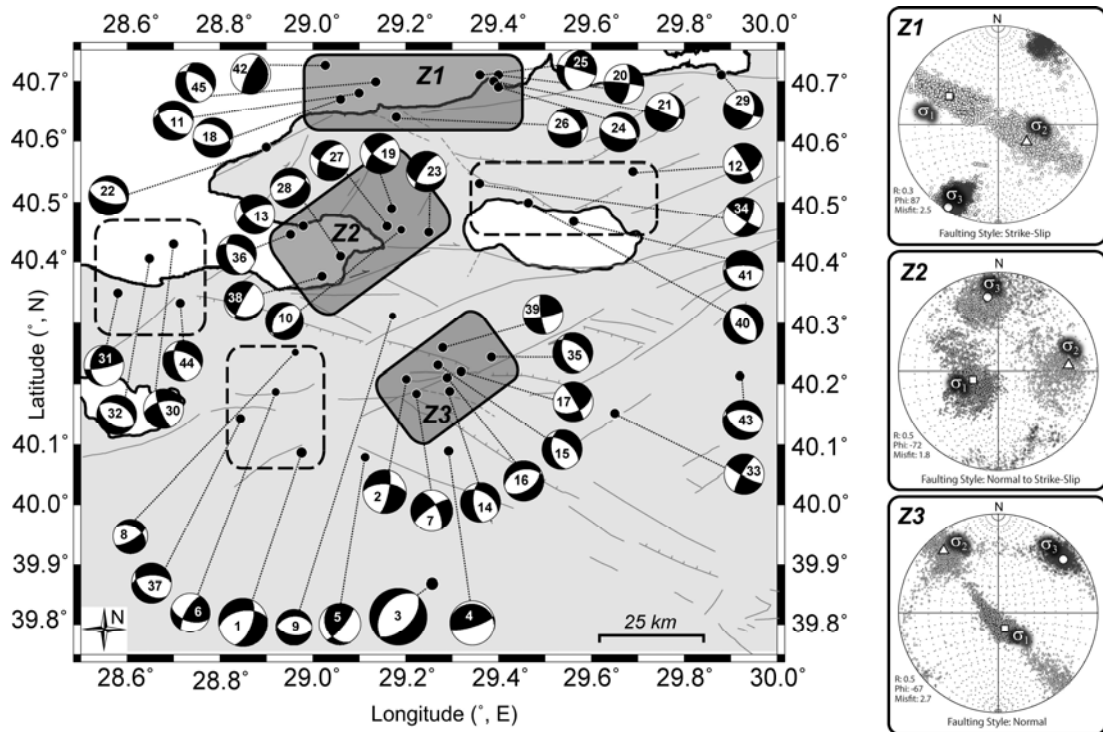


Figure 2.12 Stress tensor inversion for 45 focal mechanisms compiled from Harvard CMT. Gurbuz et al. (2000), Ozturk et al. (2009); Polat et al. (2002a,b), Sellami et al. (1997) and this study. Four subset seismogenic zones (Z1, Z2, and Z3) of the fault plane solutions generally indicate extension regime with σ_1 closer to the vertical except for the Z1 zone. The directions of the σ_1 and σ_3 (closer to the horizontal), and σ_2 (closer to the vertical) reveal a strike-slip regime here. The Z2 area is in between strike-slip and normal faulting regimes. Zone Z3 shows normal faulting with σ_1 closer to vertical. The areas shown with dashed rectangles could not be investigated by stress tensor inversion due to the insufficient number of focal mechanisms.

For the northern zone (Z1), the strike-slip regime was dominant according to the distribution of the stress axis. σ_1 is closer to horizontal with a vertical dip angle (Δ) of 32° and an azimuth of about $N300^\circ$. σ_3 is almost horizontal with $N208^\circ$ and $\Delta=3^\circ$, and the σ_2 trends $N118^\circ$ with $\Delta=68^\circ$. R was calculated as 0.3, consistent with a strike-slip regime for the northern part of the study area. Towards the south, in Z2 subset, the σ_1 is closer to the vertical trending $N259^\circ$ with $\Delta=54^\circ$ while σ_2 and σ_3 are near horizontal trending $N84^\circ$ with $\Delta=21^\circ$ and $N347^\circ$ with $\Delta=28^\circ$, respectively. The magnitude stress ratio was calculated as $R=0.5$ indicating a transition between

normal and strike-slip regimes. Since we have only one event (Nr.9) in the area between Z2 and Z3, we could not reveal the local stress regime there. Finally in Z3, our data are consistent with, we have a normal faulting regime with a magnitude stress ratio $R=0.5$. σ_1 was found to be nearly vertical trends $N169^\circ$ with $\Delta=83^\circ$. σ_2 and σ_3 , are closer to the horizontal trending $N321^\circ$ with $\Delta=19^\circ$ and $N47^\circ$ with $\Delta=17^\circ$ respectively.

The stress regime of the Bursa area is characterized by overall extension, which apparently differs from what might be expected from the stress inversion of the NAFZ. Different fault patterns related to structural heterogeneity caused superimposition of different tectonic regimes since the seismotectonic characteristics of the study area are not homogeneous, and the contemporary seismic deformation pattern is quite complex. The region is characterized by relatively complex active tectonics, NW-SE extensional structures driving to the development of Neogene and Quaternary basins. Our results reveal a transition in space from a strike-slip to a normal faulting regime. The northern seismotectonic domain of the study area is affected by a strike-slip regime. The large confidence areas for the σ_1 and σ_3 orientation and the misfit-phi values indicate some variability in the stress field of the different zones. The hydrothermal circulations and spring waters may be responsible for the earthquakes that occurred between the GF and Kestel area with a depth around 2km (Balderer, 1997; Eisenlohr, 1997; Greber et al., 1997; Imbach, 1997). The many normal focal mechanisms (i.e.; Nr.1, 3, 9, 10) suggest that gravitational forces dominate the maximum compressive stress (Adatepe et al., 2002; Klingele & Medici, 1997; Giampiccolo et al., 1999; Pamukcu & Yurdakul, 2008; Isik & Senel, 2009). We think that principal stress axes are representative of large-scale deformation of the study area. Bursa and the surrounding area which is associated with strike-slip faulting, is also consistent with the GPS geodetic observation particularly regarding the NE-SW strain extension (Straub, 1996).

2.6 Acknowledgements

This paper is a part of the PhD thesis of Elcin Gok. We are grateful to the staff of the GeoForschungZentrum (GFZ) of Potsdam, Germany for the installation of the temporary seismic network. We wish to thank Mahmut Parlaktuna from the Middle East Technical University (METU) in Ankara, Claus Milkereit from the GFZ (Potsdam) and Asaf Pekdeger from Frei University of Berlin, who cooperated with us during the project duration. We also acknowledge Rahmi Pinar, Zafer Akcig and Zulfikar Erhan from Dokuz Eylul University (DEU) in Izmir for facilitating our works during and after the project. We are grateful to Dogan Kalafat, Mehmet Yilmazer and Selda Altuncu from the Kandilli Observatory and Earthquake Research Institute (KOERI) for providing digital broad-band data and the zSacWin program code. Most of the figures were generated by using the GMT software package (Wessel and Smith 1995). This manuscript greatly benefited from helpful reviews by the editor, Prof. Eugenio Carminati. We would like to also express our special thanks to two anonymous reviewers for their comments and constructive criticisms which have greatly improved the earlier version of the paper. This work was supported by the TUBITAK (Turkey) and JULICH (Germany) bilateral scientific agreement (Project Nr.102Y156). This study was also granted by the Scientific Research Project of the Dokuz Eylul University (DEU-BAP 2006.KB.FEN.007). The English language was edited by Barbara Jean Isenberg (<http://www.barbarajisenberg.com>).

CHAPTER THREE

MICROTREMOR HVSR STUDY OF SITE EFFECTS IN BURSA CITY (NORTHERN MARMARA REGION, TURKEY)

3.1 Preface

The studied area is located in a region that suffers the highest seismic hazard in the Marmara Region due to the branches of the North Anatolian Fault Zone (NAFZ). The region of Bursa is one of the most seismically active areas in Turkey, where two damaging earthquakes with maximum intensity equal or greater than IX (EMS-98) have occurred in historical times. These earthquakes showed that strong site effects are characteristic of the parts of the town located on the Quaternary alluvium. The microtremor horizontal-to-vertical spectral ratio (HVSR) method was applied to free-field measurements over different geological structure in the town area in order to assess the fundamental frequency of the sediments. The aim of this study was to obtain a better knowledge of the geologic structure of the Bursa area (Figure 3.1) by using horizontal-to-vertical spectral ratios (HVSR) with ambient noise and earthquake records.

Three-component microtremor measurements were conducted at 22 sites in the northern section of the Bursa city, where the different geological structures in the study area outcrop. The fundamental frequencies of the sediments show a range between of 0.5 and 20 Hz. The lower frequencies (below 2 Hz) correspond to the Holocene and neogene deposits overlain by alluvium, forming a small basin. The higher frequencies correspond to Paleozoic and metamorphic rocks. However, variations over short distances are large.

In addition to microtremor data, earthquake records were also used to compute HVSR. The comparison between dominant frequencies obtained from earthquake records with those, obtained from microtremor measurements show similarities.

3.2 Introduction

Local site effects are one of the most important aspects in the assessment of seismic hazard. Local site response can be investigated by empirical and theoretical methods. Theoretical methods allow a detail analysis of the parameters considered in the evaluation; however, they require information of the geological structure (Dravinski et al., 1996). Empirical methods are based on seismic records on sites with different geological condition from which relative amplitudes and dominant periods may be determined directly. This approach requires of a large number of earthquakes. In regions with low seismicity, it would be necessary to wait for a long time to obtain a complete data set. For this reason, the use of ambient seismic noise is becoming popular as an alternative (Bard, 1998).

Recording and analyzing ambient noise is simple. A few minutes of microtremor data are usually sufficient. Microtremors are present continuously in time and space. A single three-component station is the only instrument required. Routine spectral techniques can be easily applied to estimate the dominant frequency of vibration of the sedimentary structure. These frequencies of vibration are closely related to the physical features of the site under study, i.e., layer thicknesses, densities and wave velocities. Estimates of these frequencies are useful to constrain the physical properties at a given site.

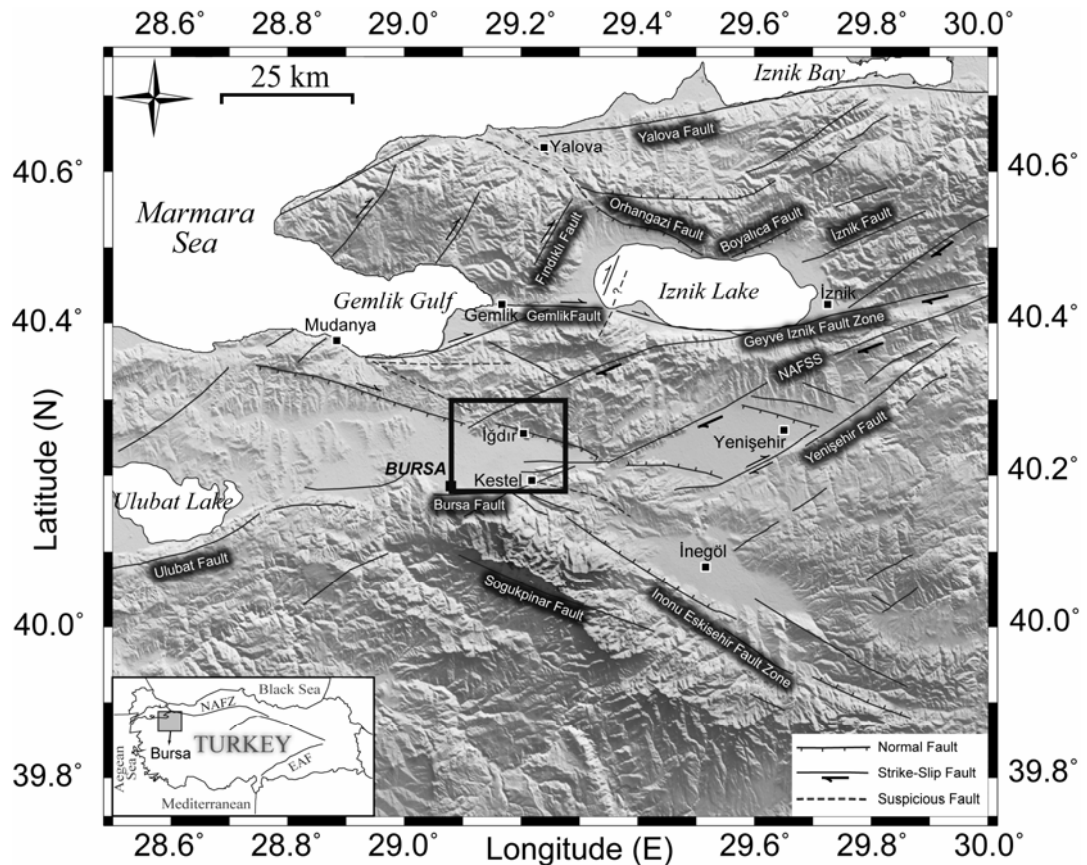


Figure 3.1 Map of Bursa. The box indicates the study area. NAFZ: North Anatolian Fault Zone, NAFSS: Southern strand of the North Anatolian Fault Zone, EAF: East Anatolian Fault Zone.

The Nakamura technique (Nakamura, 1989), based on the horizontal to vertical spectral ratio, has been commonly used to estimate the site effects. Later it has been extended to both weak motions (Ohmachi et al., 1991; Field & Jacob, 1993, 1995); and strong motions (Lermo & Chavez-Garcia, 1994; Theodulidis & Bard, 1995; Suzuki et al., 1995). Lermo & Chavez-Garcia (1993) applied this technique to estimate the empirical transfer function from the intense S-wave part of a small sample of earthquake records obtained in three cities of Mexico. Their results showed that the HVSR can estimate the dominant frequency at a site based on earthquake data.

Suzuki et al. (1995), using both microtremor and strong motion data in Hokkaido, Japan, showed that the dominant frequency obtained from HVSr was in good agreement with the predominant frequency estimated from the thickness of an alluvial layer. Lermo & Chavez-Garcia (1993) compared transfer functions computed using the Haskell method agreement with the HVSr. Lermo & Chavez-Garcia (1994) verified that the underlying assumptions of Nakamura's technique are consistent with the propagation of Rayleigh waves.

3.3 Tectonic and Geological Setting

The region of study is surrounded by many active faults; Gemlik Fault (GF), Geyve-Iznik Fault Zone (GIFZ), Yenişehir Fault, Bursa Fault (BF), Inonu-Eskisehir Fault Zone (IEFZ). The main lithological units in the vicinity of Bursa are Quaternary alluvial deposits and Neogene basement rocks. The thickness of the Quaternary deposits is larger than 300m where those are as Neogene units vary from 50 to 200m. in Bursa basin (Imbach 1997; Topal et al., 2003). South of Bursa, Paleozoic and metamorphic units are present. The simplified geological map of the study area, modified from MTA (General Directory of Mineral Research and Exploration), is shown in Figure 3.2.

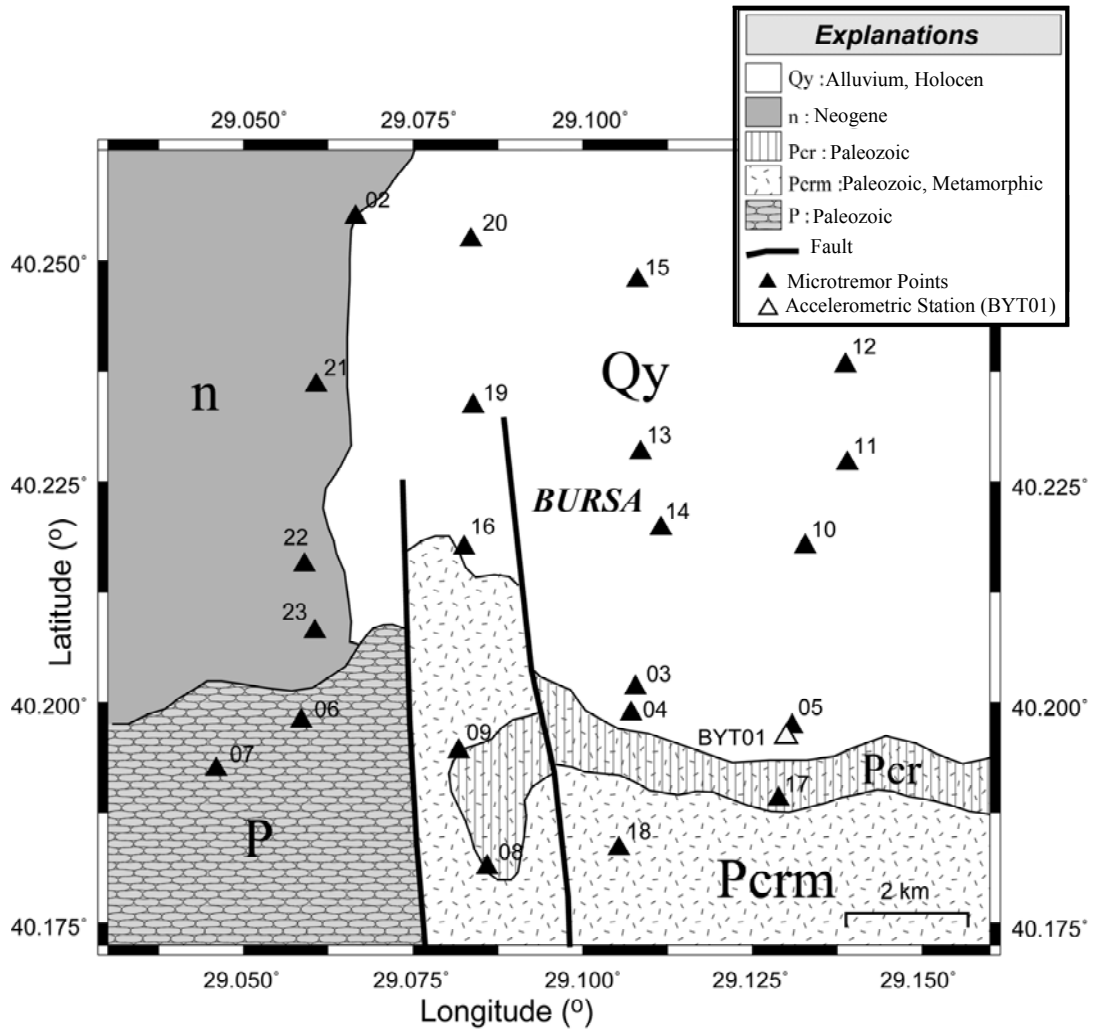


Figure 3.2 Simplified geological map of Bursa region. Black triangles indicate points of microtremor measurements; open triangle shows the location of BYT01 station (Modified after MTA, General Directory of Mineral Research and Expolaration).

Bursa city is located in the southern Marmara Region, characterised by significant historical and instrumental seismicity (Figure 3.1). Two strong earthquakes, with maximum intensities X and IX EMS-98, occurred in 1855. Seismicity is related with the activity of southern branch of the NAFZ.

3.4 Method

The microtremor HVSR method is generally used for microzonation and site responses studies. It considers that the amplification produced by a surface layer can be estimated from the ratio between the horizontal and vertical spectral amplitudes. This method is known as the Nakamura's technique.

The method supposes that microtremors are composed of Rayleigh waves which propagate in a surface layer over a half-space (Dravinski et al., 1996; Lermo & Chavez-Garcia, 1994). The motion at the interface between the layer and the half-space is not affected by the source effect. Moreover, the horizontal and vertical motions at the interface have similar amplitude due to the ellipticity of the Rayleigh waves.

HVSR is related to the ellipticity of Rayleigh waves which is frequency dependent (Bard, 1998; Bonnefoy-Claudet et al., 2006). HVSR shows a sharp peak at the fundamental frequency of the sediments, if there is a high impedance contrast between the sediments and the bottom bedrock. Criticism of the HVSR method was often related to the fact that there is no common practice for data acquisition and processing (Mucciarelli & Gallipoli, 2001). Attempts to provide standards were only made recently (SESAME, 2004). It is widely accepted today that the frequency of the peak of HVSR shows the fundamental frequency of the sediments. Its amplitude depends mainly on the impedance contrast with the bedrock and cannot be used as site amplification. Comparisons with results of standard spectral ratio method have also shown that the HVSR peak amplitude sometimes underestimates the actual site amplification. (Bard, 1998; Gosar & Martinec, 2009)

3.5 Microtremor Measurements and Analyses

3.5.1 Instruments and Data

A single seismic station was used for the microtremor measurements. It was composed of a three-component seismometer with GPS time, the passing band of this system in DC to 100 Hz. Our sampling was 100 sps, reducing the frequency to the band below 50 Hz. We recorded data at 22 different points. Record duration was set to 30 minutes. The mean distance between recording sites is approximately 2 km. The sensors were buried in the ground at each site.

3.5.2 HVSR Analyses

Microtremor measurements were made at 22 sites (Figure 3.2). Their locations were selected to avoid the influence of trees, sources of monochromatic noise, rivers, and strong topographic features. HVSR analysis was performed following SESAME (2004). Recorded time series were visually inspected to identify possible inaccurate measurements and transient pulses. Each record was split in windows between 15 to 30 s long %5 overlapping windows for which amplitude spectra in a range 0.5–20 Hz were computed using a cosine taper with 10% smoothing and Konno & Ohmachi smoothing with a constant of 40 (Konno, & Ohmachi, 1998). HVSR was then computed as the average of both horizontal component spectra divided by the vertical spectrum for each window. After produced HVSR dominant frequency and maximum amplification were determined. Figures 3.3 and 3.4 show an example of the results.

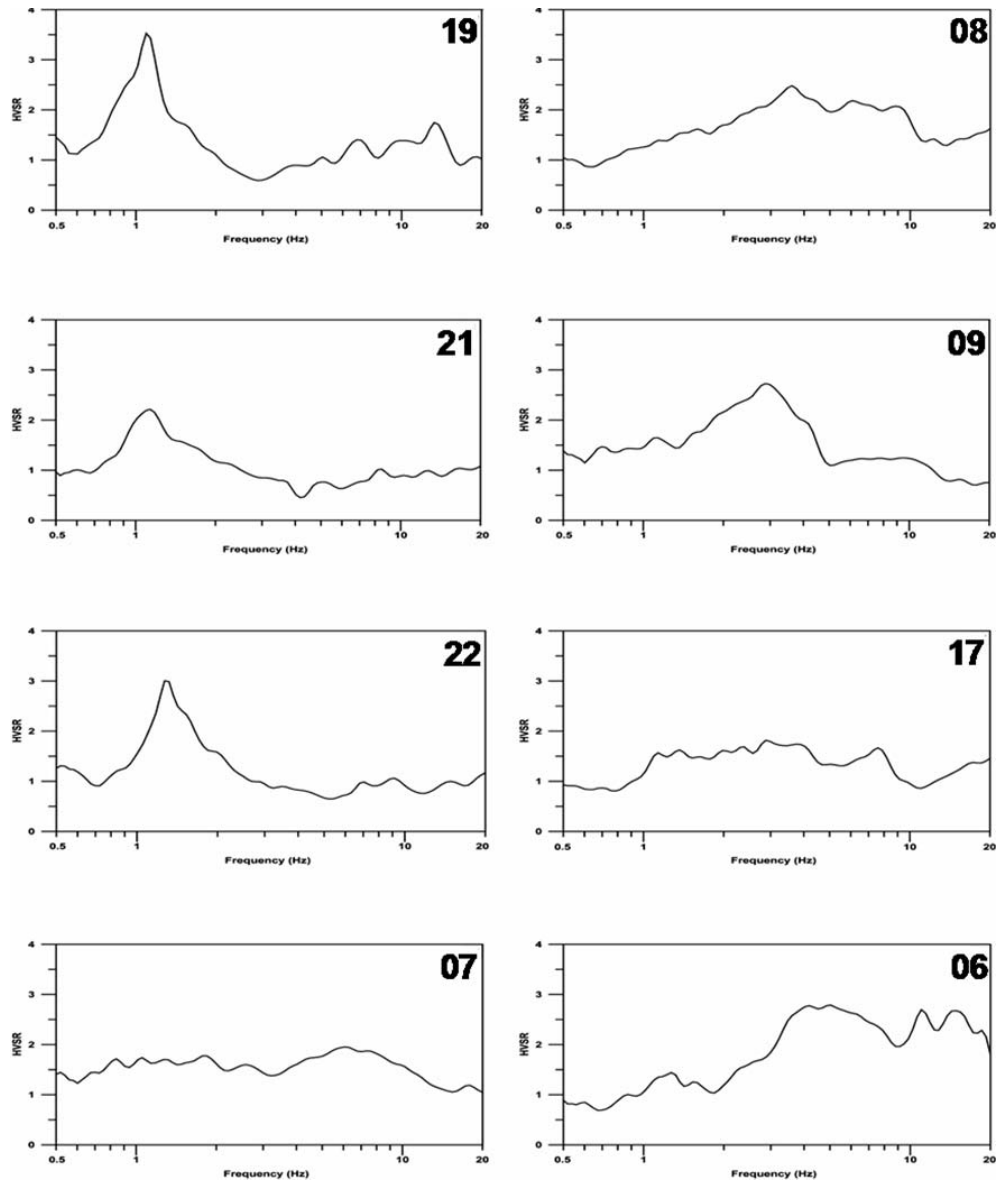


Figure 3.3 Examples of HVSR for the measurements points (19, 21, 22, 08, 09, 17, 06 and 07)

The smallest dominant frequency values (≤ 2 Hz) were obtained in the northern part of the basin, covered by the thick Neogene and Quaternary sediments (points 19, 21, 22 in Figure 3.3 and 13, 14, 12 in Figure 3.4). Frequencies in the range 2 to 4 Hz were observed on Paleozoic sediments of moderate thickness (points 08, 09, 17 in Figure 3.3). Dominant frequencies larger than 5 Hz was obtained on Paleozoic and metamorphic rocks (06, 07 in Figure 3.3 and 04, 05 in Figure 3.4). These values are characteristic for most of the Bursa area.

In some cases the microtremor measurements were unable to provide an estimate of dominant frequency (Figure 3.4). The possible reasons are: wide peak, two or more peaks in a spectrum, flat spectral ratio and very small amplitude of the peak.

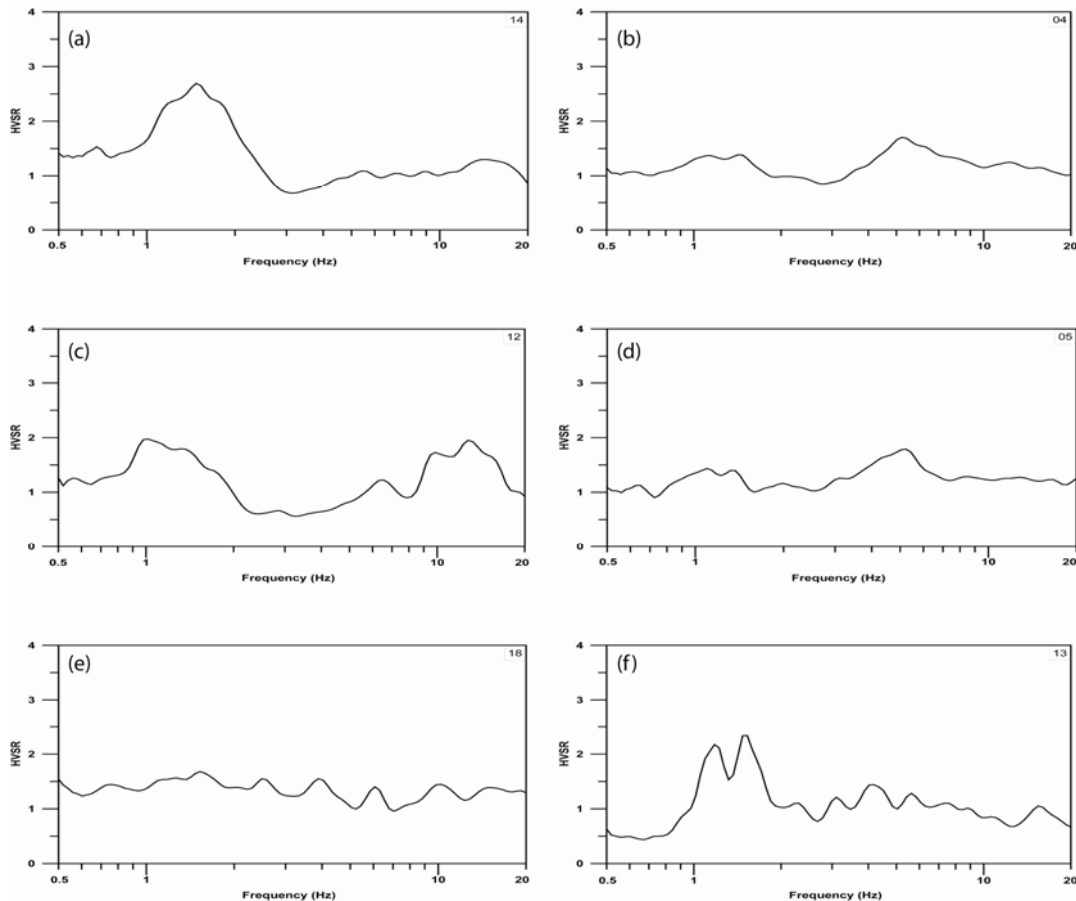


Figure 3.4 Some examples of microtremor measurements where a dominant frequency could not be identified.

Figure 3.4a shows an example of wide peak that can not be associated to a resonant frequency. Probably due to the several impedance contrasts at various depths, HVSR sometimes resulted in two or more peaks with similar amplitudes. In Figure 3.4b, the two peaks are well separated in frequency, so it can be the boundary between soft sediments and rock is related to the peak at 1.3 Hz. The second peak at 5 Hz may be related to Paleozoic rocks. However, in the case shown in Figure 4c, there are two peaks of the same amplitude at 1 Hz and 13 Hz. In such cases, we were unable to identify which one corresponds to the most significant geological boundary. Another example (Figure 3.4d) shows two different peaks at the 1.2 Hz

frequency and 5 Hz. The peak of HVSR is in this case occurs at a higher frequency (5 Hz). In some cases, we compared the dominant peak frequency with that from neighbouring measurements with more clear peaks. If the central value of the wide peak was comparable, we kept it in the database. For some measurements, we obtained almost flat spectral ratios (Figure 3.4e) with maximum amplitudes smaller than 1.5 Hz. We found no clear peak for this point but it may be correlated with Paleozoic rocks. In Figure 3.4f, two peaks are observed around 1 Hz. The shape of this HVSR curve indicates that the peak is at a similar frequency, but since it is contaminated with artificial noise, it cannot be accurately identified. The amplitudes of the peaks of HVSR are mostly in the range 1–2 Hz in Figure 3.5. Only in a few cases they are larger than 5 Hz.

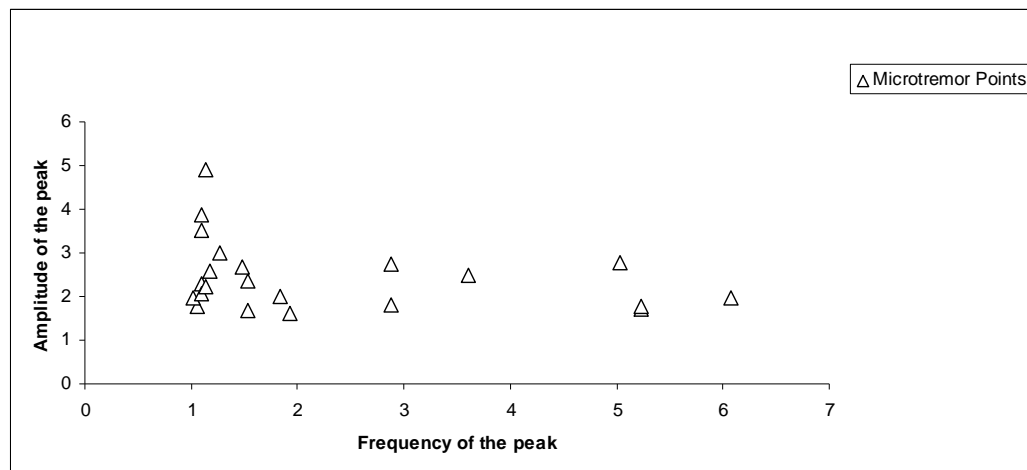


Figure 3.5 Amplitude vs. frequency graph of HVSR peaks

3.5.3 Time-dependent HVSR

The common procedure to compute the HVSR relies on average amplitude spectra of the three components of motion. Some researchers such as Almendros et al., (2004) have suggested that this approach may lead to errors. Perturbations of the wavefield may occur during the recording period and be recorded together with the microtremor data. Usually, these transients are easily identified in the spectra, and the analysis can be performed using only on data windows free of perturbations in order to obtain reliable results. In these cases, artificial peaks appear in the HVSR (Figure 3.4). These peaks affect the spectral ratio and produce inaccurate results.

Because of this problem, time-dependent HVSR has also been used to estimate spectral ratios. This approach consists of compiling HVSR to successive data windows along the traces. This procedure creates several HVSR functions that can be represented a two-dimensional contour plots versus frequency and time. This plot, that is called ratiogram, represents the evolution of the HVSR in the same way that a spectrogram represents the evolution of the spectrum versus frequency and time. (Almendros et al., 2004)

In this study, we selected a window of 25 s and slid it at intervals of 5 s along the traces. This length is suitable for the numerical fast Fourier transform (FFT) algorithm for frequencies larger than 0.5 Hz. For each window we calculated the amplitude spectra of the three components using an FFT algorithm, and smoothed it using a cosine window. Frequency-dependent window lengths have also been used keeping a constant number of cycles (Kind et al., 2005). We computed the HVSR separately for all time intervals and plotted them. An example is as a fuction of time shown in Figure 3.6.

Three component microtremor data was shown in Figure 3.6a. Using the standard technique, average HVSR are computed from individual windows (Figure 3.6b). We observed the presence of a dominant peak at about 1.2 Hz and we can conclude that the site produces amplification for this frequency. Figure 3.6c shows the time-dependent HVSR which is stationary, at least during particular time periods. An average HVSR could be obtained by stacking the HVSRs.

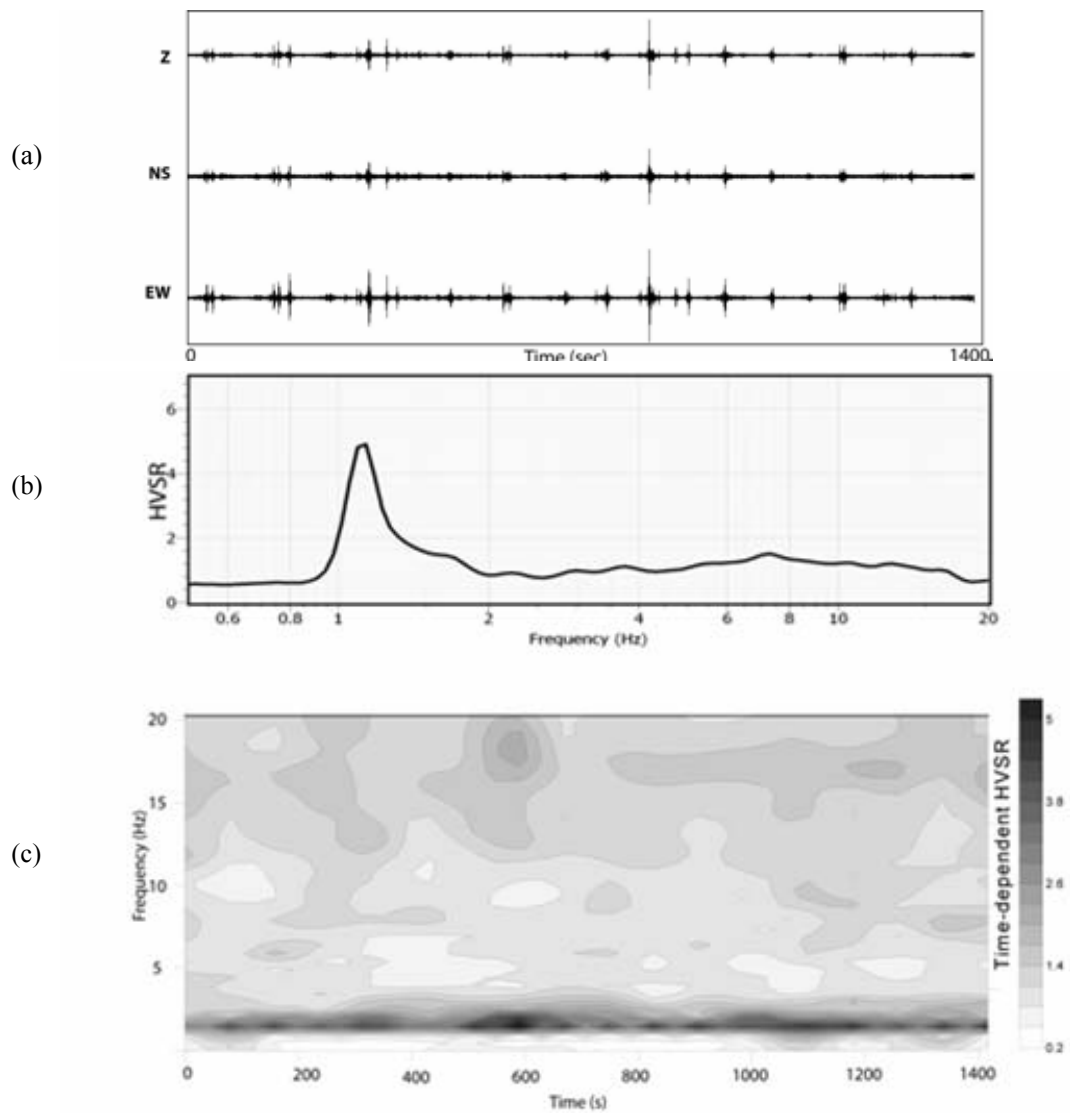


Figure 3.6 Example of the application of the time dependent HVSR method (a) three-component microtremor data (b) average HVSR using standard procedure (c) ratiogram representing the HVSR as a function of frequency and time.

3.6 HVSR Results Using Earthquake Data

Earthquake records from an accelerographic station (Figure 3.2) deployed in the city have been obtained. We used them to compare the results obtained from microtremor survey. A location of the station is given in Table 3.1.

Table 3.1 Coordinates of Station BYT01

Station Coordinates	Altitude (m)	Recorder Type	Recorder Serial Nr.
40.18240N 29.12960E	193	Etna	5035

This station has recorded four shallow earthquakes (depths smaller than 19 km.) with magnitudes (Md) between 3.6 and 5.2. Locations of the events are given in Table 3.2. Spectral ratios have been computed using the HVSR technique (Figure 3.7). We have used events for which the signal to noise level is larger than 3 in the frequency range 0.5-20 Hz. The selected window has duration of 15 second beginning 2-3 sec before S-wave arrival. The analysis included a cosine taper before Fourier transform and smoothing with a factor of 40 using the window by Konno & Ohmachi, 1998.

Table 3.2 Recorded earthquakes in BYT01 (location parameters were taken from AFAD-ERD).

Earthquake Date and Time (GMT)	Earthquake Coordinates	Depth	Magnitude (Md)
20/10/2006	40.2519N-27.9792E	16.7	5.2
24/10/2006	40.4221N-28.9937E	7.9	5.2
25/10/2006	40.3698N-29.0059E	10.7	3.6
19/12/2006	40.3400N-28.3200E	18.5	4.2

A dominant frequency around 5 Hz is observed for events 20061020 and 20061025 in the HVSr results (Figure 3.7). Events 20061024 and 20061219 show a different dominant frequency, between 2 Hz and 4 Hz. The BYT01 station is very close to the microtremor point Nr. 05, and shows similar results with ambient noise measurements.

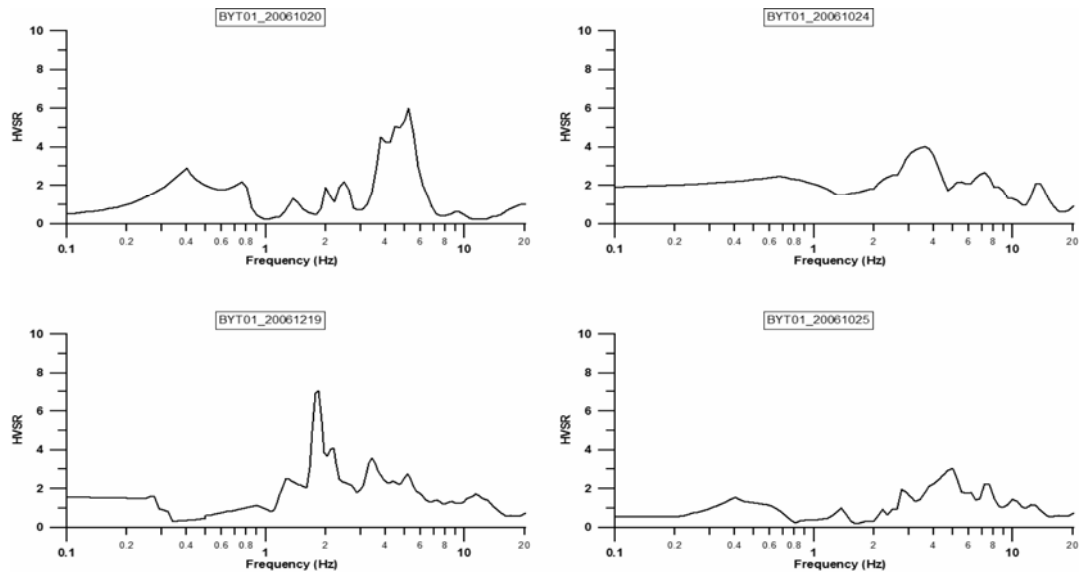


Figure 3.7 The HVSr results of four earthquakes.

3.7 Conclusion and Discussion

The 22 values of dominant frequency and maximum relative amplification (HVSr) were used to draw the contours shown in Figure 3.8. The contours of dominant frequency values coincide with surficial geology (Figure 3.8a), the maximum amplification values vary between 1 and 5 (Figure 3.8b).

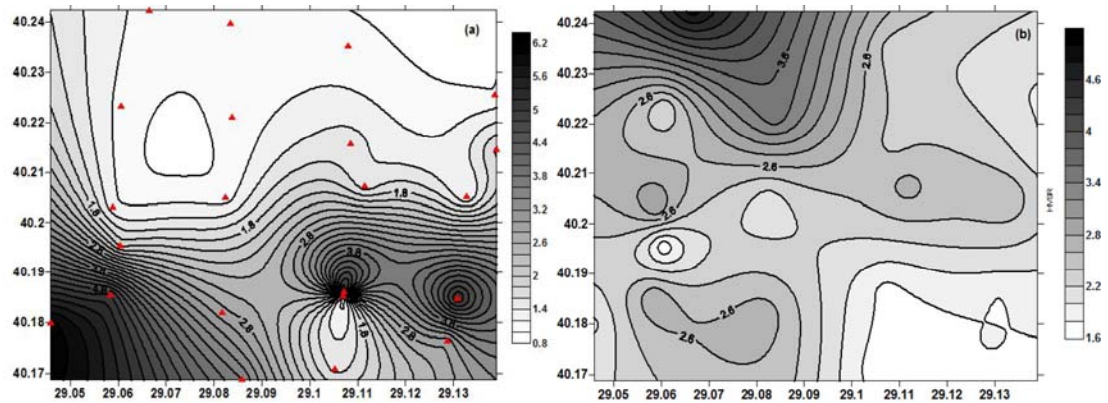


Figure 3.8 (a) Dominant frequency and (b) HVSR map of the study area.

Figure 3.9 shows examples of ratiograms obtained at two different sites. In each case, the top panel shows the three-components of ambient noise: The bottom panel shows the calculated ratiogram and the right panel shows the average HVSR. The gray scale on the right represents the values of the time-dependent HVSR in both ratiograms. In the first case (Figure 3.9a), the average HVSR does not show a dominant frequency. The flat response is seen with an amplification level approximately equal to one. In the second case (Figure 3.9b); a clear dominant frequency of 1.2 Hz appears throughout the duration of the records. Ratiograms like these have been calculated for the entire data set.

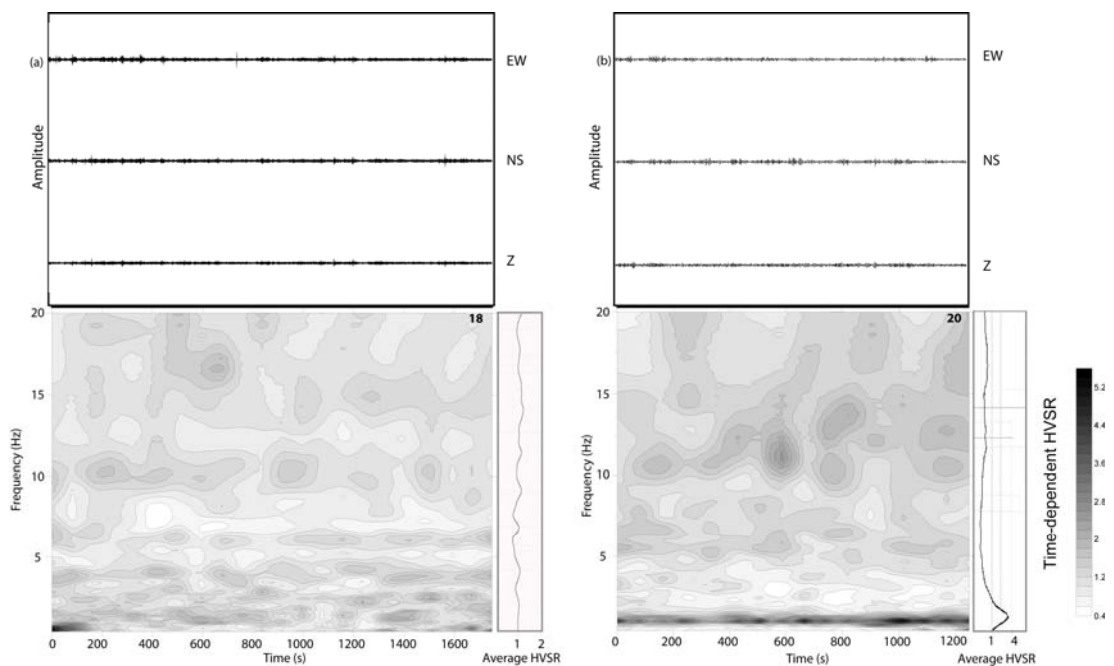


Figure 3.9 Two examples of ratiograms and average HVSRs obtained from microtremors recorded at stations a) 18, and b) 20.

In general, the smaller values of dominant frequency show that (1-2 Hz) correlate with alluvium and Neogene sediments. Peaks at larger frequencies are correlated to Paleozoic and metamorphic rocks. Our measurements show that there are transient zones between different geologic structures (alluvium and Paleozoic rocks).

The map of fundamental soil frequency derived from free-field microtremor measurements should be confirmed by independent information from boreholes, geophysical investigations or earthquake recordings in the future, since the interpretation of microtremors is restricted to identifying the resonance frequency and gives no information on the amplification of seismic ground motion. The HVSR provides an estimate of the bandwidth over which the ground motion is amplified. This is especially important for any microzonation.

The HVSR analysis of four earthquakes and microtremor at 22 points gives similar results: Dominant frequencies and spectral ratios correlate well with geological structures in the Bursa city.

Microtremor measurements at 22 points and analysis of contribute valuable preliminary microzonation and site response information. However a more complete study of city-scale earthquake hazard, it is still necessary. More microtremor points and events are necessary to understand site response in Bursa City.

CHAPTER FOUR

IZMIRNET: A STRONG-MOTION NETWORK IN METROPOLITAN IZMIR, WESTERN ANATOLIA, TURKEY

(PAPER 2)

Orhan Polat ^{1,2}, Ulubey Ceken ³, Tulay Uran ³, Elcin Gok ², Nazan Yilmaz ³, Murat Beyhan ³, Nurcan Koc ³, Berna Arslan ⁴, Doguser Yilmaz ¹, and Mehmet Utku ¹

- ¹ Dokuz Eylul University, Engineering Faculty, Department of Geophysics, Izmir Turkey
- ² Dokuz Eylul University, Earthquake Research and Implementation Center, Izmir, Turkey
- ³ Earthquake Research Department, General Directorate of Disaster Affairs, Ankara, Turkey
- ⁴ Metropolitan Municipality of Izmir, Directorate of Construction Affairs, Izmir, Turkey

Published in Seismological Research Letters

4.1 Introduction

A 16-station strong-motion seismic monitoring network covering metropolitan Izmir and the surrounding region was established in July 2008. The seismic network was installed as a cooperative effort involving the Earthquake Research and Implementation Center (ERIC-DAUM) of Dokuz Eylül University (DEU, Izmir), the Earthquake Research Department (ERD) of the General Directorate of Disaster Affairs (GDDA, Ankara), the Izmir Metropolitan Municipality, and the Ministry of Public Works and Settlement. The project was funded by the Scientific and Technological Research Council of Turkey (TUBITAK) to collect strong-motion data for earthquake hazard assessment studies and to develop a real-time monitoring system in Turkey (Inan et al. 2007) to address public safety issues. The network is critically important to addressing earthquake hazard issues in western Turkey, an area known to have historically damaging earthquakes. Izmir is the third largest city in Turkey in terms of population, industrial density, economic capacity, and contribution to the national economy, and the economic and human consequences of a damaging earthquake in the Izmir area would be significant. A primary goal of this project is to acquire strong ground motion data in order to understand propagation and site response characteristics of the Quaternary and Neogene sediments that underlie the Izmir metropolitan area and are thought to produce large site amplification and seismic hazard (Aydinoglu 2000; Masure et al. 2000). These data will complement laboratory data to characterize the properties of the soft soils underlying the Izmir metropolitan residential area so that engineers and architects can design appropriate earthquake resistant structures for the region. This project is also a first step toward developing a “Rapid Response and Damage Prediction System” for metropolitan Izmir where near real-time strong ground-motion records can be used to compute ground-shaking maps showing the areas most strongly affected by earthquakes.

4.2 Seismotectonic Setting

The tectonic framework of western Anatolia is dominated by crustal extension. The Aegean region to the south of 39.50N extends in a N-S direction with an upper bound rate of 20 mm/y, while the north Anatolian fault zone (NAFZ) and east Anatolian fault (EAF) are characterized by strike-slip deformation (Figure 4.1; see also Jackson and McKenzie 1984; Saroglu et al. 1992). Within this extensional framework, the study area is located at the western termination of the Gediz graben system (GGS), close to the city of Manisa in the north and Doganbey cap (DC) in the south (Pamukcu and Yurdakul 2008; Polat et al. 2008). The 16 stations comprising the IzmirNet are shown in Figure 4.2. Dominant tectonic features in the study area are the Izmir fault (IF); the Orhanli fault zone (OFZ); and the Seferihisar, Urla, Gulbahce, and Karaburun faults (SF, UF, GF and KF, respectively; Ocakoglu et al. 2005; Uzel and Sozbilir 2008). The IF, trending in an E-W direction, is a normal fault bounding the southern Gulf of Izmir. Its activity has been well documented, with the occurrence of strong events including the 688 and 1668 events (both with $I_0 = IX$, Ergin et al. 1967) and the earthquake of 10 July 1688 ($I_0 = X$; Ambraseys and Finkel 1995). The OFZ and SF run between Doganbey Cap and the Izmir Gulf. Here the dominant character of these faults is right-lateral strike-slip (Uzel and Sozbilir 2008). A strong earthquake on 6 November 1992 ($M_w = 6.0$) occurred along this zone, revealing a right-lateral fault plane solution (Tan et al. 2008). The most devastating earthquake along the UF from the historical period is reported on 15 October 1883 ($I_0 = IX$, Ergin et al. 1967). Toward the west, the 17–21 October 2005 ($M_s = 5.9$) earthquake series occurred along the GF and near the KF, at the north of Sigacik Bay. Fault movement of most of the events reveals pure strike-slip faults as evidenced from focal mechanism solutions (Aktar et al. 2007; Benetatos et al. 2006). The region is situated in the first-degree hazard zone in the Official Earthquake Hazard Regionalization Map of Turkey. By using historical (since 5th century B.C.) and instrumental (from 1911 on) data. Papazachos et al. (2004) postulated the possibility of a severe earthquake with magnitude larger than 6.4 in the study area. Koravos et al. (2003) proposed a maximum earthquake magnitude 7.2 ± 0.1 near KF by using a combination of instrumental, historical, and geodetic data. Since

devastating earthquakes occur relatively infrequently in the region, this should be treated with caution. A missed opportunity for proper recording of the ground motions these events produce represents the loss of important and irreplaceable scientific data in metropolitan Izmir and the surrounding area. High-density strong-motion networks are justified because if effects of these rare occurrences are recorded, they could provide valuable insight to engineers and seismologists about what to expect in a future damaging earthquake.

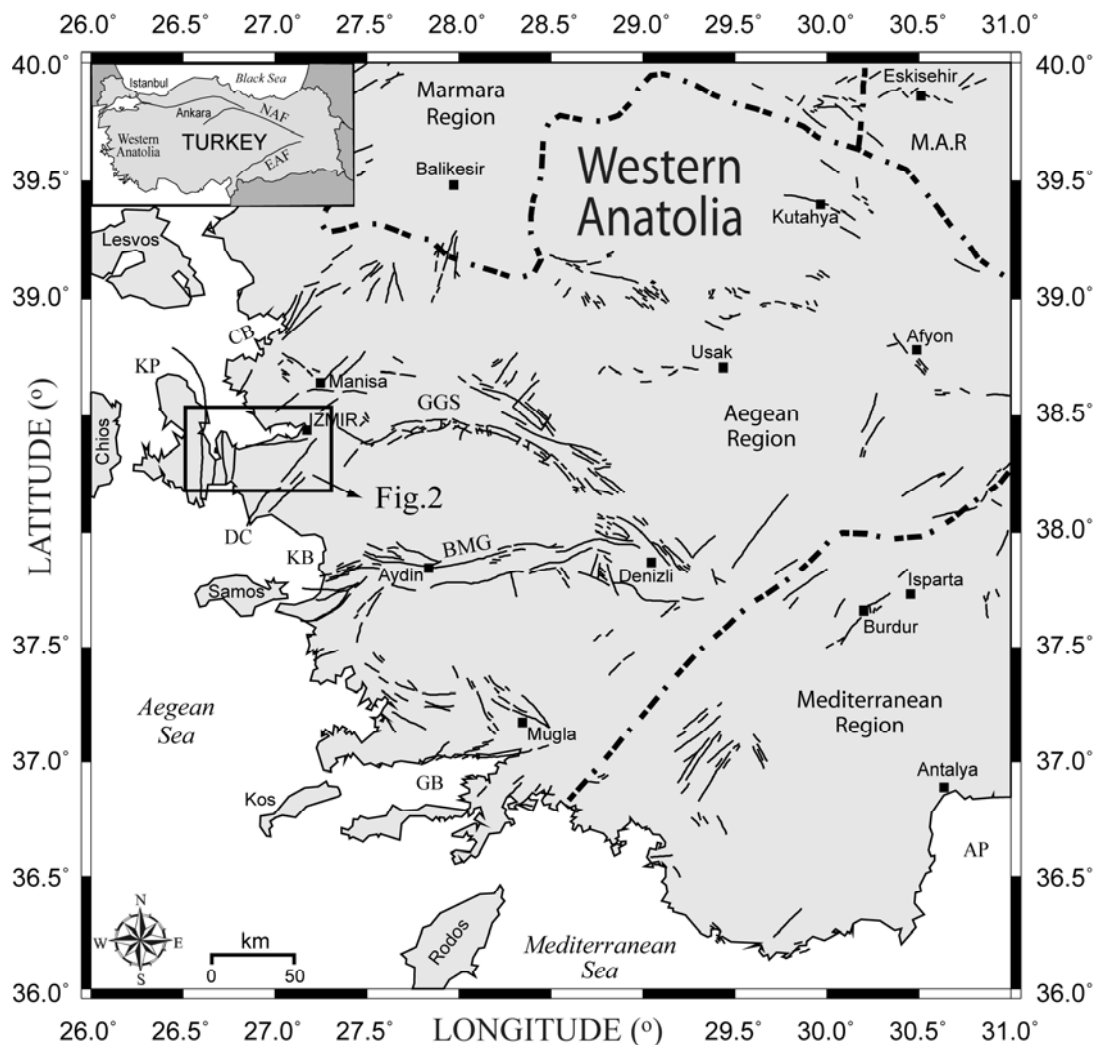


Figure 4.1 Principal tectonic features of the Aegean region of Turkey, western Anatolia (compiled from Saroglu et al. 1992). GA—Gulf of Antalya, BMG—Buyuk Menderes graben, CB—Candarli Bay, DC—Doganbey cap, GB—Gokova Bay, GGS—Gediz graben system, KP—Karaburun Peninsula, KB—Kusadasi Bay. Inset Map: NAF—North Anatolian fault, EAF—East Anatolian fault.

4.3 Description of IzmirNET

The main conceptual aims of the new network are: 1) adequate coverage of the various sedimentary environments in Izmir and surroundings, 2) station locations close to potential fault planes, 3) free-field station installations wherever logistically possible, 4) remote accessibility to the data, and 5) continuous recording (as opposed to triggered recording) so that relatively small events are recorded at all stations. The IzmirNet covers an area of approximately 50 km × 20 km around the Gulf of Izmir and is deployed over the active fault system. A list of the basic parameters for all stations is given in Table 4.1.

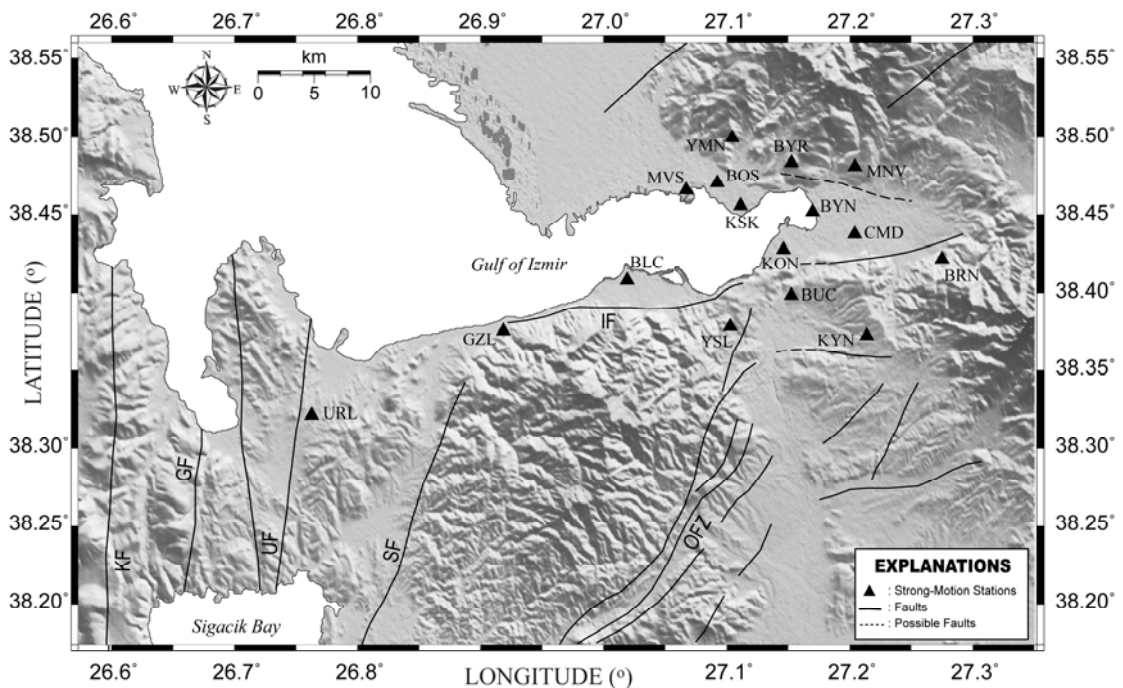


Figure 4.2 Main tectonic elements near metropolitan Izmir, Aegean region of Turkey. Tectonic features are mainly compiled from Ocakoglu et al. (2005) and Uzel and Sozibilir (2008). KF—Karaburun fault, GF—Gulbahce fault, IF—Izmir fault, SF—Seferihisar fault, OFZ—Orhanli fault zone, UF—Urla fault.

4.3.1 Station Hardware

All stations are free-field and equipped with three-component CMG-5TD accelerographs (Guralp Systems, Reading, UK) with CMG-5T force balance accelerometer and built-in 24-bit AD converter for data acquisition. The system contains two supply boxes for communication and uninterruptible power and also a serial modem (Figure 4.3). A complete health status is available that assists in the diagnosis of system component failure or malfunction.

Table 4.1 Station parameters of the IzmirNet strong-motion network

Code	Lon. deg E	Lat. deg N	Elev. (m)	Location	Environment	Installation Date *
BLC	27.04300	38.40900	3	Balçova	Institute of Marine Sciences and	6/22/2008
BRN	27.25630	38.42130	76	Bornova	FIGSAN Spicery Factory	7/16/2008
BUC	27.15160	38.40090	79	Buca	Zübeyde Hanım Nursing Home	6/22/2008
BYN	27.16710	38.45840	2	Bayındırlık	Province Directorate of	6/21/2008
BYR	27.15810	38.47620	197	Bayraklı	Local Health Home of Karşıyaka	7/16/2008
BOS	27.09404	38.46498	4	Bostanlı	Mehmet-Seniye Özbey Primary	7/17/2008
GZL	26.89077	38.37066	17	Güzelbahçe	Municipality Sport Hall	6/22/2008
KYN	27.19364	38.37560	136	Kaynaklar	Main University Campus of DEU	7/16/2008
KON	27.14350	38.43120	7	Konak	Izmir Fair	7/17/2008
KSK	27.11124	38.45250	10	Karşıyaka	Province Directorate of Forest	6/21/2008
MNV	27.21110	38.47800	184	Manavkuyu	Atatürk Public Library	6/21/2008
MVS	27.07720	38.46780	1	Mavişehir	Deniz-Kent Municipality	7/17/2008
CMD	27.19870	38.43570	68	Çamdibi	21st Family Health Center	7/17/2008
URL	26.77063	38.32823	76	Urla	Municipality Sports Hall	6/22/2008
YMN	27.10730	38.49690	64	Yamanlar	Müyesser Turfan Nursing Home	6/21/2008
YSL	27.10840	38.37230	106	Yeşilyurt	Naci Şensoy high school	6/21/2008
* : Connection is DSL (Digital Subscriber Line), DEU: Dokuz Eylül University of Izmir						



Figure 4.3 Typical installation of IzmirNet strong-motion network. (A) Recording stations are housed in the standardized small galvanized hut as shown at KSK location. (B) Inner view of a container with a typical installation of free-field station. CMG-5TD built-in system is mounted on a prefabricated concrete block.

An asymmetric digital subscriber line (ADSL) system controls the stations and downloads real-time continuous data. It runs SCREAM! data acquisition software developed by Guralp Systems for the Windows and Linux platforms. Continuous waveform data, sampled at 100 sps (samples per second), are stored in Guralp compressed format (GCF) file format containing time and station information as well. This format is compatible and convertible with several software packages including SAC (Goldstein and Snoko 2005) and SEISAN (Haskov and Ottemoeller 1999) seismic analysis software. The IzmirNet stations use the ADSL technology to download and store data in the central processing laboratories in Izmir and Ankara.

4.3.2 Site Characterization

Earthquake resistant but economical structures can be designed and constructed only if the nature of the ground motion is understood. This understanding can only come from direct measurement and subsequent analysis of the strong ground motion recorded during actual earthquakes. Many studies have demonstrated the ability of geologic conditions to alter observed seismic motions and to affect the amount of

damage. Site amplification is considerably effective on the building response especially for the near field and/or large scale earthquakes.

Izmir city and metropolitan area is located very close to active faults and is sited on thick Quaternary–Neogene-age sediments. Since unconsolidated deposits in the Izmir basin may significantly change the propagation of ground motions to the surface, the assessment of seismic hazard for the Izmir region is an important issue. The IzmirNet strong-motion seismic array has been established to calculate the site response characteristics in the region, which are of interest in the engineering seismology and earthquake engineering disciplines. We performed borehole drilling, microtremor, electrical resistivity, and seismic refraction techniques, as well as multichannel analysis of surface waves (MASW) measurements in the IzmirNet stations in order to determine the geological, geophysical, and geotechnical site characterization as a function of depth (up to 30 m). A sample is shown in Figure 4.4. The data obtained by the application of these techniques will be input to make a reliable probabilistic seismic hazard analysis for metropolitan Izmir and its vicinity.

The acceleration recorders were installed mainly at sites where thick Quaternary and Neogene formations are exposed. Stations are mainly distributed on these units in the Izmir Bay area. They are in Bornova basin at the east, the Karsiyaka-Mavisehir area at the north, and between Balçova and Urla at the south. Quaternary sediments and cretaceous flysch are the main units near the Balçova area, with a sedimentary fill up to 180 m. Here, the Izmir fault plays an important role in the development of one of the most important geothermal areas in western Anatolia. Some stations are also near Buca settlement toward the south extremity of the city, where geological units generally exhibit limestone and marl.

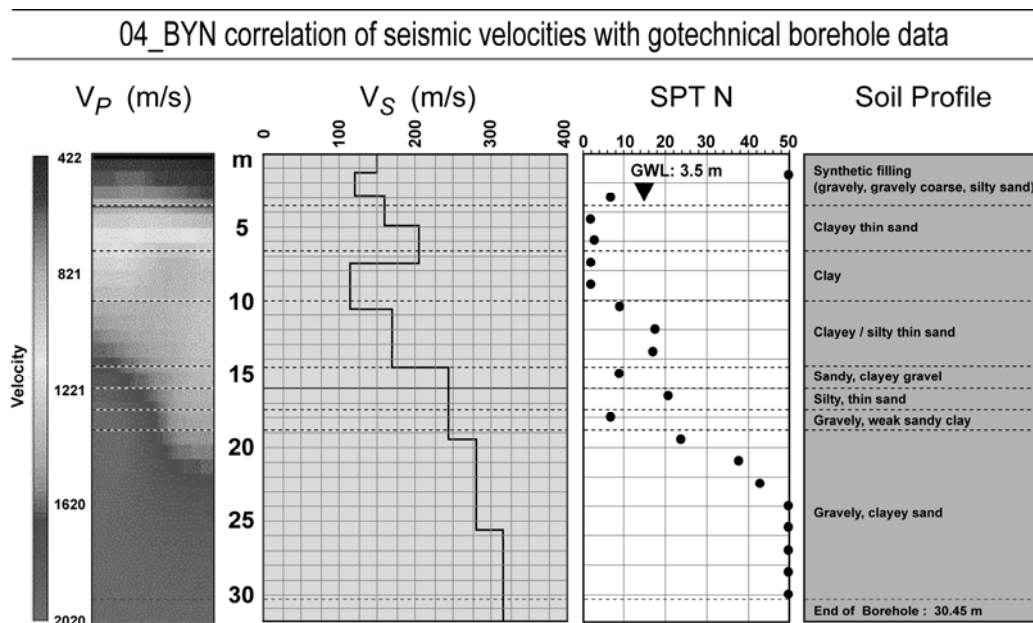


Figure 4.4 Local soil information for station 04_BYN (modified from METU 2007).

4.4 Sample Data

Figure 4.5 shows an example from time and frequency domain analysis for the earthquake ($M_d = 3.0$) that occurred on 10 August 2008. A horizontal-component accelerogram (SH) was used to analyze the site and source characteristics of the selected event. We plan to compute source size, spectral level (W_0), seismic moment, stress drop, and validity of corner and cut-off frequency (f_{max}), with a discussion of the effect of various attenuation models on the source spectra. Two horizontal motions are combined in the Z-component to infer the particle motion characteristics. This study procedure allows a detailed analysis of frequencies at which the ground motion is the largest and most polarized. Particle motion in the horizontal plane represents an ellipse, and it is a very important measure of horizontal shaking that provides a complete description of the magnitude of motions. Here, we estimated mainly north and east directions for the KSK and KYN stations, respectively, for the selected event of 10 August 2008. Figure 4.6 shows the data quality and selected earthquakes recorded by IzmirNet. The three-component event that occurred on 3 September 2008 ($M_D = 2.8$) has a 10-km hypocentral distance. The earthquake of 10 August 2008 ($M_D = 3.0$) was recorded by at least 13 stations. These data examples present local microearthquakes with a good S/N ratio. Since all

stations are remotely accessible, we plan to use the data to perform a rapid calculation of intensities.

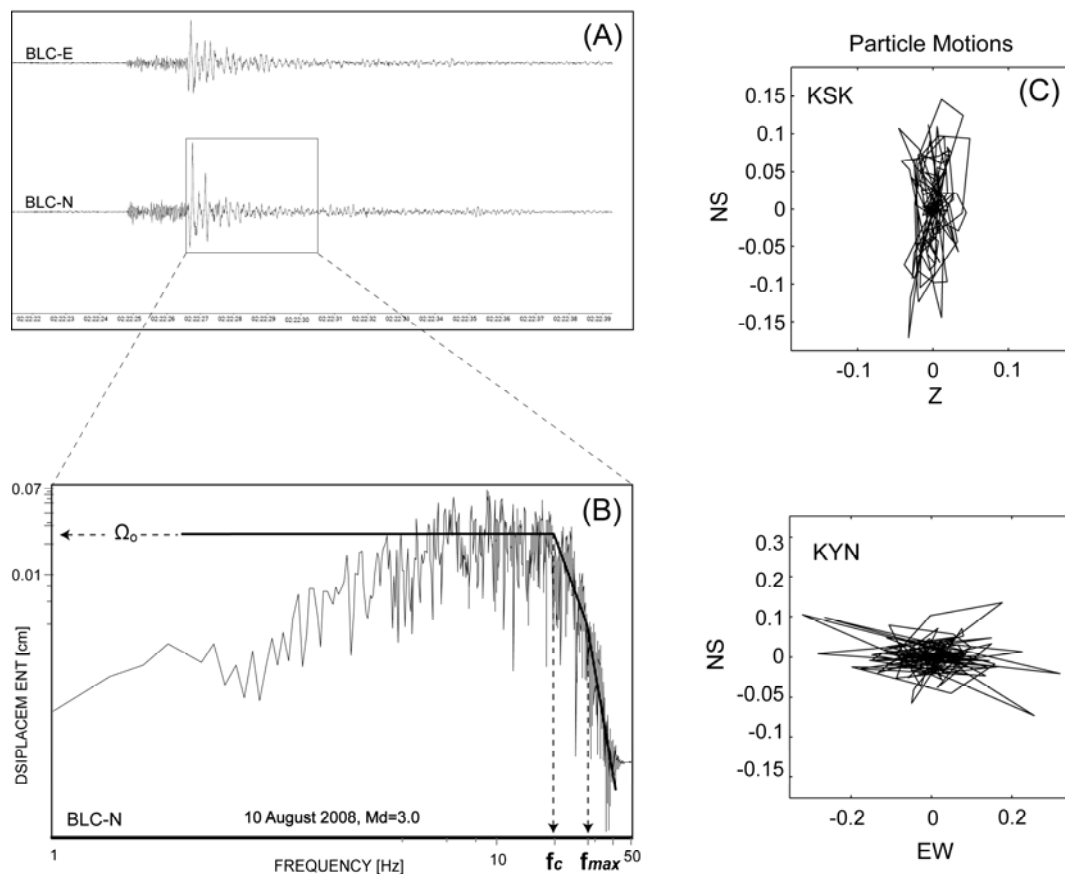


Figure 4.5 Sample analysis of the event of 10 August 2008 ($M_d = 3.0$). (A) Two horizontal components of the BLC station in time domain. (B) Displacement spectra of the event showing corner frequency (f_c), f_{max} (Hanks 1982), and spectral level (Ω_o) to compute source parameters for Brune's (1970) model. (C) Examples of the particle motion analysis at KSK and KYN stations in the plane NS-Z and EW-Z.

4.5 Future Plans

Due to its high density, wide dynamic range (flat response from DC to 50 Hz), and advanced data-acquisition and datatransmission technologies, IzmirNet will become the core infrastructure of a prototype "Rapid Response and Damage Prediction System" in metropolitan Izmir. In the near future, it will be devoted to real-time estimation of magnitude and earthquake location to calculate rapid ground-shaking maps for the whole of the city.

The principal aim of the network is to address site-response issues in Izmir. But IzmirNet will also contribute to emergency response in the near future by increasing the number of stations in the region and connecting to a broader system for reporting earthquake locations and magnitudes and computing the shakemaps. The information provided by the network during the first few seconds of a potentially damaging seismic event will be used to activate several types of security measures, such as the shutdown of critical systems, i.e., gas or oil pipelines or water, sewer, and electricity lines, etc. Hence, the IzmirNet is closely concerned with the lifeline systems and public social life. The network will provide precise peak ground acceleration (PGA) distribution, which is one of the most important parameters when projecting loss estimates as the result of a potential strong earthquake. In the near future, ground-shaking maps will also play an important role in reducing the negative impact of destructive earthquakes in urban areas. This local array will be used to fully exploit the PGA distribution during the earthquake and exhibit critical settlement areas of the city (Ulusay et al. 2004).

4.6 Conclusions

The IzmirNet strong-motion network has been fully operational since August 2008. It promises to be useful for research and implementation in engineering and strong-motion seismology. The array is already recording small-scale earthquakes in the Gulf of Izmir and the surrounding area (Figure 4.6). Location parameters are given in Table 2. Most of the events are low magnitude, but they lay the groundwork for studying a future large earthquake and predicting its ground motion. To make accurate epicenter locations and to produce more reliable ground-shaking maps after a strong earthquake in or around Izmir, we plan to install additional recorders near the Gulf of Izmir in locations north of Karaburun Peninsula (to the west), the western half of the Cigli and Mavisehir districts (in the north), and near the Gaziemir district (to the south). These additional stations will be equipped with the same instruments and communication protocols to retrieve peak ground parameters.

IzmirNet is part of the national strong-motion network of the GDDA (Ankara) that is already operating and includes several local arrays in western Anatolia. The long-sought goal of the GDDA is to increase the total number of accelerographs in Turkey (Gulkan et al. 2007). Currently, the national network consists of about 220 strong-motion recorders; the local IzmirNet array, a joint operation between ERIC in Izmir and ERD in Ankara, will help reduce the chances of missing important seismological data if a moderate-to-large earthquake were to hit the Aegean region and western Anatolia.

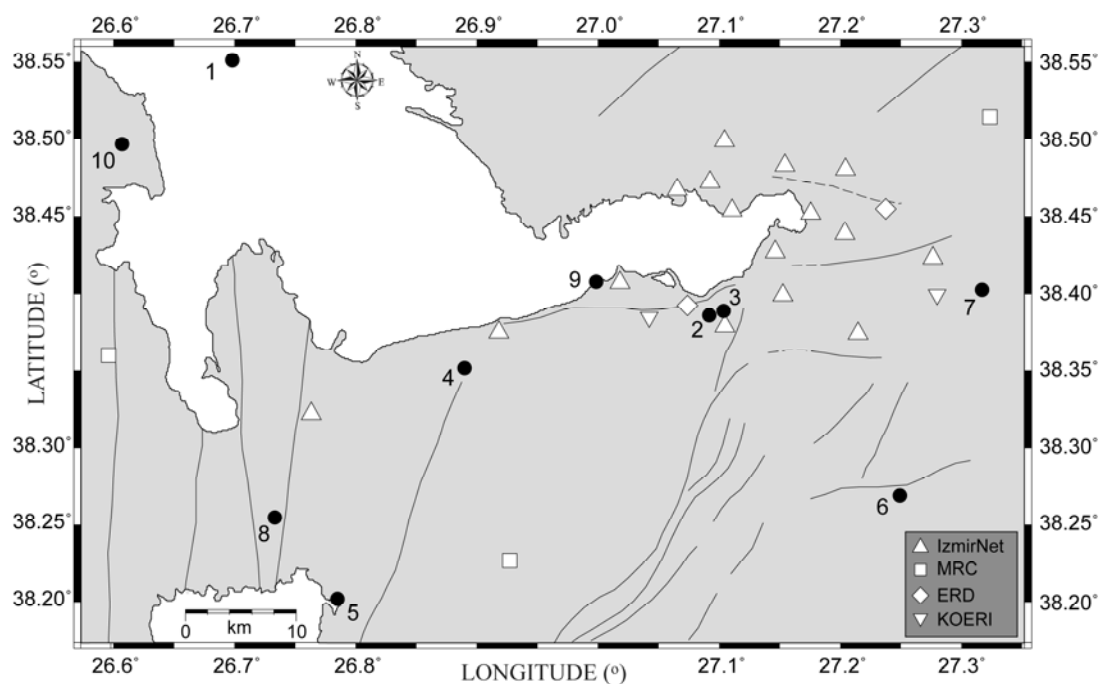


Figure 4.6 Recorded earthquakes by IzmirNet strong-motion network. See Table 2 for earthquake location parameters. MRC: Local stations of TUBITAK Marmara Research Center, Gebze, Kocaeli; ERD: National stations of Earthquake Research Department of GDDA, Ankara; KOERI: National stations of Kandilli Observatory and Earthquake Research Institute, Istanbul.

Table 4.2 Selected earthquake locations recorded by IzmirNet strong-motion network

Event No	Date	Time	Epical Coordinates		Md	Depth (km)
			N (o)	E (o)		
1	04.08.2008	23:07	38.5552	26.6998	2.8	7.0
2	10.08.2008	02:22	38.3805	27.0913	3.0	10.6
3	10.08.2008	02:55	38.3803	27.0858	2.7	7.0
4	19.08.2008	07:46	38.3520	26.8897	2.6	7.0
5	22.08.2008	02:10	38.2025	26.7848	2.8	7.0
6	26.08.2008	04:17	38.2693	27.2493	2.8	7.3
7	27.08.2008	09:36	38.4032	27.3170	2.6	7.0
8	30.08.2008	18:10	38.2552	26.7330	2.7	12.5
9	03.09.2008	11:58	38.4080	27.0125	2.8	7.0
10	18.09.2008	18:36	38.4973	26.6067	3.1	28.7

4.7 Acknowledgements

The IzmirNet strong-motion network was funded by the TUBITAK Scientific and Technological Research Council of the Turkish Republic under the category of the Public Research Grant Committee (KAMAG) of Support Program for Research Projects of Public Institutions (1007). This contribution is from Seismology Work Group-1 of the Izmir Earthquake Project, which is financially supported by TUBITAK under the project number KAMAG-106G159. This study is a part of the PhD thesis of Elcin Gok. The authors acknowledge an anonymous reviewer for constructive comments and wish to thank our project consultants (Professor Resat Ulusay and Assoc. Professors Esref Yalcinkaya, Oguz Ozel, and Ahmet Yakut) for their helpful advice in finalizing the site selection of the strong-motion stations. We also thank the staff of geophysicists, geologists, and civil engineers of Dokuz Eylül University (Izmir) and the Earthquake Research Department (Ankara) for their help during the strong-motion station studies. We wish to acknowledge the Governorship of Izmir, mayors of metropolitan Izmir and Karsiyaka municipalities, and also FIGSAN Company, Izmir. We have received enormous support and great help from Ismail Asi, Oksan Mersin, Oznur Zorlu, Latif Bilgin, Mete Mirzaoglu, Naki Hozer, Kamuran Turkun, and Rafael Benveniste. Numerous individuals have been of great help during our bureaucratic travails and station installations. We are grateful for their encouragement. Because we are afraid that a list may leave someone out, we thank them very much as a group.

CHAPTER FIVE

SEISMIC ACTIVITY OF IZMIR AND SURROUNDINGS

Active tectonics of Izmir and its vicinity have been separated into two parts regarding the study area: the first part is related to the regional tectonics, and the second part consists of local tectonics.

5.1 Regional Tectonics in the Western Anatolia

Western Anatolia is one of the most seismically active and expeditiously extending regions in the world (Bozkurt, 2001). The large-scale deformation in the Western Anatolia is dominated by the collision of the African and Arabian plates with Eurasia: the continental collision between northwestern Greece and Albania with the Apulia- Adriatic platform and the Hellenic subduction zone in the south (Taymaz et al., 1991). The rates of the movement between the African and Arabian plates with respect to stable Eurasia are of 10 mm/y towards northeast and 18-25 mm/y towards northwest (McClusky et al., 2000). The results of these collisions are deformation of the Bitlis Zagros Suture Zone in the east and the Aegean and Cyprean Arc Zones in the west (Figure 5.1). The collision of the Arabian plate with the Eurasian plate causes a westward migration of the Anatolian block from the Karliova (K) in the east to the Aegean Sea in the west. The westward motion of the Anatolian plate is accommodated by the North and East Anatolian Fault zones (NAF and EAF). These tectonics are at the origin of four different neotectonic provinces in Turkey. They are the North Anatolian Province, Central Anatolian “Ova” Province, East Anatolian Contractional Province and West Anatolian Extensional Province (Şengör et al., 1985; Bozkurt, 2001) (Figure 5.1). The Aegean Region is extending in an N-S direction at a rate of approximately 30-40 mm / year. (Oral et al., 1995; Le Pichon et al., 1995)

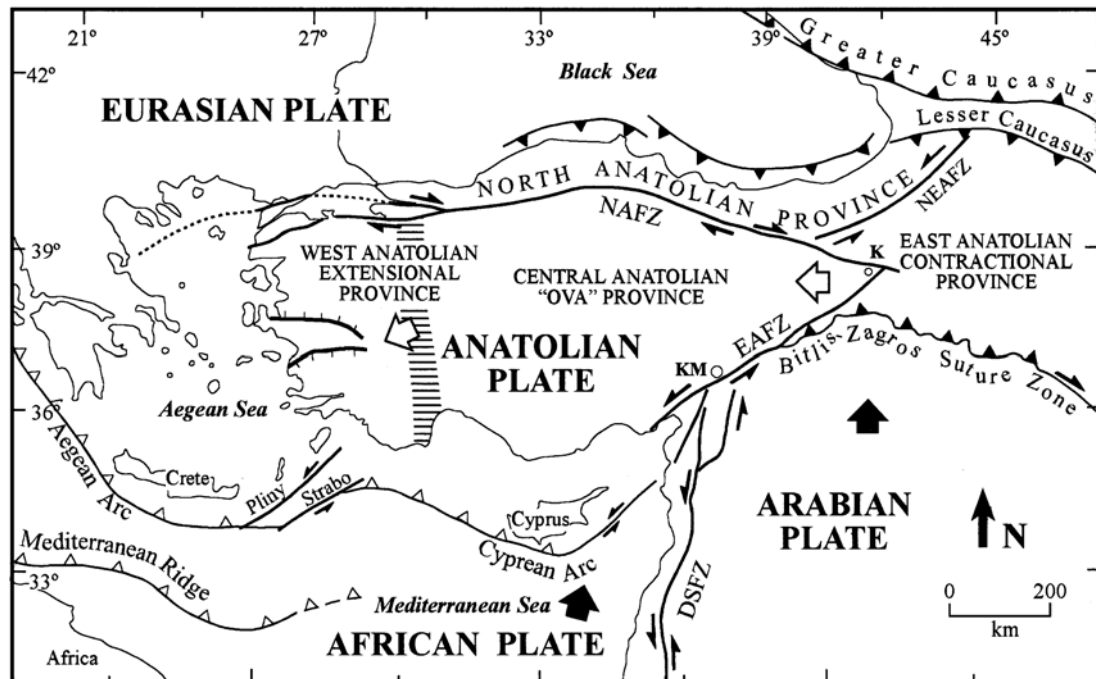


Figure 5.1 Tectonic map of Turkey showing major neotectonic structures and neotectonic provinces compiled from Sengör et al., 1985; Barka, 1992. K – Karlıova, KM – Kahramanmaraş, DSFZ – Dead Sea Fault Zone, EAFZ – East Anatolian Fault Zone, NAFZ – North Anatolian Fault Zone, NEAFZ – Northeast Anatolian Fault Zone.

The westward migration of the Anatolian block is accommodated mainly along the North Anatolian Fault zone, and this movement is continued into the North Aegean Sea. The extension observed on both sides of the Aegean Sea is due to the subduction of the African plate along the Hellenic Arc and the associated extension of the overriding plate. The extension of the Aegean region in Turkey is accommodated by large, approximately east-west trending normal fault systems like Gediz Graben, Büyük Menderes Graben and Küçük Menderes Graben (Figure 5.2). The orientation of the faults is more west-northwest in the mainland of Greece and more east-northeast in western Turkey. Several studies have suggested that when the central Anatolian block moves westwards it has a counter-clockwise rotation at the westernmost part of Turkey and parts of the eastern Aegean area rotate counter-clockwise to have a more southward direction with respect to a fixed Eurasian plate (Westaway, 1990).

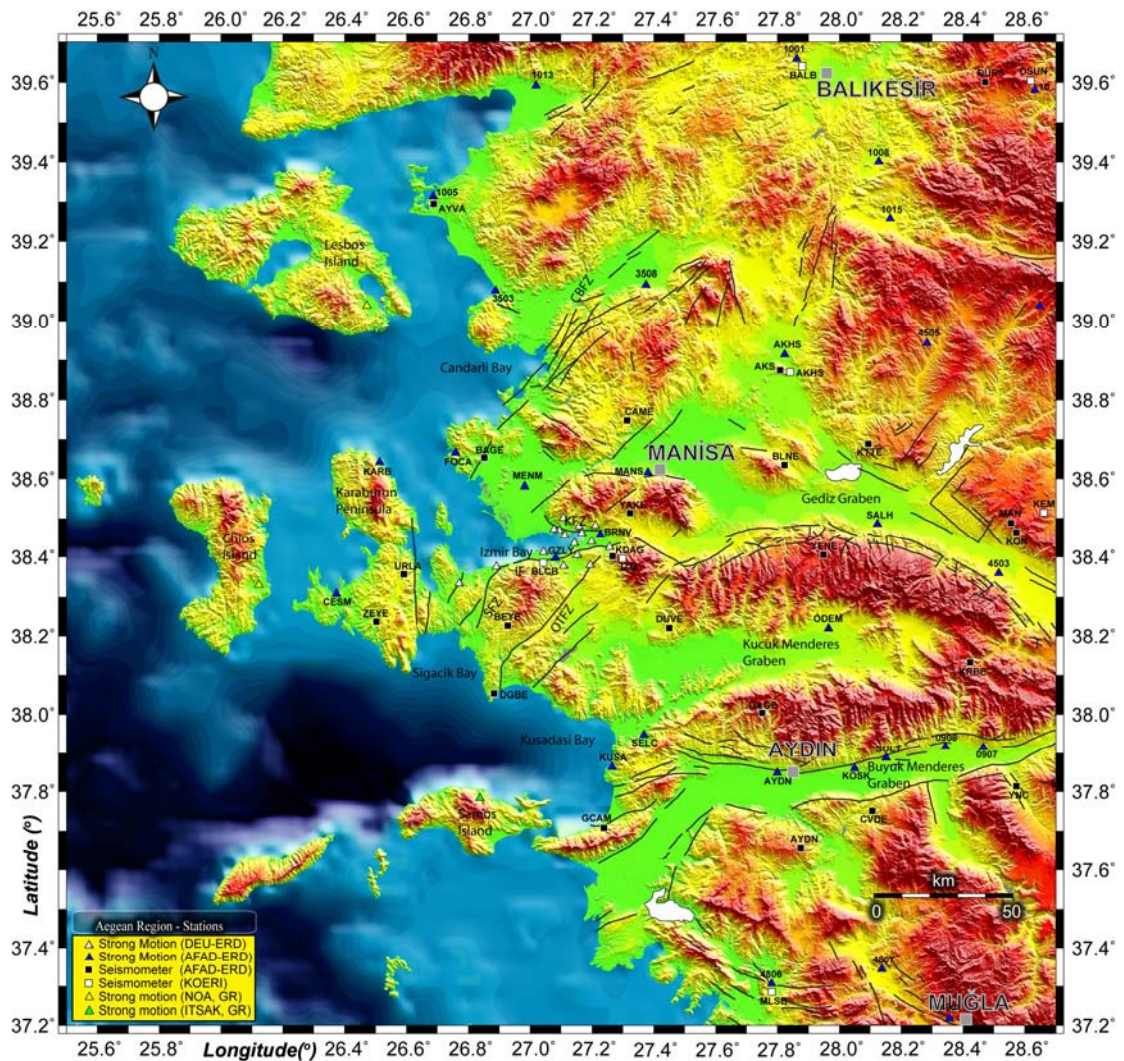


Figure 5.2 Active faults and grabens in the Aegean region

Western Anatolia also has some NE–SW-trending strike-slip fault zones, such as Orhanlı Tuzla Fault Zone (OTFZ) and Canderlı–Bergama Fault Zone (CBFZ; Saroglu et al., 1992; Emre & Barka, 2000; Genc et al., 2001). Most researchers have noticed that these strike-slip faults accommodate local relative motions, between adjacent normal fault segments (e.g., Kaya, 1979; Sengor et al., 1985; Genc et al., 2001). In Western Anatolia, basins are generally bounded by NE–SW-trending strike-slip faults and E–W-trending normal faults oriented obliquely to the strike-slip faults (Uzel & Sözbilir 2005a, 2005b).

Because of the high seismicity level of the Aegean Region of Turkey, many institutes have installed seismometers to monitor seismic activity. In Figure 5.2,

white squares represent a few seismometers from Bogazici University Kandilli Observatory and Earthquake Research Institute (KOERI), dark squares indicate the location of seismographs belonging to Republic of Turkey Prime Ministry Disaster and Emergency Management Presidency Earthquake Department (AFAD-ERD) and blue triangles show stations operated by the Strong Ground Motion Working Group of the AFAD-ERD. IzmirNET stations are shown with white triangles.

5.2 The seismicity of Western Anatolia

Tectonic deformation in Western Anatolia produces high seismic activity. During historical times, Izmir and its surroundings have experienced several destructive earthquakes. The historical events listed in Table 5.1 indicate significant historical seismicity in both the Izmir and north-east section of the OTFZ as seen in Figure 5.3. These two faults are the most active ones in the area, and are also the ones producing the largest intensities in Izmir. The latest large earthquake with epicenter near Izmir occurred in 1778 with a maximum intensity of IX following two earlier events occurring in 1688 and 1723. During the earthquake in 1688 ($M=6.8$) it was observed that the city center of Izmir, located on the hanging wall block of the Izmir fault, had subsided 60 cm (Papazachos et al., 1997; Papazachos & Papazachou, 1997; and Ambraseys & Finkel, 1995).

Table 5.1 Historical earthquakes parameters of Western Anatolia (Papazachos et al., 1997; Papazachos & Papazachou, 1997; and Ambraseys & Finkel, 1995).

Year	Latitude	Longitude	Magnitude	Intensity	Region
47	37.84	27.16	6.9	VIII	Samos
178	38.3	27.1	6.5	VIII	Izmir
688	38.33	27.12	7.5	IX	Izmir
1039	38.4	27.3	6.8	VIII	Izmir
1056	38.32	27.31	7.5	VIII	Izmir
1625	39.2	27.8	7.0	VII	Manisa
1654	38.5	27.1	6.4	VIII	Izmir
1674	38.4	26.3	6.2	VII	Chios
1680	38.4	27.2	6.2	VII	Izmir
1688	38.38	27.17	6.8	X	Izmir
1690	38.6	27.4	6.4	VII	Izmir
1702	37.7	29.1	7	X	Denizli
1723	38.4	27.0	6.4	VII	Izmir
1739	38.4	26.9	6.8	IX	Foca
1772	38.8	26.7	6.4	VIII	Foca
1778	38.4	26.8	6.4	IX	Izmir
1845	38.6	27.5	6.7	IX	Manisa
1845	39.1	26.3	6.7	X	Lesbos
1865	39.4	26.2	6.2	IX	Lesbos
1865	37.7	27.0	6	VII	Samos
1867	39.25	26.21	6.8	X	Lesbos
1868	37.6	26.9	6	VII	Samos
1869	36.98	28.32	6.8	IX	SW.Turkey
1873	37.8	27.1	6.5	VII	Samos
1880	38.5	27.2	6.7	IX	W.Turkey
1883	38.3	26.6	6.8	IX	Cesme
1889	39.2	25.9	6.8	IX	Lesbos
1904	37.66	26.93	6.8	VIII	Samos

There has also been historical seismic activity at the north, around Lesbos Island, and west of Samos Island on the NE-SW direction. These earthquakes caused significant destruction in Izmir (Papazachos et al., 1997; Papazachos & Papazachou, 1997; and Ambraseys & Finkel, 1995).

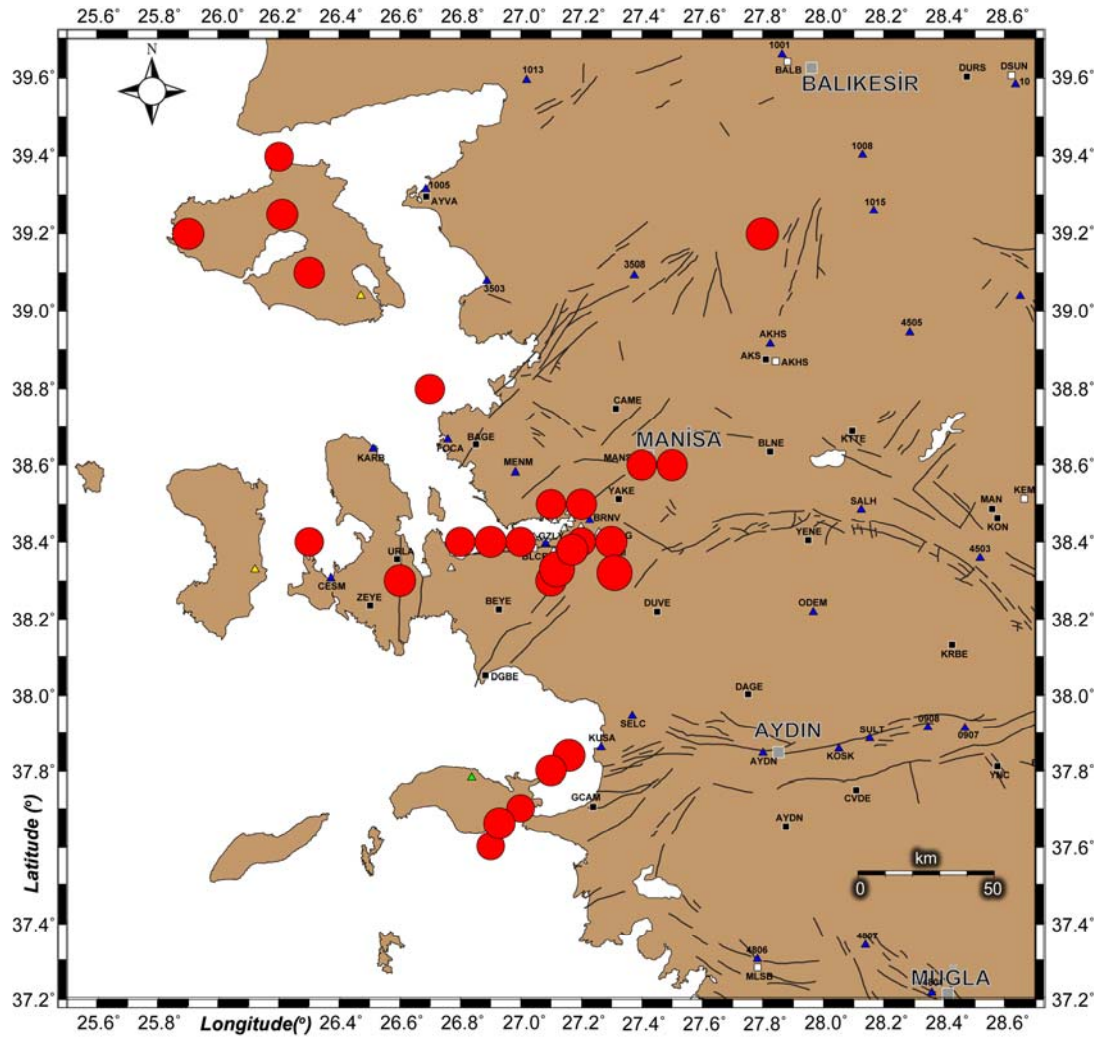


Figure 5.3 Destructive earthquakes in the West Anatolia, during the historical periods (see table 5.1).

Aegean Region of Turkey shows high seismic activity during the instrumental periods as seen in Figure 5.4. Four strong earthquakes occurred around Izmir. In 1928, Torbalı earthquake ($M=6.5$; Salomon-Calvi & Kleinsorge, 1940), the 1949 Karaburun earthquake ($M=6.6$; Pinar, 1950, Jackson & McKenzie 1984), the 1992 Seferihisar earthquake ($M=6.0$; Türkelli et al., 1994; Pinar, 1998) and the 2005 Sigacik Gulf earthquake ($M=5.9$). All of them affected Izmir. The Seferihisar earthquake in 2003 ($M=5.7$) caused a small amount damage in the city.

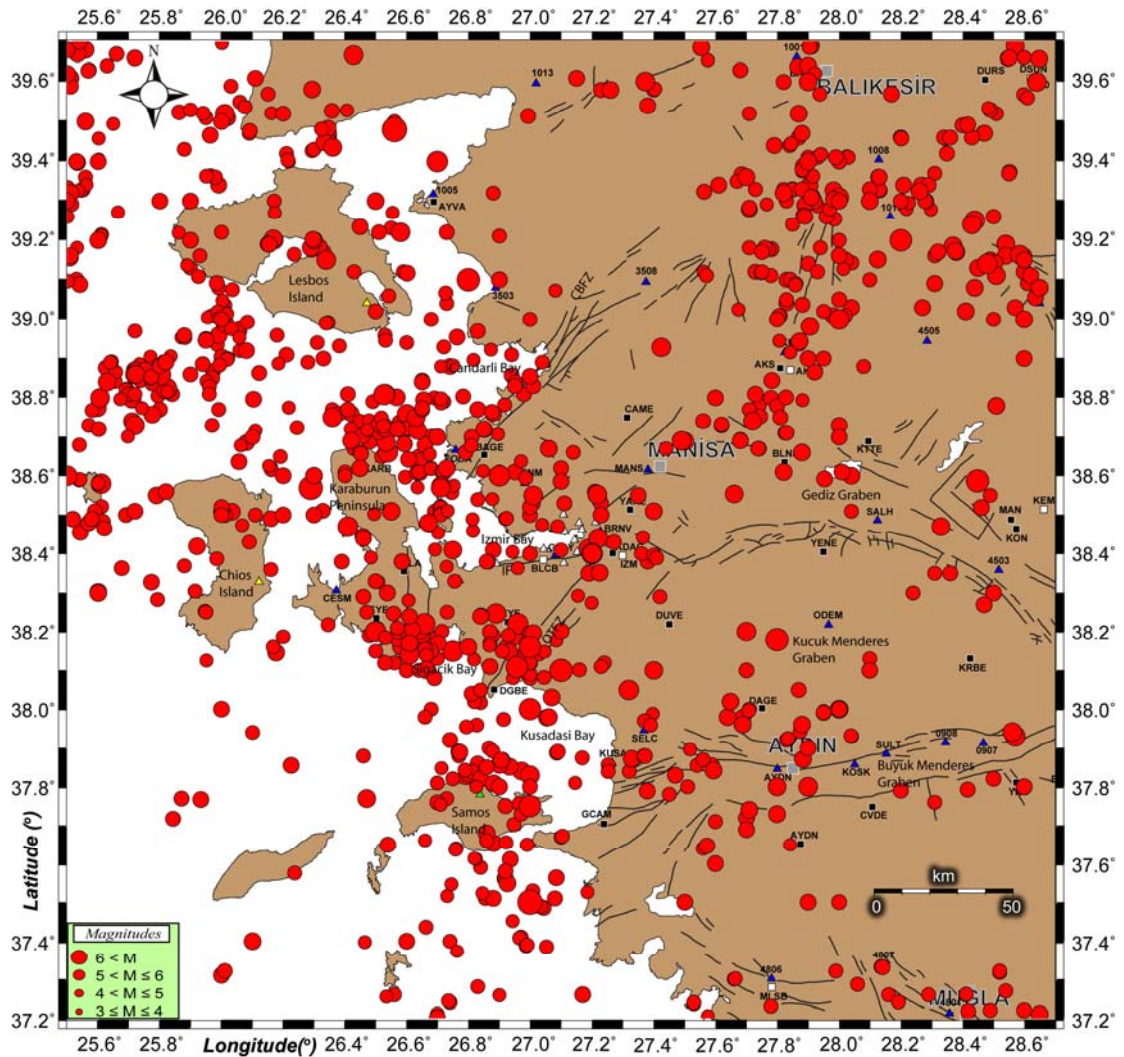


Figure 5.4 Seismicity of the Aegean Region of Turkey between 1900 and 2011 (www.deprem.gov.tr).

Instrumental seismicity shows some swarms and epicenter alignments in the Aegean region of Turkey (Figure 5.4). Three swarms are located around Izmir Bay. These are the Sigacik Bay swarm at the SW of the Izmir Bay, the OTFZ seismicity at the south of the gulf of Izmir and the Karaburun seismic zone at the north of the Karaburun Peninsula which is aligned on the NW-SE direction along the outer part of the Izmir Bay. Linear distribution of seismicity is present on the south of CBFZ following the coastal area of Candarli Bay. There is also significant seismic activity SW of Lesbos Island aligned on a SW-NE direction. We also observed a swarm Samos Island located mainly North and East of the island. No seismicity is observed along some large geologic structures such as the Buyuk and Kucuk Menderes and

Gediz Grabens. Only scattered seismic activity is observed in that area. The region, between Manisa and Balikesir shows diffused seismic activity.

Seismic activity around Sigacik Bay which implies high risk for Izmir city was reported as L-type swarm (Aktar et al., 2007; Benetatos et al., 2006). Recently, in 2005 some seismic activity ($M \geq 3.2$) was observed in the Gulf of Sigacik from 17 to 31 October. Two earthquakes with magnitude of $M_s=5.9$ took occurred.

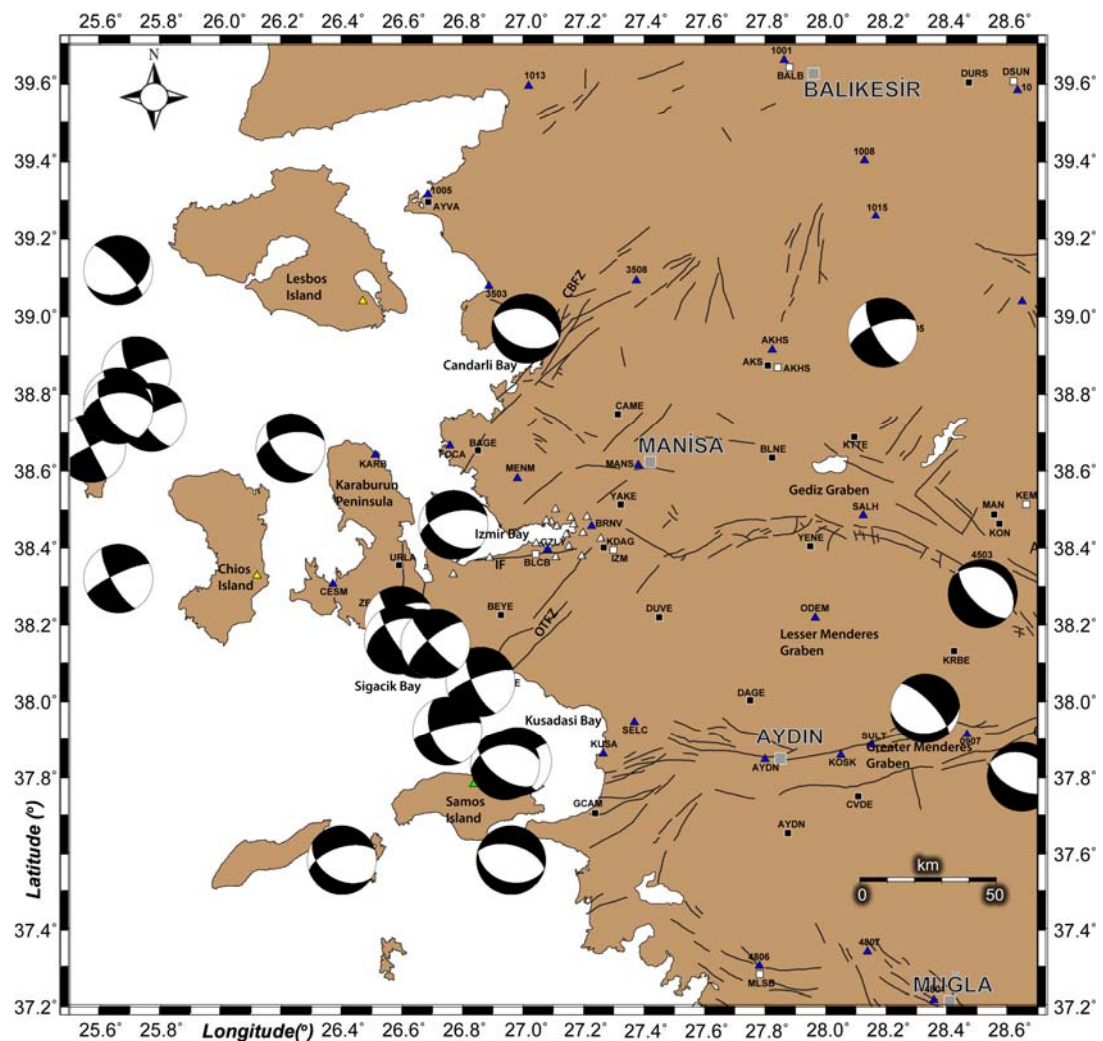


Figure 5.5 Fault plane solutions compiled from the Harvard-CMT.

The focal mechanisms of the earthquakes in the area are mainly east-west striking normal faultings, which is a result of the extension of the Aegean Region. Effects of the westward movement of the Anatolian plate is accommodated by large

(approximately) east-west trending normal fault systems like the Gediz Graben and Buyuk Menderes Graben in the east. There are also many examples of strike slip faults along OTFZ.

5.3. Local tectonics of Izmir and surroundings

The Mineral Research and Exploration Institute, Ankara, Turkey (MTA) has reported more than 40 active faults in the vicinity of the Izmir city as shown in figure 5.6. Active faults of the study area were studied by Uzel & Sözbilir (2008; in figure 5.6).

5.3.1 Major Tectonic Structures around Izmir

Dominant faulting characters of this area are normal faults. However, strike slip faults are also observed along the OTFZ, Karaburun Fault (KF), and CBFZ. The study area is controlled by the E–W trending normal faults and NE–SW strike-slip faults (Sözbilir et al., 2008). Miocene basement units and Plio–Quaternary basin deposits are usually separated by strike-slip faults (Kaya, 1979; Genc et al., 2001). Normal faults indicating southern Izmir Gulf oriented E–W direction such as Izmir Fault (IF). The normal faults include regularly strike-slip components. The strike-slip faults generally have sinistral character such as NE–SW trending OTFZ and Seferihisar Fault (SF). Izmir City is settled along the shoreline of the Izmir Bay which is covered by Plio-Quaternary terrestrial and marine deposits.

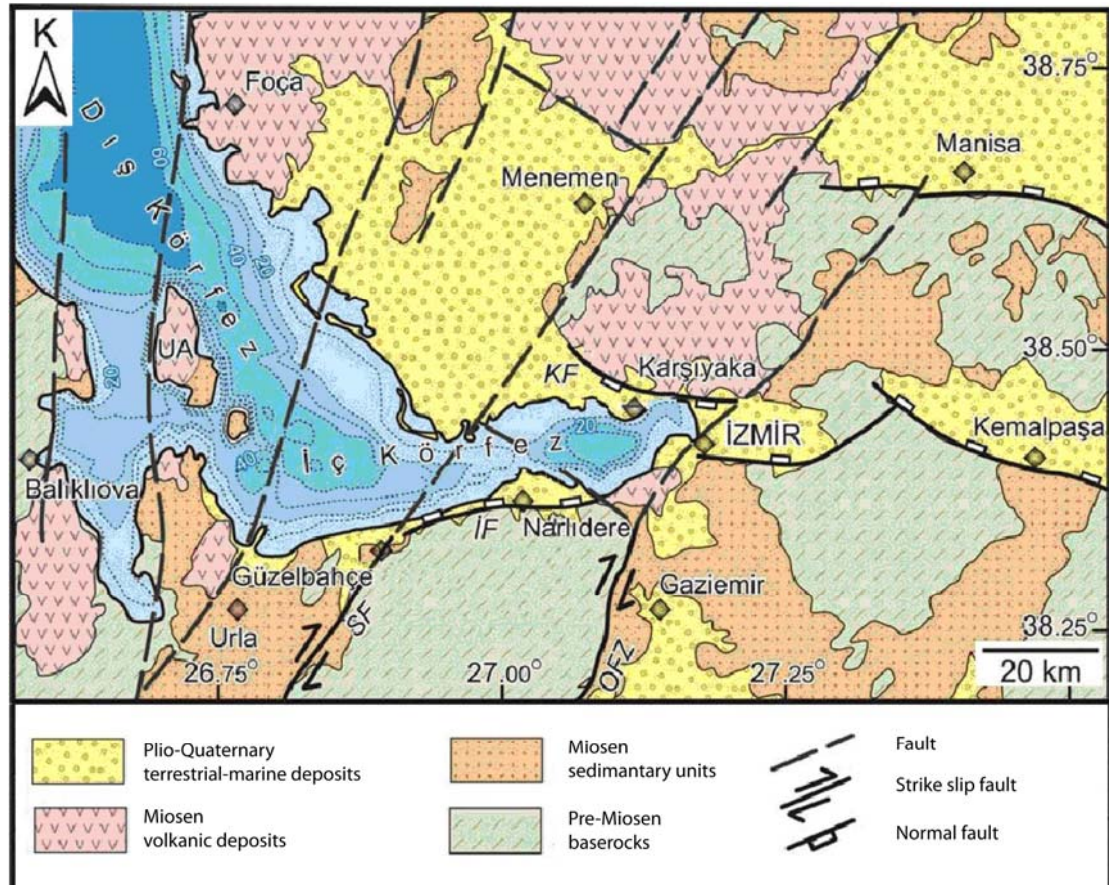


Figure 5.6 Simplified geological map of Izmir Gulf; İç Körfez: Inner Bay, Dış Körfez: Outer Bay, IF: Izmir Fault, KF: Karşıyaka Fault, OFZ: Orhanlı Tuzla Fault Zone, SF: Seferihisar Fault, UA: Uzunada island (modified from Sözbilir et al. 2008).

5.3.1.1. The Izmir Bay

The Izmir Metropolitan settlement is divided into two parts by Izmir Bay. Izmir Bay is an L-shaped basin limited by NE-, NW and E–W-trending active faults (Aksu et al., 1987). These faults cross over the Izmir Bay such as Seferihisar Fault, Urla Fault. Izmir Bay is a about NW-trending basin, 20-km-wide and 40-km-long. It is limited by the Karaburun Peninsula to the west and the Foça high and the Menemen plain to the north (Uzel et al., 2010). The Southern part of the Bay is bounded with a between Urla and Balçova basin due to the high mountain at the south.

5.3.1.2. Faults

The important tectonic features of the study area are the Izmir Fault, Karşıyaka Fault, Orhanlı Tuzla Fault and Seferihisar Fault Zone (Figure 5.7).

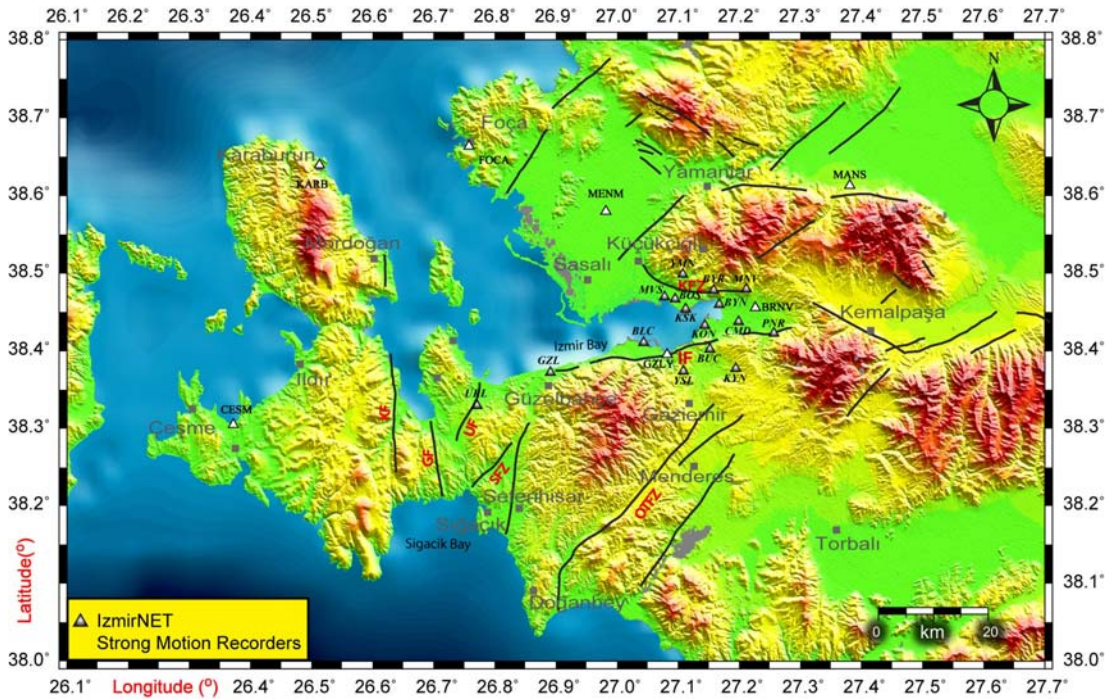


Figure 5.7 Map of Izmir and location of IzmirNET strong motion recorders.

Izmir Fault: Izmir fault makes up the southern margin of the Izmir Bay in the E-W direction. It is an approximately 2-4 km wide, 40 km long active normal fault zone. The eastern part of Izmir Fault between Izmir and Pınarbaşı has two small sections. Izmir Fault is limited by the Seferihisar and Nifdağı Highs to the north. The western part of Izmir Fault is surrounded by Güzelbahçe and Üçkuyular villages. (Erdik et al., 1999; Emre & Barka, 2000).

During the period whose seismicity has been observed instrumentally, two earthquakes have occurred on Izmir fault: One in 1977 and another in 1979. The moment magnitude of these events was 5.5 and 5.3 respectively (Emre et al., 2005b).

Orhanlı Tuzla Fault zone and Seferihisar Fault Zone: Seismically active areas south and southwest of Izmir city are Seferihisar (SFZ) and Orhanlı Tuzla fault zone (OTFZ). The Seferihisar fault is located west of the Tuzla fault and east of the city Urla. The fault starts in the south in the Gulf of Sigacik and ends in the north, close to the Izmir fault. SFZ is a 2–5-km-wide, 30-km long and NE-trending dextral fault zone (Figures 5.7; Inci et al., 2003; Ocakoğlu et al., 2004, 2005; Emre et al., 2005; Sözbilir et al., 2008). The Seferihisar fault is known to have ruptured in recent times, latest one in 2003, where an earthquake with a moment magnitude of 5.6 was recorded (Emre et al., 2005b).

The OTFZ is located to the south of Izmir and is aligned in the NE-SW direction cutting the Izmir settlement area. For this reason it is the most important structure around the study area. The OTFZ is bounded by Cumaovası basin at the west and the Seferihisar High to the east. The most important earthquake than has occurred on the OTFZ is the November 6, 1992 Doğanbey Earthquake (M=6) which affected Izmir Metropolitan settlement (Tan & Taymaz, 2001).

Karşıyaka Fault Zone: It is a 0.5–2.5 km-wide, 20-km-long normal fault, located north of Izmir. This fault zone is aligned in an EW direction, defined by a concave fault shape trace. Karşıyaka fault zone (KFZ) is an antithetic fault to the IFZ (Izmir Fault Zone) and affects Karşıyaka and Bayraklı districts (Uzel & Sözbilir 2008).

5.4 Seismic Activity around Izmir

IzmirNET accelerometric stations (Figure 5.7) were installed primarily to investigate the soil characteristics and site response at station sites. During the duration of the project they have also been used for seismological studies such as the analysis of the distribution of seismic activity, focal mechanisms and stress tensor determination.

All stations are installed in the free field and the instruments were produced by Guralp Systems in UK (5TD built in accelerometers). IzmirNET stations are equipped with a GPS antenna, UPS supply and an ADSL communications line.

Stations are recording the data continuously and transmit it to AFAD-ERD laboratory in Ankara. Seismology Laboratory in Izmir receives the data by internet connections from AFAD-ERD. Data are routinely processed and stored in Izmir (Figure 5.8).

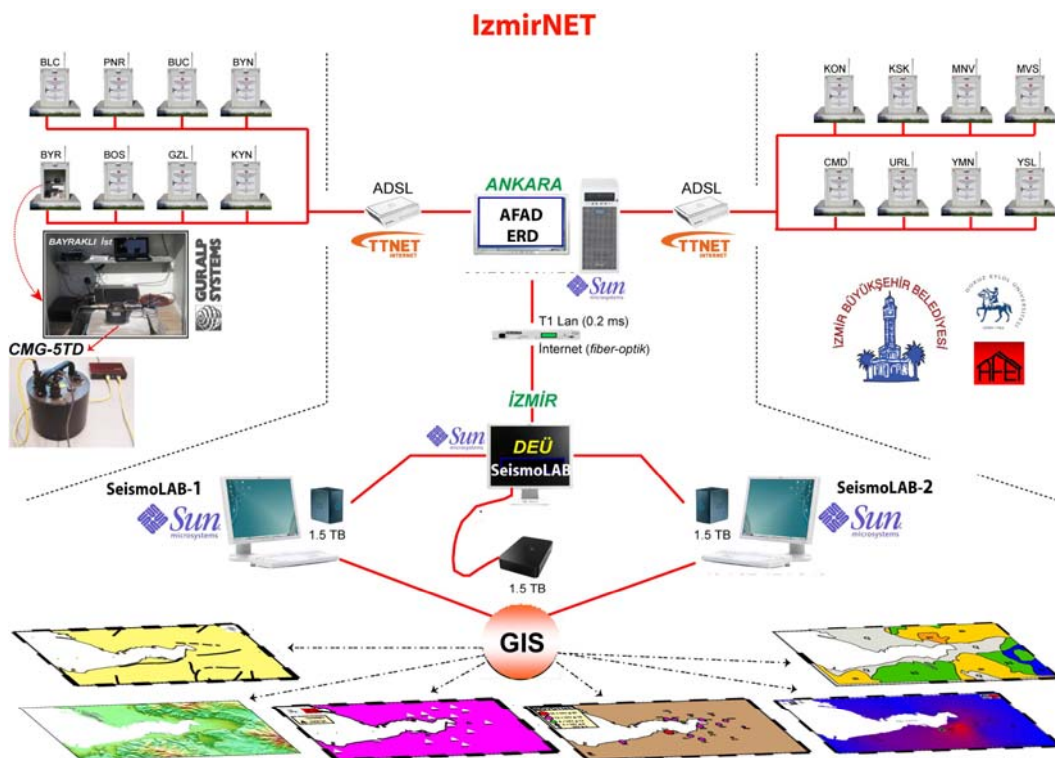


Figure 5.8 IzmirNET Infrastructure of Data communication

The Seisan software package is used (Havskov & Ottomoller, 1999) to pick P and S arrivals, to read amplitudes and to compute earthquake parameters such as origin time, location, RMS and magnitude.

During the project, we recorded 943 micro-earthquakes together with the AFAD-ERD stations. Figure 5.9 shows the seismic activity for the period end of August 2008 to 2011 April. Only well located 150 events ($RMS \leq 0.2$) are plotted. The magnitude of these events is comprised between 1.7 and 4.8. Depths range from 1 to 28 km.

Some local cluster areas were detected near Menemen, west of the Narlıdere, Kemalpaşa basin and Bornova basin. During the project, we also located diffused seismic activity near Sigacık Bay. Around the outer gulf epicenters align on a NW-SE direction.

Digital waveforms of the stations operated by ERD in Ankara were also used during the seismological analysis since our stations are concentrated around the Gulf.

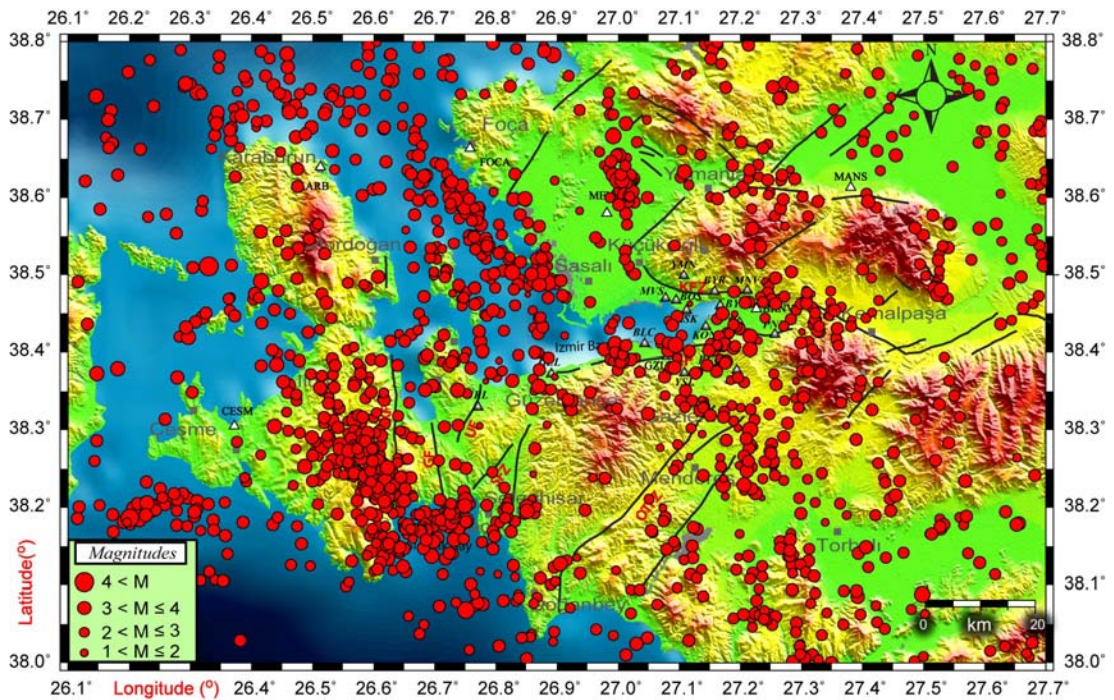


Figure 5.9 Seismic activity of study area during the project time (DEU+AFAD-ERD, 2008-2011).

To locate events, we used the velocity model proposed by Kaypak & Gokkaya (2011). It was observed that most of the events are concentrated in the upper part of the earth crust with depths smaller than 28 km.

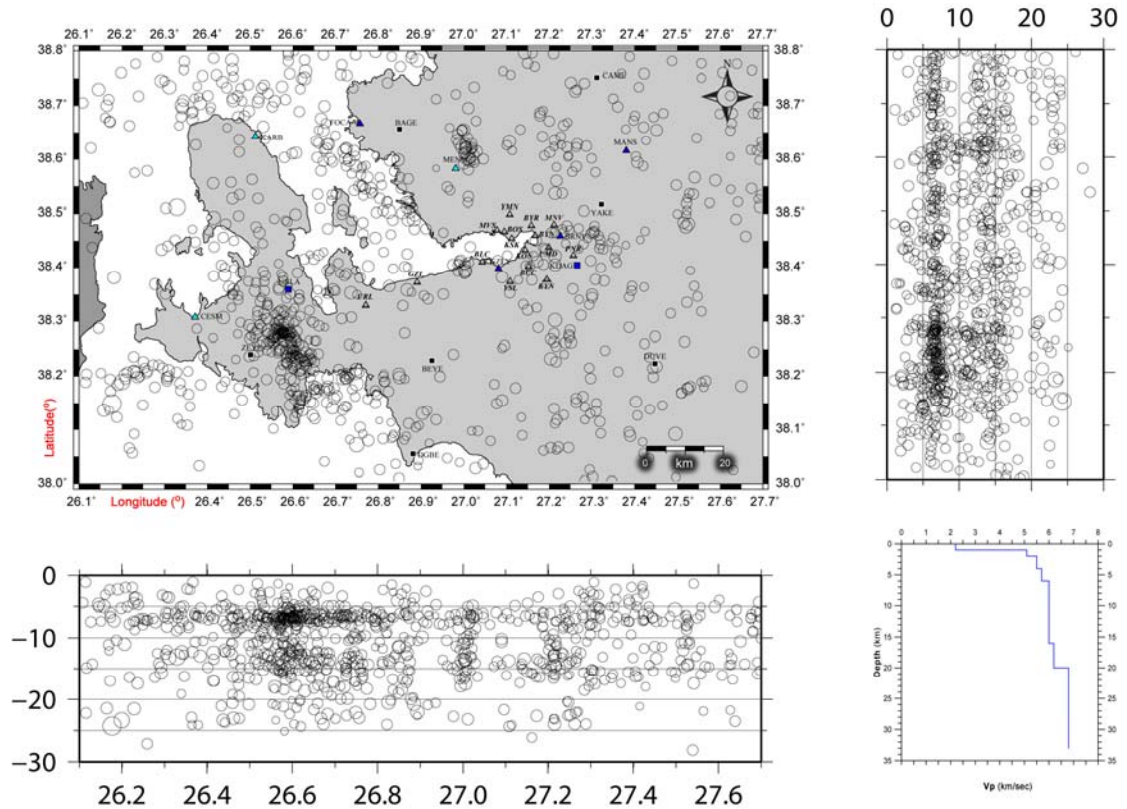


Figure 5.10 Seismic activity with the Longitude and Latitude depth cross sections of the located events of this study. Velocity model was taken from Kaypak & Gokkaya, 2011.

After locating the micro-earthquakes focal mechanisms were determined using P wave first motion polarities in the program FOCMEC (Snoko, 2003). We computed 27 focal mechanism solutions (Table 5.2) each one using at least 11 reliable polarities with an azimuthal range less than 180° .

Our focal mechanisms indicate normal faulting as seen in figure 5.11. Three mechanisms show normal faulting (Number 3, 4, 5) at the west of the Izmir Fault Zone (IFZ). E-W trending normal faulting mechanisms were obtained at the north of IFZ (12, 14, 15 and 27). Strike slip faulting mechanisms (events numbers 18 and 21) were observed at the east border of the Izmir Bay. Strike slip faulting is also observed along the OTFZ, as shown by event number 1. A normal faulting mechanism with a strike slip component was found around SFZ. Dextral strike slip fault (event number of 6) was observed in the outer Gulf along the suspicious fault.

Table 5.2 Parameters of focal mechanism solutions

Date and Time	Longitude	Latitude	Depth	Azimuth	Dip	Rake	MI	RMS	GAP
1_20080810_02h22	27.098	38.376	10.6	193.0	60.0	14.0	3.0	0.19	111
2_20081009_03h15	27.240	38.387	24.0	80.0	51.0	-145.0	3.3	0.07	178
3_20081118_20h06	27.010	38.389	13.5	1.0	86.0	-74.0	3.2	0.17	151
4_20081118_20h11	27.012	38.396	17.8	1.0	1.0	-179.0	3.1	0.19	113
5_20081119_06h07	27.016	38.389	2.8	200.0	62.0	-46.0	2.2	0.18	104
6_20090204_00h19	26.828	38.508	14.9	197.0	83.0	146.0	3.0	0.18	106
7_20090215_14h01	27.100	38.421	18.4	129.0	69.0	10.0	3.1	0.11	165
8_20090227_14h51	26.914	38.318	25.3	83.6	80.0	-78.0	3.3	0.17	108
9_20090401_23h27	26.957	38.393	7.0	157.0	62.0	-8.0	2.5	0.08	118
10_20090522_16h11	26.906	38.345	7.0	101.0	39.0	-80.0	2.7	0.18	135
11_20090527_14h54	26.909	38.346	7.0	69.0	48.0	-111.0	2.5	0.12	160
12_20090822_19h21	27.069	38.409	7.0	79.0	22.0	-103.0	3.6	0.16	139
13_20090822_19h29	26.986	38.368	7.1	324.0	65.2	-53.1	2.6	0.09	171
14_20090828_00h44	27.076	38.414	7.0	96.0	50.0	-84.0	2.9	0.16	175
15_20090830_08h06	27.074	38.415	6.9	116.0	49.0	-65.0	2.9	0.08	103
16_20091125_18h35	27.109	38.428	7.0	228.8	39.9	-75.9	2.7	0.16	101
17_20091219_14h43	27.137	38.437	26.3	359.0	41.0	-12.0	2.7	0.13	113
18_20091219_18h42	27.165	38.44	7.0	313.0	79.0	-6.0	2.5	0.17	98
19_20091221_07h33	27.126	38.517	7.0	223.7	35.8	-69.2	2.8	0.18	112
20_20091221_12h21	27.129	38.512	8.5	228.0	34.0	-60.0	2.5	0.14	115
21_20100123_19h24	27.171	38.468	25.7	87.5	83.6	39.6	3.5	0.20	98
22_20100306_18h26	27.143	38.569	15.2	250.1	78.9	-10.2	2.5	0.20	172
23_20090708_19h29	27.169	38.449	6.9	326.0	68.0	-34.0	3.1	0.13	84
24_20091218_00h28	27.173	38.404	11.0	289.5	87.1	-34.1	2.5	0.19	109
25_20091220_06h17	27.162	38.408	7.0	72.4	86.7	41.9	2.5	0.16	161
26_20100522_21h21	27.181	38.424	8.0	274.4	45.5	-45.5	2.5	0.18	91
27_20100815_13h49	27.069	38.417	9.0	333.0	27.0	-71.0	2.6	0.07	114

The mechanism solutions we determined are in good agreement with the morphology of the faults. We observe dextral strike slip components together with normal faulting. These solutions are not to explain the kinematics of the suspicious fault. We need more focal mechanisms to complete interpretation of the morphological features of all the faults.

To understand the stress regime around Izmir region, we computed the carried out stress tensor inversion proposed by Michael (1987; figure 5.12). This technique has been widely used by different researches to estimate principal stress directions from focal mechanism solutions. We used 27 focal mechanism solutions to calculate stress axes.

The results show the max. principal stress axis sigma 1 (σ_1) close to vertical. The min. principal stress axis sigma 3 (σ_3) is close to horizontal. Our results indicate that

the studied area is influenced by the N-S extension evident from the dominant normal faulting, with a minor strike-slip component.

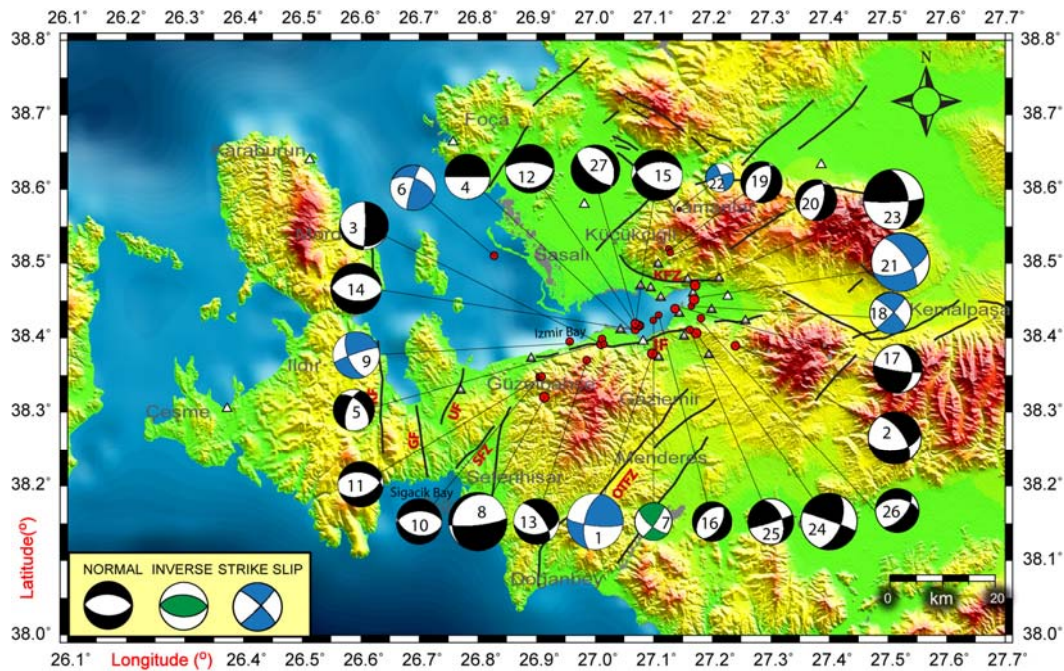


Figure 5.11 Focal mechanism solutions obtained from this study. Triangles indicate accelerometric stations belong to both DEU and AFAD-ERD.

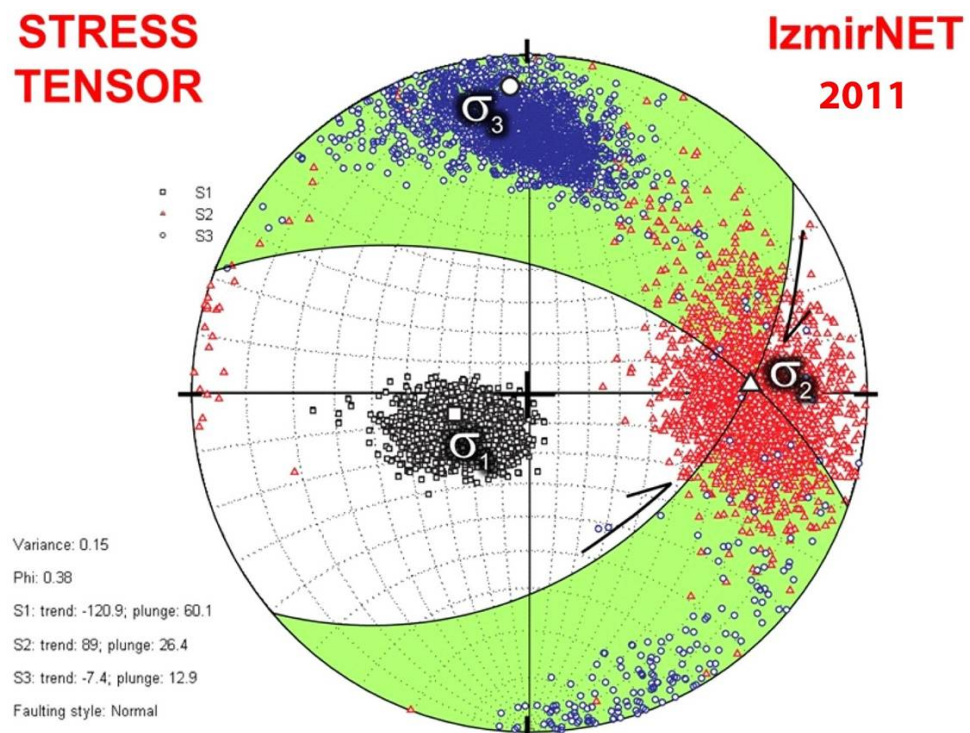


Figure 5.12 Results of stress tensor inversion from 27 focal mechanisms solutions.

CHAPTER SIX
LOCAL SITE EFFECTS IN IZMIR, AEGEAN REGION OF TURKEY
(PAPER 3)

Elcin Gok^{a,*} and Orhan Polat^b

^a Dokuz Eylul University, Earthquake Research and Implementation Center, Izmir
Turkey

^b Dokuz Eylul University, Engineering Faculty, Department of Geophysics, Izmir
Turkey

Submitted to Tectonophysics (2011)

Abstract

Local geological conditions of Izmir Metropolitan city, Aegean region of Turkey, has been studied by using earthquake-based data obtained from the IzmirNET local strong-motion network which was installed in 2008. Using data from low intensity events which occurred during 2009 and 2010, a preliminary evaluation of site amplification effects has been carried out. Fourier amplitude spectra of the accelerograms for each site, for 10 different events distributed in a wide range of azimuths were computed. We used only a limited portion of the record that containing predominantly S waves. The spectral shapes were smoothed and amplitude ratios with respect to the rock site were calculated. For each site, mean amplification was computed. We also performed microtremor measurements at each location sites. These results show a clear influence of the site soil conditions on the amplification of ground motion. This amplification can be quite different depending on the frequency range considered. No amplification of ground motion with respect to rock on Paleocene limestones, Miocene volcanics and flysch. Amplification reveals a maximum amplification of 7.9 (at 0.98 Hz) in Mavisehir district where old river bed presents over there. Other remarkable peaks are on Quaternary alluvial in Karsiyaka, Bostanli, Balcova ve Konak stations.

Keywords: Site effect, amplification, resonance frequency, strong-motion network

6.1 Introduction

Correlation of structural damage with local site geology and soil properties is commonly observed after a strong earthquake. Structural damage may implicitly measure the relation between ground-motion characteristics and local site conditions. Izmir is the 3rd largest city of Turkey, after Istanbul and Ankara, with more than 3.5 million inhabitants. Seismic microzonation, urban planning, land-use management, and mitigation of urban earthquake risk require assessment of site effects in earthquake-prone urban areas (Ozel et al., 2002). However, available strong-motion instruments in Izmir are not adequate to study the local site effects. For this reason, a local accelerograph array (IzmirNET; Polat et al., 2009) has been installed in Izmir, Aegean region of Turkey, in the frame of a bilateral cooperation between Dokuz Eylul University (DEU), in Izmir, and Earthquake Directorate Department of the Presidency of Disaster and Emergency Management Directorate (AFAD-DDB), in Ankara. This accelerometric network was deployed within a rectangle of 15 km x 30 km. Most stations sample different surface geology, so that local site effects on ground motions may be studied using earthquake and microtremor data.

In this paper, we studied site response in Izmir city using earthquake standard spectral ratios (SRR) and microtremor horizontal-to-vertical spectral ratios (HV). We used earthquake data recorded by IzmirNET to estimate amplification at different sites. We investigated effects of local topography, soil type and azimuth to the source. We have also compared SSR with HV in Izmir city. Hence, one of the principal aim of this study is to reveal about usage of the low-cost ambient noise measurements at stations sites as a satisfactory alternative where already reported for Avcilar, Turkey, case (Ergin et al., 2004; Ozel et al., 2002) after influenced by unexpected heavy damage due to the Izmit-Kocaeli earthquake ($M_s=7.4$) occurred on August 17, 1999 (Polat et al. 2002a, b) at the western extremity of the North Anatolian Fault Zone (NAF; Cisternas et al., 2004; Gurbuz et al., 2000).

6.2 Geological Setting and Instruments

The Aegean region (AR) of Turkey is characterized by wide scale extension, and several large scale graben structures oriented on the E-W direction. Damaging earthquakes in these grabens show normal fault mechanisms in agreement with the N-S extensional tectonics (Angelier, 1978; Aktar et al., 2007; Bozkurt, 2001; Eyidogan & Jackson, 1985; LePichon & Angelier, 1981; McKenzie, 1978; Sengor et al., 1984; Taymaz et al., 2007). Recent studies based on surface morphology and marine seismic reflection provide evidence of active faults in the area (Emre & Barka, 2000; Ocakoglu et al., 2004, 2005). The potential seismic risk is high in Manisa, Aydin, and Usak cities. Moderate size earthquakes also occur near the study area (Polat et al., 2008).

Geology and tectonics at Figure 6.1 have been studied based on mapping of geological structures at a scale of 1/25.000, measurements of stratigraphic sedimentologic sections of the units, and documentation of faults and of their kinematics. Izmir Bay is a shallow marine basin that is controlled by active faults, in the West Anatolian Extensional Province. The bay comprises Paleocene (Bornova) flysch zone, Miocene sedimentary sequence (sandstones, mudstones) belonging to the Yenikoy-Kizilca formation, Miocene (Yamanlar) volcanics, and Pliocene-Quaternary alluvial deposits (Sozbulir et al., 2008, 2010; Uzel et al., 2010).

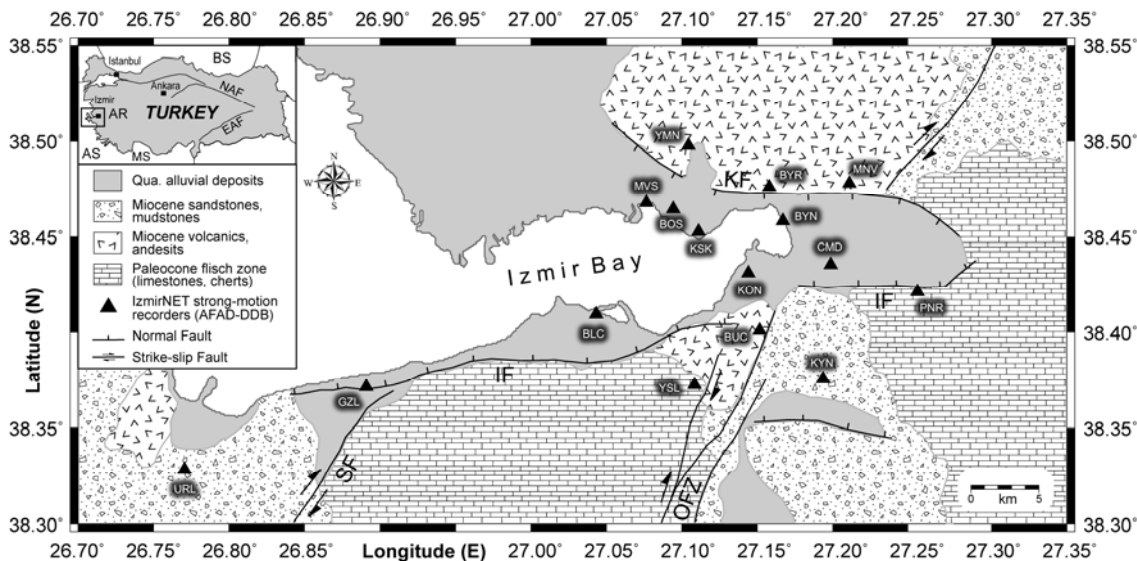


Figure 6.1 Simplified geologic and tectonic map of Izmir and surrounding area (compiled from Sozbilir et al., 2008, 2010; Uzel et al., 2010). Thick lines indicate active faults. IzmirNET accelerometric array is shown as solid triangles. IF is the Izmir Fault, KF is Karsiyaka Fault, SF is the Seferihisar Fault, and OFZ is the Orhanli Fault Zone. Inset Map: AR is the Aegean Region of Turkey, AS is the Aegean Sea, BS is the Black Sea, EAFZ is the East Anatolian Fault Zone, MS is the Mediterranean Sea, and NAFZ is the North Anatolian Fault Zone.

GPS measurements and present seismicity indicate that the study area is under E-W shortening in addition to N-S extension (McClusky et al., 2000). Recent GPS surveys and seismic studies show E-W trending normal faults and N-S oriented crustal extension which increases in amplitude from north to south (Aktug & Kilicoglu, 2006; Aktar et al., 2007).

The 16 observation sites are located on different geological units. Surface geology in the Izmir area consists of Quaternary alluvium. Eight stations (BLC, BOS, BYN, CMD, GZL, KON, KSK, MVS) are deployed on this unit. MVS and Bostanli station are located close to an old river (Gediz) with high water table and liquefable sand. PNR and YSL stations are installed on Cretaceous-Paleocene aged Bornova flysch zone. Two stations (KYN, URL) are on Miocene upper sedimentary units which belong to Yenikoy-Kizilca formation. But the site around URL was altered by a broad marl zone (Sozbilir et al., 2010). BYR and MNV are deployed on Miocene aged Yamanlar andesites (Uzel et al., 2010). BUC is close to the Yenikoy-Kizilca

formation, and YMN is close to the boundary of alluvial deposits. MNV is taken as reference station in the present study.

6.3 Method and Data Analysis

To quantify the site characteristics near station locations, we used both standard spectral ratio (SSR) and horizontal to vertical (HV) spectral ratio techniques. The SSR is considered a very reliable method to estimate site effects. After introduced by Borchardt (1970), it has been widely used and discussed in the literature (Chavez-Garcia et al. 1990; Lachet et al., 1996; Ozel et al., 2002). The HV method was widely spread by Nakamura (1989).

We first used the SSR method from the same earthquake to obtain the relative amplification between the two sites. The critical assumption in the spectral-ratio method is that the two sites share the same source spectrum and have comparable propagation path effects for the phases included in the sample window. For the narrow range of azimuths and epicentral distances that are covered by our data, any effects of radiation pattern should be minimal. On the basis of these assumptions, we eliminate the source and path effects by taking the spectral ratios of sample windows when the distance to the reference site is small compared with the source to site distance. The technique also assumes that the reference site is transparent and has no site complexity of its own. The calculation of spectral ratios from weak motion records is one of the most frequently applied techniques for the estimation of site response. In practice, this method consists of taking the spectral ratio between the site of interest and a nearby hard-rock (reference) site. In some cases, a suitable hard-rock reference site may not be available close to the site of interest. In this case, the vertical component is used as reference, and transfer functions can be estimated using HVSR on earthquake data (Lermo & Chavez-Garcia, 1993).

We have used 10 regional earthquakes with good signal-to-noise (S/N) ratio and wide azimuthal coverage. The epicentral locations are shown in Figure 6.2, and location parameters are listed in Table 6.1. Local magnitudes vary from 3.9 to 4.8

and focal depths are between 3 and 28 km. Table 6.2 shows the matrix of events and recording stations. The focal distance and azimuth distribution of the selected events for each station are given in Table 6.3. Hypocentral distances vary between 50 and 216 km. Maximum epicentral distance between reference site (MNV) and other stations are 42 km (with URL station deployed at the western extremity of the study area). All epicentral distances are less than their hypocentral distances from the sources. Therefore it is probably good assumption that the path effects on the records are similar.

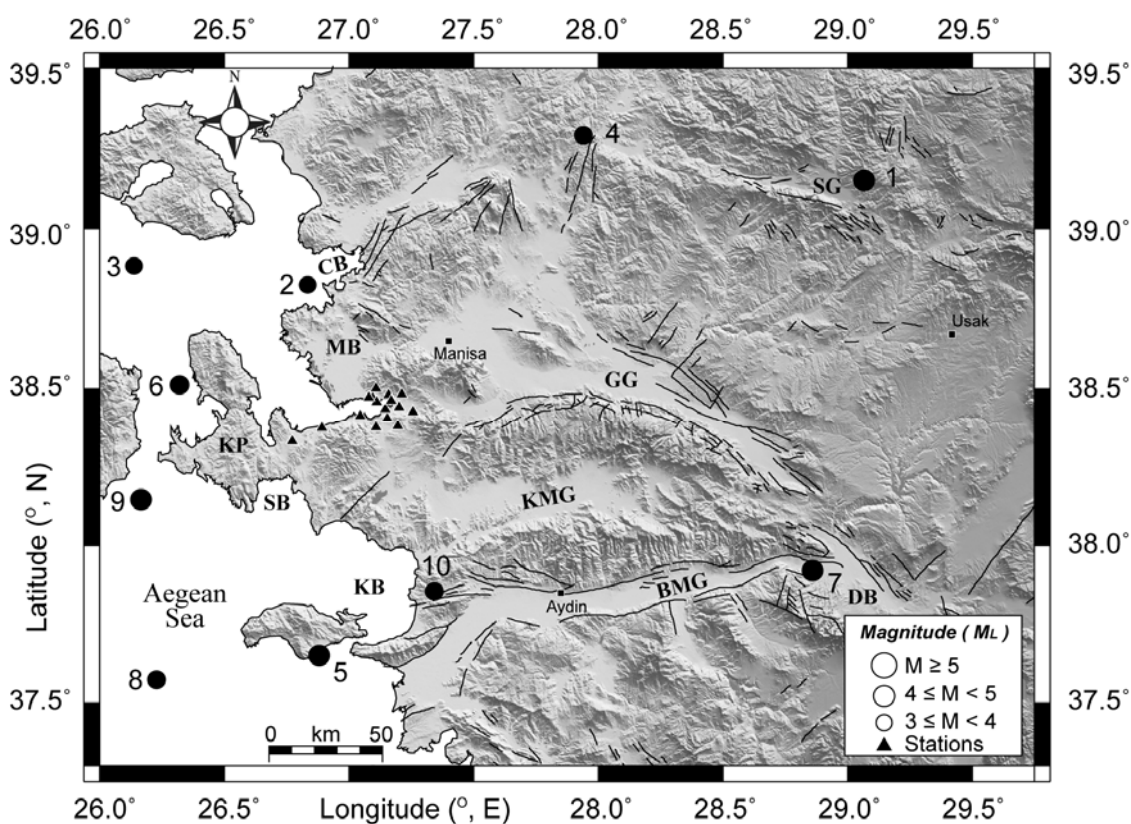


Figure 6.2 Epicenters are shown with solid circles. Triangles are IzmirNET accelerometric array. BMG is Greater Menderes Graben, CB is Candarli Bay, DB is Denizli Basin, GG is Gediz Graben, KB is Kusadasi Bay, KMG is Lesser Menderes Graben, KP is Karaburun Peninsula, MB is Menemen Basin, SB is Sigacik Bay and SG is Simav Graben.

Table 6.3 Focal distance (R) and azimuth (Az) of the earthquakes.

Nr.	BLC		BOS		BUC		BYN		BYR		CMD		GZL		KON	
	R (km)	Az(°)	R (km)	Az(°)	R (km)	Az(°)	R (km)	Az(°)	R (km)	Az(°)	R (km)	Az(°)	R (km)	Az(°)	R (km)	Az(°)
1	191	65	185	67	183	64	179	65	179	66	178	65	205	61	182	65
2	98	338	98	329	105	329	103	323	101	222	59	323	90	355	57	329
3	55	303	52	299	60	302	56	298	54	297	107	298	57	311	103	300
4	127	39	119	39	122	35	116	35	115	37	117	34	139	42	120	37
5	85	190	92	192	86	196	93	196	95	195	91	198	80	181	90	195
6	68	280	72	274	77	279	77	274	77	273	80	276	-	-	76	278
7	168	109	166	111	158	110	159	112	161	113	156	111	179	106	160	110
8	120	218	127	217	125	221	131	220	-	-	131	221	108	213	127	220
9	84	249	91	246	-	-	96	249	96	246	98	250	71	248	93	250
10	70	157	73	162	66	164	72	167	73	167	69	170	72	146	69	164

Nr.	KSK		KYN		MNV		MVS		PNR		URL		YMN		YSL	
	R (km)	Az(°)	R (km)	Az(°)	R (km)	Az(°)	R (km)	Az(°)	R (km)	Az(°)	R (km)	Az(°)	R (km)	Az(°)	R (km)	Az(°)
1	184	66	181	62	175	65	186	67	174	63	216	66	182	67	-	-
3	54	329	110	328	56	319	51	231	112	321	60	6	50	325	60	335
2	99	299	64	301	105	295	97	299	63	298	86	318	97	298	104	304
4	120	38	123	33	113	35	120	39	116	32	149	44	116	39	127	36
5	91	190	85	199	96	197	92	192	92	201	76	173	-	-	82	195
6	73	275	81	282	81	273	70	274	85	278	50	298	73	272	75	282
7	164	111	154	110	157	114	167	111	151	111	188	104	166	104	161	108
8	127	218	126	223	135	221	127	217	133	225	100	210	131	216	120	220
9	92	248	96	254	101	248	-	-	102	253	61	247	93	244	88	252
10	72	164	62	168	73	172	74	161	66	173	74	137	76	165	64	160

The success of the standard spectral ratio technique relies on the availability of a good reference station. Site effect may affect ground motion even on hard rock, as discussed in detail in Buech et al. (2010). As already noted, the MNV reference site chosen in this study was located on hard Miocene andesite outcrop. Figure 6.3 shows accelerograms of the 20 June 2009 earthquake (Nr. 5 in Table 6.1) which was recorded at all sites except YMN (Table 6.2). Amplitudes are much higher and durations longer at other sites compared to the reference station, as was also typically observed for other earthquakes. As seen in the plotted figure, the frequency content of the YSL (represents Cretaceous-Paleocene flysch) is quite different from the URL and KON stations. As expected, the rock site MNV, located in NE of Izmir Bay, has the smallest amplitudes, and the soil site KON has remarkably high amplitudes as compared with other three sites. The studies showed that for epicentral distances greater than 50 km, peak accelerations are strongly influenced by surface geology, acceleration being lowest on rock sites and high on alluvial deposits (Boore et al. 1989; Ergin et al., 2004; Ozel et al., 2002). On the other hand, radiation pattern and/or source directivity may have caused the amplitude differences. We verified these amplitude differences in the range of azimuth and focal distances that was covered by our data, and found no noticeable differences as explained in detail in Results section.

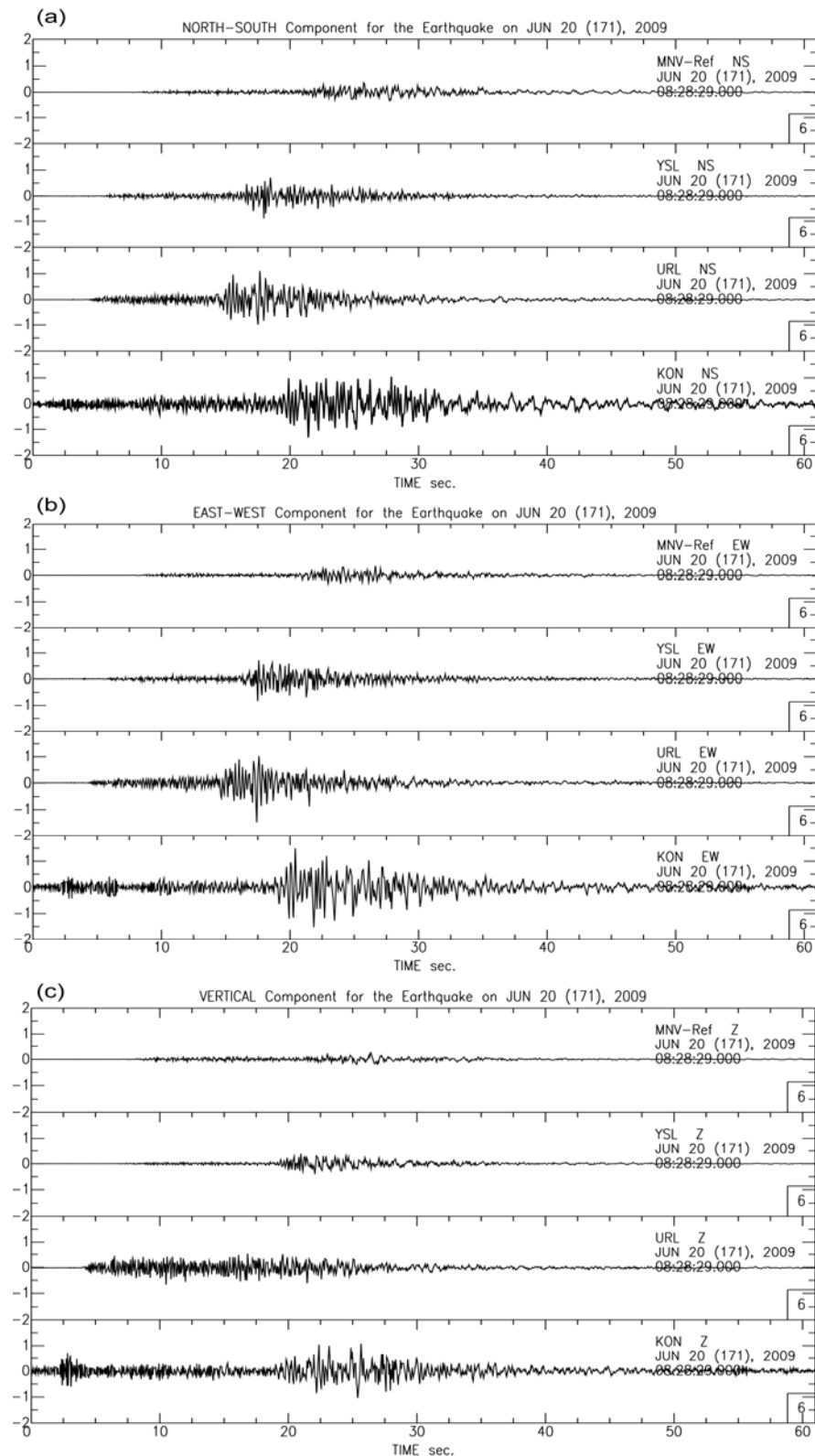


Figure 6.3 Comparison of three-component unfiltered accelerograms for the event Nr. 5 (Table 6.1) recorded at four sites, including reference site MNV. (a) North-South component, (b) East-West component, (c) Vertical component. All accelerograms are fitted to the same scale.

Processing of signals is as follows. Seismograms were corrected for system response and spectral amplitudes were computed. Different time window lengths were used for each event, starting 3 s before and ending 7-10 s after the S arrival. This ensured that S-wave was included. A cosine taper was applied over the 10% of each record before taking the Fourier transform. The average horizontal spectrum was computed by adding the squared moduli of the horizontal spectra before taking the square root. Spectrums were smoothed by a simple moving average filter.

We also estimated site response using HV technique. It is a good tool to determine the fundamental soil frequency and to reveal site characteristics. Basic assumption of this method is that the vertical component is not influenced by the local site geologic structure, whereas the horizontal components contain the local geological properties underlying the recording site. Site response is obtained by deconvolving the vertical component from the horizontal component. In the frequency domain, this corresponds to the division of horizontal spectrum by the vertical spectrum (H/V). This approach was applied to the microtremor data by Nakamura (1989). Experimental studies using this technique showed some encouraging results, suggesting the possible use of this technique for the microzonation studies. Simultaneously, these studies suggested that such HVSR analysis might be meaningful not only for microtremor measurements, but also for weak-motion recordings, although questions are still unresolved about the validity of the ground-motion amplification factors obtained by this technique (Ergin et al., 2004; Marcellini, 2006; Ozel et al., 2002).

Single-station microtremor measurements were conducted at the station locations during 30 minutes. Ambient vibrations were recorded using Guralp CMG-6TD with a built-in broad-band seismometer with a 100-sps sampling rate. Signals were processed with the Geopsy software (<http://www.geopsy.org>). 10 to 40 s windows were processed, selected with an anti-trigger criteria using $STA = 1$ s, $LTA = 30$ s, and low and high thresholds of 0.2 and 2.5 respectively. Before averaging, each individual spectrum was smoothed using the window with a constant parameter of 40 (Konno & Ohmachi, 1998).

6.4 Results

Figure 6.4 illustrates results for SSR at 15 sites relative to MNV. Spectral ratios were arithmetically averaged. The resonance frequency peaks for the 8 stations deployed on quaternary alluvial deposits (Figure 6.4) are consistent with the conventional site categories of the NEHRP (Rodriguez-Marek et al., 2001). Maximum spectral amplifications vary from 2.8 to 7.9 at CMD and MVS stations, respectively. We observed variation in peaks between 0.6 and 2.8 Hz frequency band on the EW component of the CMD site. Secondary peaks with decreasing slightly between 1.8 and 2.0 Hz, were observed on the NS component of BYN, and EW components of KON and MVS sites around an amplification value of 4. The largest amplification is at MVS, reaching 7.9 at 0.98 Hz on the EW component. It is deployed at the center of Mavisehir district and this area is located on old river delta. We observed no amplification at KYN site which is deployed on Miocene sandstone, mudstone and partitioned limestone units. It can be also thought a possible reference site. Further west towards the URL, we detected amplification with a value of 4 at 1.3 Hz resonance frequency on the same geologic units comprising some marl levels, additionally. The PNR site, located on flysch and limestone units, show nearly flat response both on EW and NS components. Amplification is 1.8 at 8.2 Hz on the EW, and 1.9 at 8.0 Hz on NS components. Whether we observed similar maximum frequencies for YSL site (7.0 Hz at NS, and 8.4 Hz at EW) representing same geological units as PNR site, we also noticed slight increases in amplifications (from 1.0 to 3.0) starting from 0.8 Hz to 8.4 Hz. Increasing is linear on NS component. Similar augmentations towards higher frequencies also exist at YMN (both component) and at BYR (only NS comp.) sites deployed on Miocene volcanics and andesites. Amplification reaches a maximum of 3 (for 8.0 Hz) at EW component of YMN site, while it is 1.7 (for 3.0 Hz) on the NS component of BYR. It is ~3.8 in 1.3 Hz (on EW) at BUC site which is located on similar units. Its location is very close to the boundary of Miocene sandstone and mudstone units. Figure 6.5 shows the relation between the fundamental-resonance frequencies and peak amplification of the sites from SSR technique. Most of the larger amplifications (%73) occur at low frequencies (0.6 – 3.0 Hz).

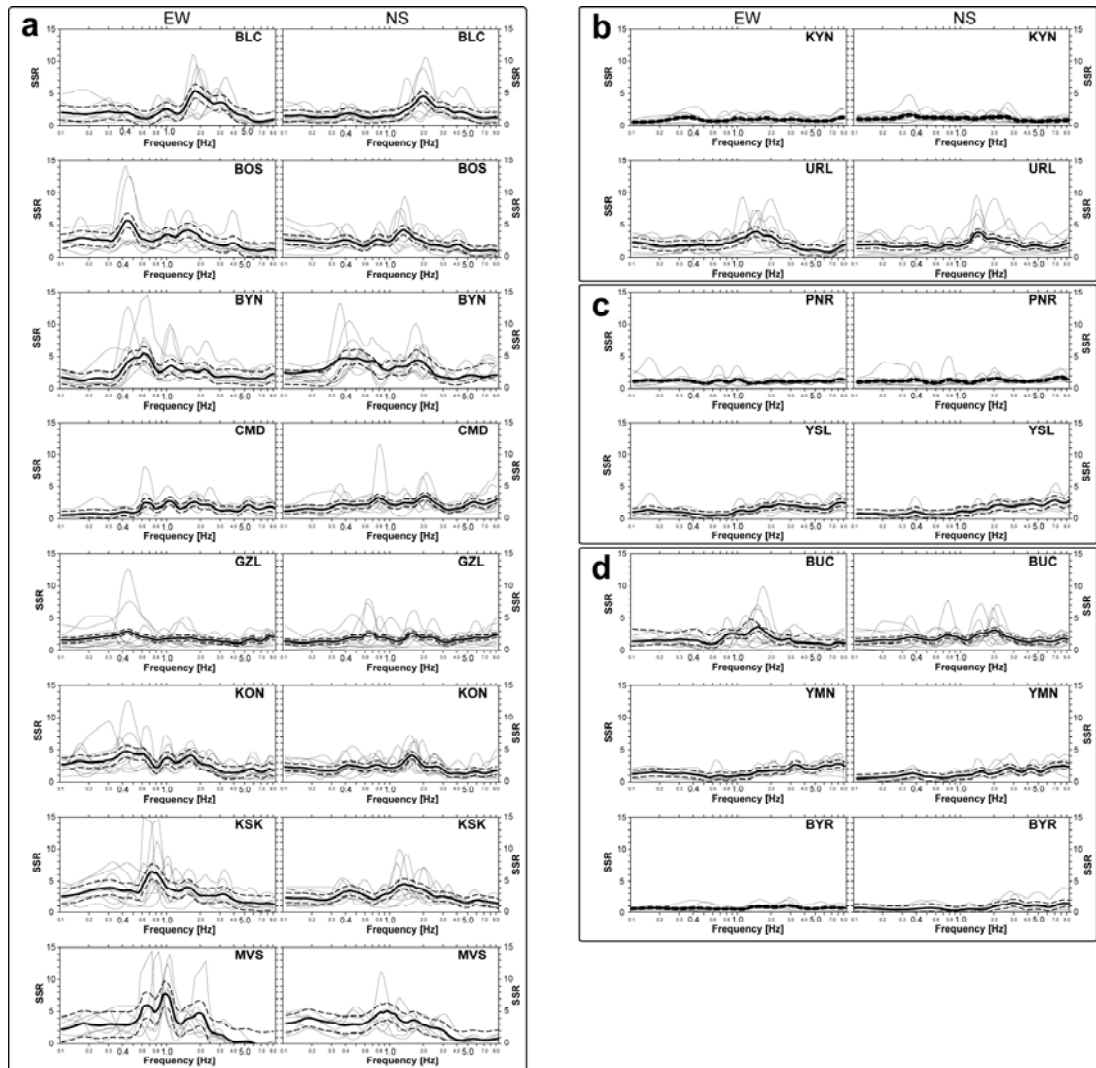


Figure 6.4 Comparison of S-wave spectral ratio at each site relative to the reference site, using the SSR method, for all recorded events as given in Table 6.2.

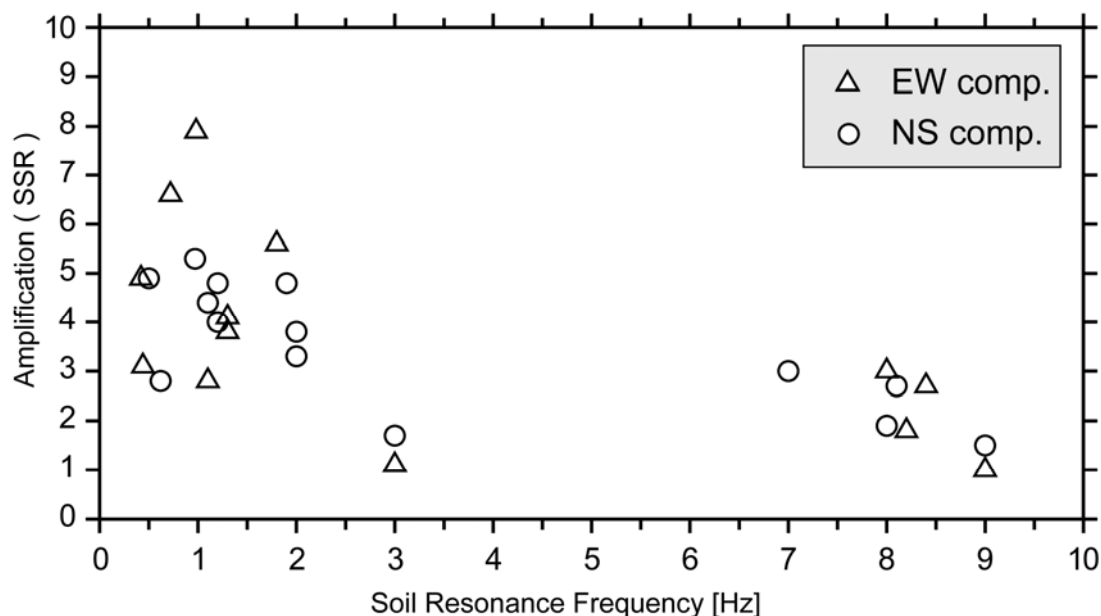


Figure 6.5 Correlation between variables of soil resonance frequency and amplification obtained for 15 sites. Open triangles and circles denote the results of EW and NS horizontal components, respectively.

Directionality of ground motions has been discussed in relation to fault rupture direction based on the observation records obtained in the study area. This is interesting from the point of structural response (e.g., Motosaka & Somer, 2002). Hence we realized that the mean amplification for each event is a good target to investigate the ground motion directionality since station sites were spanned by these events (Figure 6.6). The maximum amplification as a factor of 6.5 on the EW component was observed for the event Nr. 10, at the south of the network. Other prominent amplification by revealing 5.9 on the EW was detected towards to the east (for the event Nr. 7). We also obtained high ratios for the events Nr. 2 (at the north), and Nr. 9 (in the west) as a factor of 4.9 and 4.1, respectively. Generally speaking, southern events (Nr. 5, 8, 10) show significant amplification on their EW components. We did not observe a systematic focal distance dependency by comparing the amplifications (on EW components) for the event pairs (Nr. 5 - Nr.1 or Nr. 5 - Nr. 7) which have same magnitudes and different focal distances. Similar non-systematic results were also obtained for the northern and western events. There is no randomly augmentation in amplification when magnitude increases (for the same focal distances) as we observed for the events the Nr. 6 and Nr. 9 inside the

western group and sharing same epicentral area. Similar observation can be also thought for the events Nr. 5 and Nr. 10, at the south. Amplification is not growing by increasing the magnitude for the same focal distances. No systematic variation in amplification was observed comparing with the magnitude and distance for each seismic source. Similar results can be concluded for the observations on the NS components of the investigated events.

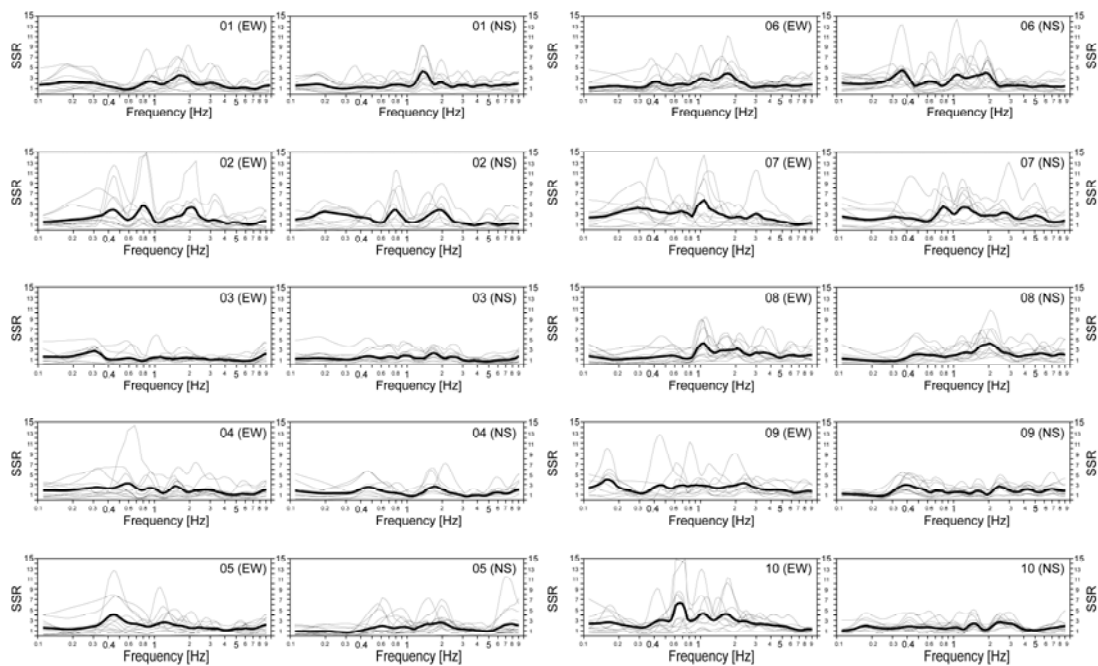


Figure 6.6 Stacked spectral ratios for each event from all sites, using SSR method.

Added to these studies, further analysis was also performed to infer the relation of directivity by comprising the recorded events in the same directional area. For this purpose, an integrated amplification study was realized for each station by stacking all spectra. And they were separately partitioned into four groups (Figure 6.7) according to their azimuth: east (events 1, 7), south (events 5, 8, 10), west (events 3, 6, 9), and north (2, 4). The eastern group consists of best records in terms of S/N ratio and magnitude. Hypocentral distances in this group are important for testing the focal distance (azimuthal) dependence of site amplification. Event Nr. 4 in the north, and Nr. 8 at the south are aligned on the NE-SW direction. Magnitudes, depths and hypocentral distance of these events are the same. Mean amplification was observed as 3.8 on EW components for the northern (at 0.82 Hz) and southern (1.1 Hz) events.

Nearly same amplification was observed on the NS components as a factor of 3.2 (at 1.8 Hz) for the northern, and 3.8 (at 2.0 Hz) for the southern events. The EW amplification for western events is 3.5 (at 1.7 Hz) while it is 3.4 (at 0.45 Hz) for the eastern events. Whether frequency peaks are a bit different on the NS components (1.6 Hz for western and 1.9 Hz for eastern events), amplifications are the similar (~ 3.0). We have three records from west covering a broad area from NW (Nr. 3) to SW (Nr. 9). A common spectral peak from 0.46 Hz to 1.7 Hz is observed for EW azimuths, although the northern and southern events seem to cause slightly higher amplification comparing with the western and eastern events. The peaks are clustered around 0.8 Hz, with amplification reaching a factor of 3.8. This factor is higher at 5 stations by reaching from 4 to 13. Significant but smaller amplification has a peak at 1.6 Hz for the eastern events. One of the largest events (Nr.1) was occurred at a hypocentral distance of ~ 216 km on the NE direction. Considering the distance and magnitude level, spectral ratios for this event have been investigated. Like for the other events, amplification by a factor of 2.5–3.5 was observed between 0.45 and 1.4 Hz at the stations deployed on alluvial units.

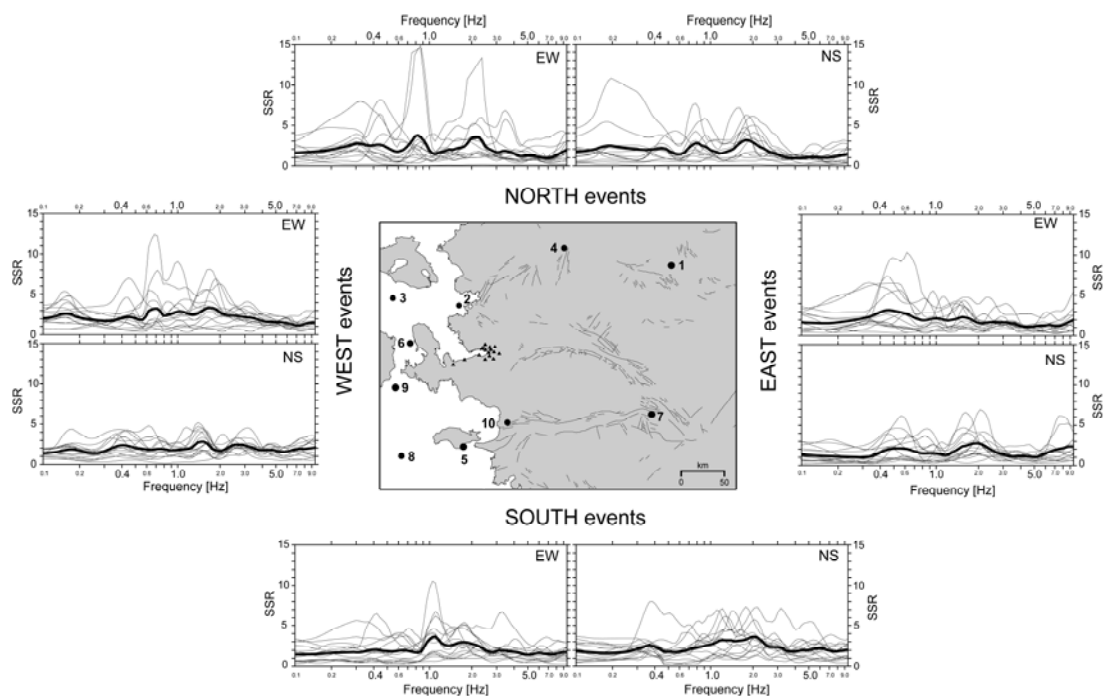


Figure 6.7 Stacked spectral ratios for all sites, for events grouped by north, east, south and west azimuths, using SSR method.

In this study, we also used microtremor measurements to estimate local site effects at IzmirNET. We present the results of HV (Figure 6.8) sampling four different geological units. Most sites show peaks between 0.6 Hz and 1.2 Hz. The maximum amplification 7.6 (at 0.7 Hz) was observed at BYN. Similar resonance frequency but different amplification factor (5.7) as obtained from SSR technique. The eight sites representing quaternary alluvial deposits indicate amplitude peaks around 5.0 for MVS and CMD sites which reveal lower amplitudes comparing the results of SSR. The HV result of KON is higher than that of obtained from SSR. But both sites reveal peak frequencies near 0.7 Hz. There is no good coherency for BLC and BOS stations from microtremor study, and their HV curves. Broad peak was detected in KSK site. Other variation (three peaks) in amplification was also observed at CMD site between 0.6 Hz to 1.5 Hz. One of the large amplitude was detected at KON, reaching to a factor of 6.3 at 0.7 Hz. This site was deployed close to the sea side at the south of Izmir Bay. There is no substantial amplitude at KYN which is located on sandstones and marls. Broad and varied peaks were detected at URL with a maximum HV of 4.8. Its amplitude was same as in SSR, but the resonance frequency is different. The YSL and PNR stations where located on flysch and limestones, show flat response. Both sites reveal coherent results with the SSR. No clear HV were obtained for the BUC, BYR and YMN on andesites.

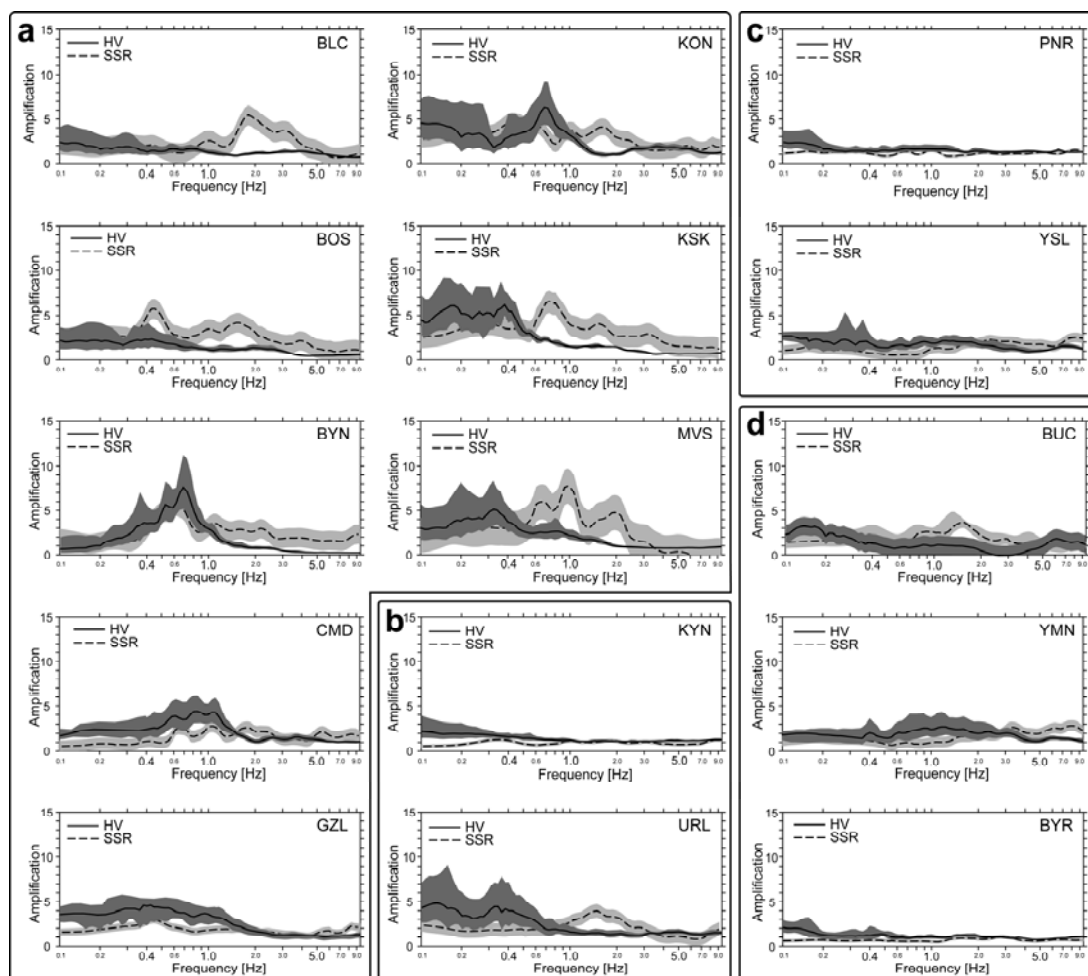


Figure 6.8 Comparison between mean amplification factors for the horizontal component estimated at 15 stations. a) 8 sites on alluvial deposits, b) 2 sites on flysch and marl, c) 2 sites on limestone, d) 3 sites on volcanic rocks. In all graphs the thick continues lines represent the results of the microtremor measurements (HV) and dashed curves are the results of the SSR method. The shaded areas indicate the mean \pm one standard deviation.

In most cases the HV spectrums have similar results as observed in SSR except the URL station. We observed peak frequency around 0.3 Hz while it was 1.3 Hz in SSR. Amplifications were the same (3.5 and 4). Amplitudes were detected slightly higher at BYN and KON sites regarding to SSR. Other largest spectral ratios were observed at KSK and MVS sites. These results should be the effect of alluvial deposits, around the costs of the Gulf of Izmir. Similarities at most sites were obtained from the HV and SSR.

6.5 Discussions

The systematic survey of the site response in Izmir, using both the SSR and HV methods, has shown that significant ground amplification at lower frequencies exists. The SSR method can provide more details about the nature of the ground according to the selection of reference site. On the other hand, the HV may indicate more reliable resonance frequency for some stations in accordance with the data quality. However, we could not obtain clear results to better describe the amplifications and resonance frequencies.

Amplitudes at four different geologic units with respect to a hard rock site, computed from the SSR, have shown that significant amplifications between 1.8 (PNR) and 7.9 (MVS) occur in the frequency range from 0.45 Hz (KON) to 3.0 Hz (BYR). At the same time, the HV detected peak amplitudes at lower frequencies for the sites located on Quaternary alluvial deposits such as BYN, CMD, GZL, KON, KSK and MVS revealing resonance frequencies of 0.7, 0.82, 0.4, 0.7, 0.38, and 0.32 Hz, respectively. Whether no coherency was noticed for the BLC and BOS sites (on the same unit), a slight increase towards to lower frequencies (below 0.8 Hz) was observed at both stations. We observed that the ground motion was amplified nearly by a factor of 7.9 at 0.98 Hz at MVS (Mavisehir) site which is located on old (Gediz) river delta, north of Izmir Bay comprising high water table and organic peat. Similar results were also obtained from the HV method indicating a resonance frequency at 0.32 Hz. A first-order estimate of the thickness H of the resonating layer can be calculated as $H=V_s/(4*F_0)$ where V_s is the S-wave velocity (Seth & Wohlenberg, 1999). If an average S-wave velocity of 200 m/s is taken, the thickness for the resonating layer can thus be estimated from ambient noise as 140 m for MVS and KON (at 0.5 Hz). Hence, the large amplification factors could be then attributed to deposits at these sites. Reverberations are also clearly seen following the arrival of the S-wave train, nearly on all accelerograms in Figure 6.3. With its present site characteristics, the sites on alluvium need special attention to perform additional geophysical and geotechnical studies. We thus conclude that the unconsolidated low-

velocity sediment overlying rock basement play the primary role in the local site response.

No remarkable amplifications were detected for the rest of the sites, except the URL and BUC stations where deployed on Miocene mudstones-marl and on a transition zone between volcanics and mudstones, respectively. We noticed that the slight increase towards to high frequencies, exist on the NS component of YSL, YMN and BYR sites. We believe that the topography of the basin affects these amplitudes since they are located on slightly slopped hills having ~100 m for YSL-YMN, and ~150 m altitudes for BYR sites. As already reported in many studies, the topography play key roles in causing amplification effects of seismic ground motion even the site geology was dominated by rocks (Aki, 1993; Ashford, 1997; Assimaki & Gazetas, 2004, Buech et al., 2010; Chavez-Garcia et al., 1996).

In addition to frequency characteristics, we also investigated the dependence of amplification on epicentral distance, azimuth and magnitude of the earthquakes that were recorded. Frequency dependence of the site amplification has shown common properties at all sites for 10 events. The analysis has clearly shown that effective amplification by a factor between 2.8 and 5.9 (on EW components) occurs in the low frequency band. A secondary amplification is generally observed between 1.8 and 3.0 Hz, especially on the NS components for events 2, 4, 5, 6 and 9. However, no significant amplification is observed in the higher frequency band (above 3 Hz). It is also clear that the amplification does not depend on the azimuth of the seismic source. In other words, waves coming from any direction cause similar amplification (3.4 for eastern and 3.8 for southern events) at all sites as we have shown the mean stacked results for the same directional area. But it is true that remarkable amplifications were observed for the events 5, 8 and 10 showing a factor of 4.3, 4.3 and 6.5 (on EW components), respectively. Event Nr. 10, at the western extremity of Greater Menderes Graben (BMG), aligned on the E-W directional faulting may cause significant effect for the city of Izmir. For instance the event 5, occurred on the same direction located towards to the west, was revealed pure normal faulting mechanisms (<http://bbnet.gein.noa.gr>), and widely felt not only in close settlement area but also in

Izmir. Two strong earthquakes were occurred between 17 and 21 October 2005 revealing similar magnitudes (M_w 5.9) in the Sigacik Bay (SB), and caused long-term broad panic in the region. Whether no interruption is reported in the lifeline systems, these events have augmented the structural damage and the post-earthquake stress of the people living in Izmir and neighboring cities such as Manisa and Aydin. Event Nr. 8 is on the same path as Sigacik Bay earthquake. Towards to the west of the network, Event Nr. 9 was located in between Karaburun Peninsula (KP) and Chios Island (CI). This earthquake was occurred on March 26, 2010 (20h35 local time) with a magnitude of M_L 4.7, and again was widely felt by the inhabitant of Izmir city. It showed dominant normal faulting mechanisms (with minor strike-slip component) as one observed similarly for the event 5 (<http://bbnet.gein.noa.gr>). Since dominance of the normal fault has been reported in relation to fault rupture direction and directivity effect (Somerville et al., 1997), earthquakes occurred one of these areas may contribute significant effect for structures with the strength directionality.

In Izmir, the maximum amplifications are seen at high frequencies. Peak frequencies of the soils and the fundamental frequencies of the buildings are reciprocally close in the city. Since our analysis identifies the resonance effects, i.e., soil-structure or ground motion-soil-structure, they can play an important in the future earthquake, and contribute significant damage in the area. Hence, investigations should be additionally enhanced to methods dealing with 2D or even 3D shape of the basins in the city.

6.6 Acknowledgements

This research is a part of PhD study of Elcin Gok. It is performed in the framework of a joint collaboration between Dokuz Eylul University in Izmir and Presidency of Disaster and Emergency Management Directorate (AFAD) belongs to the Prime Ministry in Ankara, Turkey. We thank Murat Nurlu, Zafer Akcig, Ulubey Ceken, Murat Kececioglu and Mustafa Akgun for their support. The GMT (Wessel and Smith, 1995), SAC (Goldstein et al., 2003), and Geopsy (<http://www.geopsy.org>) software packages were used to generate most figures. This work was granted by TUBITAK (Project Nr. 106G159).

CHAPTER SEVEN

CONCLUSIONS

In this thesis, earthquake and ambient noise data recorded both Bursa and Izmir cities were analyzed to understand the present seismicity, to describe the fault kinematics and relate current stress regime with focal mechanisms, and to investigate the local site response. In the first part of the thesis, the seismic activity, ambient noise measurements and earthquake data have been studied for Bursa and related to the current knowledge of seismotectonics and geology. In the second part, the Izmir city was investigated using a similar dataset and analysis as for Bursa city.

From the seismic activity of Bursa, 384 events out of a total 582 recorded have been well located with an $RMS \leq 0.2$ s. Depths of most events concentrate in the first 29 km of the earth crust. Magnitude (M_L) was comprised between 0.3 and 5.4. Clusters of seismicity were detected around Uludag Mountain, near Kestel-Igdir alignment, and an area between Gemlik Bay and Iznik Lake along the south of Gemlik Fault. Fault plane solutions of 10 earthquakes were obtained and then used for stress tensor inversion. Faulting regime is compatible with dominant normal faulting overall the study area. However, this observation changes when this computation was repeated in sub-regions, for which the results exhibit a transition regime from normal to strike slip faulting from the north to the south of the studied area. The principal stress tensor axis σ_1 was shown to how a dips (δ) of 81° , and a strike (ϕ) of $N182^\circ$. Dip and strike of σ_2 and σ_3 were computed as $\delta=3^\circ \phi=291^\circ$ and $\delta=8^\circ \phi=21^\circ$, respectively.

The local site effect of Bursa was studied using the HVSR ambient vibration method. The purpose was to contribute to seismic hazard and risk mitigation in the urban area. Although the physical basis and reliability of the site effects estimates obtained with this method are still being discussed, the HVSR peak frequencies were obtained on HVSR curves to estimate the fundamental resonance frequency on different geologic units. Some earthquakes were recorded by a station (BYT01) in

Bursa, and these events were analyzed to define the HVSR amplitude of the station site. The peak frequencies of HVSR of ambient noise measurements at 22 sites on different geologic units (Quaternary alluvium, Neogene, Paleozoic and Metamorphic rocks) show a distribution between 1 and 10 Hz. The smaller frequencies (below 2 Hz) correspond to the Alluvial and Neogene deposits at the north of the study area whereas the Paleozoic and metamorphic rocks exhibit fundamental frequencies at higher frequencies. Amplitude of resonance frequencies of microtremors vary between 1 and 5. The HVSR analysis of the events recorded at BYT01 sites show a dominant frequency between 2.0 Hz and 3.5 Hz. This site is very close to the Paleozoic units and shows dominant frequencies similar with spectral ratios obtained from the microtremor measurement. The peak frequencies coincide with the surficial geology in the study area. HVSR provide a good estimate of the actual bandwidth over which the ground motion is amplified. However, the amplification factor could not be defined in this thesis due to the limitations of the method, and lack of the dense strong-motion array in the study area.

Regarding the seismic activity of Izmir, 150 events out of a total 943 recorded were well located with $RMS \leq 0.2$ s. Most events occur between 1 and 28 km depth. Magnitudes (M_L) are comprised between 1.7 and 4.8. Swarms are observed around Menemen in the north, Narlidere at the west, and on a line between Bornova and Kemalpaşa basins. During the project, no clusters were observed in the Izmir Bay. Fault plane solutions of 27 earthquakes were obtained and then used to compute a stress tensor inversion. Faulting regime is compatible with normal faulting. The principal stress tensor axis σ_1 was computed with a dip (δ) of 60° , and a strike (ϕ) of $N240^\circ$. Dip and strike of σ_2 and σ_3 were computed as $\delta=26^\circ$ $\phi=N89^\circ$ and $\delta=13^\circ$ $\phi=N353^\circ$, respectively.

Local site effects at Izmir were studied using the SSR (Standard Spectral Ratio) and HVSR methods at IzmirNET stations. The results indicate that there is no amplification of ground motion with respect to rock on Paleocene limestones. Sites located on Miocene volcanics and flysch show amplification to 4.1 (on the sandstone marls units), and reach a maximum amplification of 7.9 at 0.98 Hz in Mavisehir area

(at the North of Izmir Bay) on old terrestrial and marine deposits. On Quaternary alluvial deposits we observed as a amplification factor of 6.6 (site KSK) and 5.8 (site BOS). The BYN and BLC sites also show high amplification with a factor of 5.7 and 5.6, respectively.

Bursa and Izmir cities are two different settlements in the Marmara and Aegean regions of Turkey. Two different projects were performed in those cities to investigate the seismic activity, seismotectonic properties and local site effects (Table 7.1).

Table 7.1 Comparison of Bursa and Izmir Metropolitan cities in terms of administrative and scientific statistics.

Administrative Statistics	Bursa	Izmir
Engaged departmental region in Turkey	Marmara	Aegean
Population of city center*	1 905 570	2 774 103
Total population*	2 605 495	3 948 848
Total population order in 81 cities*	4	3
Contribution order to National Economy in 81 cities †	5	3
Socio-Economic development order in 81 cities †	5	3
National income per person †	\$ 10 500 5th order over 81 city	\$ 13 500 3th order over 81 city

Table 7.1 (continue ...)

Scientific Statistics (this study)	Bursa	Izmir
Base of the study	JULICH – TUBITAK (Germany – Turkey) Project Nr : 102Y156	TUBITAK – KAMAG (DEU Izmir – AFAD Ankara) Project Nr : 106G159
Project Duration	6 month (2003 – 2004)	3 years (2008-2011)
Geology		
Analyzed Dataset	<ul style="list-style-type: none"> • Event locations from temporary seismometer array (11 seismographs) • Microtremor measurements • Acceleration records of earthquakes 	<ul style="list-style-type: none"> • Event locations from permanent strong-motion network (16 accelerographs) • Microtremor measurements • Acceleration records of earthquakes
Used Data	Earthquake + Microtremor	Earthquake + Microtremor
Used Method	HVSR of earthquakes HVSR of microtremor	SSR (Standard Spectral Ratio) HVSR of microtremor
Used Software	SEISAN (Hypo71, FocMec) ZMAP Geopsy	SEISAN (Hypo71, FocMec) ZMAP Geopsy
Number of located events	384 (over 582) RMS \leq 0.2	150 (over 943) RMS \leq 0.2
Observed seismic activity	Moderate type $0.3 \leq M_L \leq 5.4$ $0.5 \leq \text{Depth} \leq 29$ km	Moderate type $1.7 \leq M_d \leq 4.8$ $1.0 \leq \text{Depth} \leq 28$ km
Focal Mechanism Solutions	10 (from P, SV waves)	27 (from P, SV waves)
Stress regime	Extension, Transition (from Normal to Strike) $\sigma_1 = 81$ $\sigma_2 = 03$ $\sigma_3 = 08$ R = 0.5	Extension (Normal) $\sigma_1 = 60$ $\sigma_2 = 26$ $\sigma_3 = 13$ R = 0.3
Local site effects	Alluvial and Neogene deposits: Amplitudes are between 1 and 5 at 1 - 10 Hz peak frequencies	Alluvial deposits: Amplifications are between 2.8 and 7.9

* Turkish Statistical Institute (TUIK; <http://www.tuik.gov.tr>)

† Stane Planning Organization (DPT; <http://www.dpt.gov.tr>)

This thesis had the objective to evaluate the available data obtained from the international/national scale collaborations and to disseminate the results individually for two different urbans and settlement areas. Although it is not easy to correlate and comparison for great cities, the influence and behaviour of local geologic conditions on earthquake ground motions have been studied thoroughly in the frame of this thesis for the case of Bursa and Izmir which are prone to earthquake.

REFERENCES

- Adatepe, F., Demirel, S., & Alpar, B. (2002). Tectonic setting of the southern Marmara Sea region based on seismic reflection data and gravity modelling. *Mar. Geol.*, *190*, 383–395.
- Aki, K. (1993). Local site effects on weak and strong ground motion. *Tectonophysics* *218*, 93-111.
- Aksu, A.E., Piper, D.J.W., & Konuk, T., (1987). Late Quaternary tectonic and sedimentary history of outer Izmir and Candarli bays, western Turkey. *Marine Geology* *76*, 89–104.
- Aktar, M., Karabulut, H., Ozalaybey, S., & Childs, D. (2007). A conjugate strike-slip fault system within the extensional tectonics of Western Turkey. *Geophysical Journal International*; doi: 10.1111/j.1365-246X.2007.03598.x, 1–13.
- Aktug, M., Kilicoglu, A. (2006). Recent crustal deformation of Izmir, Western Anatolia and surrounding regions as deduced from repeated GPS measurements and strain field. *J. Geodynam.* *41*, 471-484.
- Almendros, J., Luzo'n, F., & Posadas, A. (2004). Microtremors analysis at Teide Volcano (Canary Islands, Spain): assessment of natural frequencies of vibration using time-dependent horizontal-to-vertical spectral ratios, *Pure and Applied Geophysics*, *161*, 1579–1596.
- Alpar, B., & Yaltirak, C. (2002), Characteristic features of the North Anatolian Fault in the Eastern Marmara region and its tectonic evolution, *Marine Geology* *.190*, 329-350.

- Altuncu, S., Pinar, A., & Yilmazer, M. (2008). Moment tensor inversion solutions for event 2005 KAS earthquake by using zSacWin software, *ORFEUS workshop on Waveform Inversion*, 19-20 June 2008, Utrecht University, Netherlands.
- Ambraseys, N., & Finkel, C.F. (1995). *The Seismicity of Turkey and Adjacent Areas*, Eren Yayincilik, Istanbul-Turkey, 240 p.
- Ambraseys, N. (2000). The Seismicity of the Marmara Sea Area 1800-1899, *Journal of Earthquake Engineering*. 4, 3, 377-401.
- Ambraseys, N. (2002). The Seismic Activity of the Marmara Sea Region over the Last 2000 Years, *Bulletin of the Seismological Society of America*. 92, 1, 1-18.
- Angelier, J. (1978). Tectonic evolution of the Hellenic Arc since the late Miocene. *Tectonophysics* 49, 23-36.
- Angelier, J. (1990). Inversion of field data in fault tectonics to obtain the regional stress: A new rapid direct inversion method by analytic means, *Geophysical Journal International*. 103, 363-376.
- Angelier, J. (2002). Inversion of earthquake focal mechanisms to obtain the seismotectonic stress - a new method free of choice among nodal planes, *Geophysical Journal International*. 150, 588-609.
- Ashford, S.A., Sitar, N., Lysmer, J., & Deng, N. (1997). Topographic effects on the seismic response of steep slopes. *Bull. Seismol. Soc. Am.* 87, (3), 701-709.
- Assimaki, D., & Gazetas, G. (2004). Soil and topographic amplification on canyon banks and the 1999 Athens earthquake. *J. Earthq. Eng.* 8, (1), 1-43.
- Aydinoglu, N. (2000). *Loss Estimation of Building Stock in Izmir Earthquake Master Plan*. Bogazici University report for the RADIUS Project, Istanbul.

- Badawy, A., El-Hady, Sh., & Abdel-Fattah, A.K. (2009), Microearthquakes and Neotectonics of Abu-Dabbab, *Eastern Desert of Egypt, Seism Res Lett.* 79-1, 55-67.
- Balderer, W. (1997). Mechanisms and processes of ground water circulation in tectonically active areas. In C. Shindler, & M. Pfister (Eds.). *Active Tectonics of Northwestern Anatolia-The Marmara Poly-Project* (375-416). Hochschulverlag AG an der ETH Zurich-Swiss.
- Bard, P. Y. (1998). Microtremor measurements: A tool for site effect estimation? In Okada & Sasatani (Eds), *Proc. 2nd Intl. Symp. on The Effects of Surface Geology on Seismic Motion*, 1251-1279. Balkema.
- Barka, A., & Kadinsky-Cade, K., (1988). Strike-slip fault geometry in Turkey and its influence on earthquake activity. *Tectonics* 7, 663– 684.
- Barka A. (1992). The North Anatolian Fault zone. *Annales Tecton.* 6 (1992) 164–195.
- Benetatos, C., Kiratzi, A., Ganas, A., Ziazia, M., Plessa, A., & Drakatos, G. (2006). Strike-slip motions in the Gulf of Sigacik (western Turkey): Properties of the 17 October 2005 earthquake seismic sequence. *Tectonophysics* 426, 263–279.
- Bonnefoy-Claudet, S., Cornou, C., Bard, P. Y., Cotton, F., Moczo, P., Kristek, J., & Fah, D. (2006). H/V ratio: A tool for site effects evaluation. Results from 1-D noise simulations. *Geophysical Journal International* 167, 827–837.
- Boore, D.M., Seekins, L., & Joyner, W.B. (1989). Peak acceleration from the 17 October 1989 Loma Prieta earthquake. *Seism. Res. Lett.* 60, 151-166.
- Borcherdt, R.D. (1970). Effects of local geology on ground motions near San Francisco Bay. *Bull. Seism. Soc. Am.* 60, 29-61.

- Bozkurt, E. (2001). Neotectonics of Turkey, a Synthesis. *Geodinamica Acta* 14, 3-30.
- Bozkurt, E., & Sozbulir, H. (2004), Tectonic evolution of the Gediz Graben: field evidence for an episodic, two extension in Western Turkey, *Geological Magazine*. 141, 63-79.
- Brune, J. N. (1970). Tectonic stress and the spectra of seismic shear waves from earthquakes. *Journal of Geophysical Research* 75, 4997–5009.
- Buech, F., Davies, T.R., & Pettinga, J.R. (2010). The Little Red Hill Seismic Experimental Study: Topographic Effects on Ground Motion at a Bedrock-Dominated Mountain Edifice. *Bull. Seism. Soc. Am.* 100 (5A), 2219-2229.
- Chavez-Garcia, F.J., Pedotti, G., Hatzfeld, D., & Bard, P.-Y. (1990). An experimental study of site effects near Thessaloniki (Northern Greece). *Bull. Seism. Soc. Am.* 80, 784-806.
- Chavez-Garcia, F.J., Sanchez, L.R., & Hatzfeld, D. (1996). Topographic site effects and HVSr: A comparison between observations and theory. *Bull. Seismol. Soc. Am.* 86, (5), 1559–1573.
- Cisternas, A., Polat, O., & Rivera, L. (2004), The Marmara Sea Region: Seismic behavior in time and the likelihood of another large earthquake near Istanbul (Turkey), *Journal of Seismology*. 8, 427-437.
- Dravinski, M., Ding, G., & Wen, K. L. (1996). Analysis of Spectral Ratios for Estimating Ground Motion in Deep Basins. *Bulletin Seismological Society of America* 86, 646–654.

- Dreger, D.S. (2003), TDMT_INV: Time Domain Seismic Moment Tensor INVersion, *International Handbook of Earthquake and Engineering Seismolog, 81B*, p1627.
- Eisenlohr, T., Pfister, M., & Balderer, W. (1997) Environmental isotope study and 2-D modelling of cold and thermal karst within the Gemlik (Bursa) area of Northwestern Turkey, In C. Shindler, & M. Pfister (Eds.). *Active Tectonics of Northwestern Anatolia-The Marmara Poly-Project* (229-238). Hochschulverlag AG an der ETH Zurich-Swiss.
- Emre, Ö., & Barka, A. (2000). Active faults between Gediz graben and Aegean Sea (İzmir region). *Bati-Anadolu'nun Depremselliği Sempozyumu (BADSEM 2000)*. Dokuz Eylül University Press, İzmir, pp. 131– 132.
- Emre, Ö., Doğan, A., Özalp, S. & Yıldırım, C. (2005b). 17 Ekim 2005 Sığacık(İzmir) Depremleri Ön Değerlendirme Raporu. *Rapor No:10765, Jeoloji Etüdüleri Dairesi, MTA*.
- Erdik, E., Biro, Y.A., Onur, T., Sesetyan, K. & Birgören, B. (1999). Assessment of earthquake hazard in Turkey and neighbouring regions. *Annali di Geofisica* 42, 1125–1138.
- Ergin, K., U. Güçlü, & Z. Uz (1967). *A Catalog of Earthquakes for Turkey and Surrounding Area 11 A.D. to 1964 A.D.* Istanbul: Istanbul Technical University Press No. 24, Turkey, 169.
- Ergin, M., Ozalaybey, S., Aktar, M., Yalcin, M.N., 2004. Site amplification at Avcilar, Istanbul. *Tectonophysics* 391, 335-346.

- Eyidogan, H., & Jackson, J. (1985), A seismological study of normal faulting in the Demirci, Alasehir and Gediz earthquakes of 1969-1970 in Western Turkey: implications for the nature and geometry deformation in the continental crust, *Geophysical Journal of Royal Astronomical Society*, 81, 569-637.
- Eyidogan, H. (1988), Rates of crustal deformation in Western Turkey as deduced from major earthquakes, *Tectonophysics*. 148, 83-92
- Field, E.H., & Jacob, K., (1995). A comparison and test of various site response estimation techniques, including three that are non reference-site dependent. *Bulletin Seismological Society of America* 85, 1127–1143.
- Field E, & Jacob K. (1993). The theoretical response of sedimentary layers to ambient seismic noise. *Geophysical Research Letters*, 20 (24),2925±8.
- Genç, C., Altunkaynak, Ş., Karacık, Z., Yazman, M. & Yılmaz, Y. (2001). The Çubukludağ graben, south of İzmir: tectonic significance in the Neogene geological evolution of the Western Anatolia. *Geodin. Acta* 14, 1– 12.
- Gephart, J.W & Forsyth, D.W. (1984). An improved method for determining the regional stress tensor using earthquake focal mechanism data: application to the San Fernando Earthquake sequence. *Journal of Geophysical Research*, 89, 9305-9320.
- Giampiccolo, E., Musumeci, C., Malone, S.D., Gresta, S., & Privitera, E. (1999). Seismicity and stress-tensor inversion in the Central Washington Cascade Mountains. *Bulletin of the Seismological Society of America*. 89, 3, 811-821.
- Goldstein, P., & A. Snoke (2005). SAC availability for the IRIS community. *DMS Electronic Newsletter* 7 (1); <http://www.iris.edu/news/newsletter>.

- Goldstein, P., Dodge, D., Firpo, M., Minner, L. (2003). The SAC2000: Signal processing and analysis tools for seismologists and engineers, In: Lee, W.H.K., Kanamori, H., Jennings, P.C., Kisslinger, C. (Eds.), *The IASPEI International Handbook of Earthquake and Engineering Seismology*, Academic Press, London.
- Gosar, A. & Martinec, M. (2009). Microtremors HVSR study of site effects in the Ilirska Bristica town area (S. Slovenia), *Journal of Earthquake Engineering* 13, 50–67.
- Greber, E., Pfister, M., & Imbach, M. (1997). Hydraulic level variations in a thermal water well: impact of precipitation on the Cekirge thermal water system, In C. Shindler, & M. Pfister (Eds.). *Active Tectonics of Northwestern Anatolia-The Marmara Poly-Project* (267-274). Hochschulverlag AG an der ETH Zurich-Swiss.
- Gulkan, P., Yucemen, M.S., Bayfz, N., Kocyigit, A., Doyuran, V. (1993). A map for seismic zones in turkey according to recent data. Middle East Technical University, *Earthquake Engineering Research Center Report 93-01* (in Turkish).
- Gulkan, P., Ceken, U., Colakoglu, Z., Ugras, T., Kuru, T., Apak, A., et al. (2007). Enhancement of the National Strong-Motion Network in Turkey, *Seismological Research Letters*. 78, 429-438.
- Gurbuz, C., Kuleli, S., Bekler, T., Zor, E., Karabulut, H., & Zobu, M. (1998). Crustal structure studies in Western Turkey based on earthquake and explosion seismic data, *26th General Assembly of European Seismological Commission* (Expanded Abstract), August 23-28. p 106-111.
- Gurbuz, C., Aktar, M., Eyidogan, H., Cisternas, A., Haessler, H., Barka, A., et al. (2000), On seismotectonics of the Marmara region (Turkey): Results from a microseismic experiment, *Tectonophysics*. 316, 1-17.

- Hanks, T. (1982). Fmax. *Bulletin of the Seismological Society of America* 71 (6), 1,867–1,879.
- Hardebeck, J.L., & Hauksson, E. (2001), Stress orientations obtained from earthquake focal mechanisms: what are appropriate uncertainty estimates?. *Bulletin of the Seismological Society of America*. 91, 2, 250-262.
- Havskov, J., & Ottemoller, L. (1999). SEISAN: The Earthquake Analysis Software. *Seismological Research Letters*, 70, 532–534.
- Ibs-von Seth, M., & Wohlenberg, J. (1999). Microtremor measurements used to map thickness of soft sediments, *Bull. Seism. Soc. Am.* 89 (1), 250-259.
- Imbach, T. (1997). Geology of Mount Uludag with emphasis on the genesis of the Bursa, Northwest Anatolia, Turkey In C. Shindler, & M. Pfister (Eds.). *Active Tectonics of Northwestern Anatolia-The Marmara Poly-Project* (239-266). Hochschulverlag AG an der ETH Zurich-Swiss.
- Inan, S., Ergintav, S., Saatçilar, R., Tuzel, B., & Iravul, Y. (2007). Turkey makes major investment in earthquake research. *Eos, Transactions, American Geophysical Union* 88 (34), 333–334.
- Inci, U., Sözbilir, H., Erkül, F. & Sümer, Ö. (2003). Urla – Balıkesir arası depremlerin nedeni fosil bir fay [The reason of the earthquakes between the Urla and Balıkesir is a fossil fault]. *Cumhuriyet Gazetesi Bilim Teknik Dergisi* 848, 6–7.
- Isik, M., & Senel, H. (2009), 3D gravity modeling of Buyuk Menderes Basin in Western Anatolia using parabolic density function, *Journal of Asian Earth Science*. 34, 317-325.

- Jackson, J. A., & McKenzie, D. P. (1984). Active tectonics of Alpine– Himalayan belt between western Turkey and Pakistan. *Geophysical Journal of the Royal Astronomical Society* 77, 185–265.
- Kalafat, D., Gunes, Y., Kara, M., Deniz, P., Kekovali, K., Kuleli, H.S., Gulen, L., Yilmazer, M., & Ozel, N.(2007). *A Revised and Extended Earthquake Catalogue for Turkey since 1900 ($M \geq 4.0$)*, Bogazici University Library Cataloging. (ISBN 978-975-518-281-0) Istanbul.
- Kalafat, D., Kekovali, K., Ocal, M., & Gulen, L. (2009). Moment Tensor Catalogue of Important Earthquakes in Turkey and Surrounding Regions, *American Geophysical Union*, Fall Meeting 2009, Abstract 23A-0536, San Francisco-USA.
- Kang, T.-S., & Baag, C.-E. (2004). The 29 May 2004, $M_w = 5.1$, offshore Uljin earthquake, Korea, *Geosciences Journal*. 8, 115-123.
- Kang, T.-S., & Shin J.S. (2006). The offshore Uljin, Korea, earthquake sequence of April 2006: seismogenesis in the western margin of the Ulleung Basin, *Geosciences Journal*. 10, 2, 159-164.
- Karnik, V. (1971). *Seismicity of the European Area 2* (Prague,1971), 52 p.
- Kaya, O. (1979). Ortadoğu Ege çöküntüsünün Neojen stratigrafisi ve tektoniği (East-central Aegean depression: Neogene stratigraphy and tectonics). *Türkiye Jeoloji Kurultayı Bulteni* 22, 35–58.
- Kaypak, B., & Gokkaya, G. (2011). 3-D imaging of the upper crust beneath the Denizli geothermal region by local earthquake tomography, Western Turkey. *Journal of Volcanology and Geothermal Research*, submitted.
- Kind, F., Fah, D., & Giardini, D. (2005). Array measurements of S-wave velocities from ambient vibrations. *Geophysical Journal International*, 160, 114–126.

- Kissling E., Ellworth W.L., Eberhart-Phillips D. & Kradolfer U. (1994). Initial Reference Models in Local Earthquake Tomography. *J. Geophys. Res.*, 99, 19635-19646.
- Klinge, E., & Medici, F. (1997). Gravimetric studies of the Marmara Region. In C. Shindler, & M. Pfister (Eds.). *Active Tectonics of Northwestern Anatolia-The Marmara Poly-Project* (487-502). Hochschulverlag AG an der ETH Zurich-Swiss.
- KOERI. (2010). *Earthquake Cataloge of Turkey and surrounding region*, <http://www.koeri.boun.edu.tr/sismo/> (last access: March 28, 2011).
- Koravos, G. C., Main, I. G., Tsapanos, T. M., & Muson, R. M. W. (2003). Maximum earthquake magnitudes in the Aegean area constrained by tectonic moment release rates. *Geophysical Journal International* 152, 94–112.
- Konno, K. & Ohmachi, T. (1998). Ground-motion Characteristics Estimated from Spectral Ratio between Horizontal and Vertical Components of Microtremor. *Bulletin Seismological Society of America*, 88, 228–241.
- Kuscu, I., Okamura, M., Matsuoka, H., Yamamori, K., Awata, Y., & Ozalp, S. (2009). Recognition of active faults and stepover geometry in Gemlik Bay, Sea of Marmara, NW Turkey, *Marine Geology*. 260, 90-101.
- Lachet, C., Hatzfield, D., Bard, P.Y., Theoduludis, N., Papaianou, C. & Alekos, S. (1996). Site effects and microzonation in the city of Thessaloniki (Greece) Comparison of Different Approaches. *Bull. Seism. Soc. Am.* 86, 1692-1703.
- Lee, W. H. K. & Lahr, J. C. (1972). HYPO71: A Computer Program For determining hypocenter, magnitude, and first motion pattern of local earthquakes, *Open File Report, U. S. Geological Survey*, 100 pp.

- Le Pichon, X., Angelier, J. (1981). The Aegean Sea. *Philos. Trans. R. Soc. Lond.* A300, 357-372.
- Le Pichon X., Chamot-Rooke C., Lallemand S., Noomen R., & Veis G., (1995). Geodetic determination of the kinematics of Central Greece with respect to Europe: implications for Eastern Mediterranean tectonics. *J. Geophys. Res.* 100 (1995) 12675–12690.
- Lermo, J., & Chavez-Garcia, F. J. (1993). Site effect evaluation using spectral ratios with only one station *Bulletin Seismological Society of America*, 83, 1574–1594.
- Lermo, J., & Chavez-Garcia, F. J. (1994). Are microtremors useful in the site response evaluation?. *Bulletin Seismological Society of America*, 84, 1350–1364.
- Marcellini, A. (2006). Guidelines for the Implementation of the H/V Spectral Ratio Technique on Ambient Vibrations, *SAMCO Final Report*, 69 pp. (<http://citeseerx.ist.psu.edu/viewdoc/summary?doi=10.1.1.117.6488>).
- Masure, P., Mouroux, P., & Martin, C. (2000). *The International Decade for Natural Disaster Reduction (IDNDR) RADIUS Project: Case Study: Seismic Risk Assessment of Izmir City*.
- McClusky, S., Balassanian, S., Barka, A., Demir, C., Georgiev, I., Hamburg, et al. (2000). Global Positioning System constraints on plate kinematics and dynamics in the eastern Mediterranean and Caucasus. *J. Geophys. Res.* 105, 5695–5720.
- Mckenzie, D. (1972). Active tectonics of the Mediterranean Region. *Geophysical Journal of Royal Astronomical Society* 30, 109–185.
- Mckenzie, D. (1978). Active tectonics of the alpine-himalayan belt: the Aegean Sea and surrounding regions. *Geophysical Journal of Royal Astronomical Society* 55, 117–254.

- METU. (2007). *Seismic and Geotechnical Survey at "AI_115_BRN_BAY" Station*. Ankara, Turkey: ERD-METU TUBITAK Scientific Research Project (No. 105G016), 16 pps.
- Michael, A. J. (1984). Determination of stress from slip data: faults and folds, *J. Geophys. Res.* 89, 11517-11526.
- Michael, A. J. (1987). The use of focal mechanisms to determine stress: a control study, *J. Geophys. Res.* 92, 357-368.
- Mohamed, H.H., Kang, T-S, & Baag, C-E, (2001). Focal mechanism determination based on the polarity and SV-P amplitude ratio in the Kalabsha area, Aswan, Egypt, *Geosciences Journal* 5 (2), 165-171
- Motosaka, M., Somer, A. (2002). Ground motion directionality inferred from a survey of minaret damage during the 1999 Kocaeli and Düzce, Turkey earthquakes. *J Seism.* 6, 419-430.
- Mucciarelli, M., & Gallipoli, M. R. (2001). A critical review of 10 years of microtremor HVSR technique. *Bolletino di Geofisica Teorica ed Applicata* 42, 255–266.
- Nakamura, Y. (1989). A method for dynamic characteristics estimation of subsurface using microtremor on the ground surface. *Quarterly Report of the Japanese Railway Technical Research Institute (RTRI)*, 30(1), 25–33.
- Ocakoğlu, N., Demirbağ, E., & Kuşçu, İ. (2004). Neotectonic structures in the area offshore of Alacati, Doganbey and Kusadasi (western Turkey): evidence of strike-slip faulting in the Aegean extensional province. *Tectonophysics*, 67- 83.

- Ocakođlu, N., Demirbađ, E., & Kuşçu, İ. (2005). Neotectonic structures in Izmir Gulf and surrounding regions (western Turkey): Evidences of strikeslip faulting with compression in the Aegean extensional regime. *Marine Geology* 219, 155–171.
- Ocal, N. (1968). *Turkiye'nin sismisitesi ve zelzele cografiyasi*, Istanbul Kandilli Rasathanesi Yayini 8, Istanbul-Turkey, 119 p. (in Turkish).
- Ohmachi, T., Nakamura, Y., & Toshinawa, T. (1991). Ground motion characteristics in the San Francisco Bay area detected by microtremor measurments. In S. Prakash (Ed.), *Proceedings of the Second International Conference on Recent Advances in Geotechnical Earthquake Engeneering and Soil Dynamics*, March 11–15, St. Louis, Missouri, Univ. of Missouri-rolla, p. 1643– 1648.
- Oral M.B., Reilinger R.E., Toksöz M.N., Kong R.W., Barka A.A., Kınık I, et al. (1995). Global positioning system offers evidence of plate motions in eastern Mediterranean. *EOS Transac.* 76 (9).
- Ozel, O., Cranswick, E., Meremonte, M., Erdik, M., & Safak, E. (2002). Site Effects in Avcilar, West of Istanbul, Turkey, from Strong- and Weak-Motion Data. *Bull. Seism. Soc. Am.* 92 (1), 499-508.
- Ozturk, K., Yaltrak, C., & Alpar, B. (2009). The Relationshipbetween The Tectonic Setting of the Lake Iznik Basin and the Middle Strand of the North Anatolian Fault, *Turkish J. Earth Sci.* 18, 1-16.
- Pamukcu, O., & Yurdakul, A. (2008). Isostatic compensation in Western Anatolia with estimate of the effective elastic thickness, *Turkish Journal of Earth Sciences.* 17, 545-557.
- Papazachos, B., & Papazachou, C. (1997). *The Earthquakes of Greece: Thessaloniki*. Technical books Edition.

- Papazachos, B.C., Papaioannou, C.A., Papazachos, C.B., & Savvaidis, A.S. (1997). *Atlas of Iseismal Maps for Strong Shallow Earthquakes in Greece and Surrounding Area (426BC-1995)*: Thessaloniki. Technical books Editions.
- Papazachos, C. B., Karakaisis, G. F., Scordilis, E. M., & Papazachos, B. C. (2004). Probabilities of activation of seismic faults in critical regions of the Aegean area. *Geophysical Journal International* 159, 679–687.
- Pinar, N. (1950). Etude g'eologique et seismologique du tremblement de terre de Karaburun (Izmir) du 23 juillet 1949. *Revue de la Facult'e des Sciences de l'universit'e d'istanbul, Istanbul*, 15, 363–375
- Pinar, A., Kalafat, D., & Üçer, S. B. (1998). Rayleigh Yüzey Dalga Spektrumu, Cisim Dalgaları ve İlk Hareket Yönlerinden 1992-1997 Yıllarında Türkiye ve Civarında Oluşan Depremlerin(Ms=5.5-6.8) Analizi. *Deprem Araştırma Bülteni, Sayı 76*, 88-120.
- Plenefisch, T., & Klinge, K. (2003). Temporal variations of focal mechanisms in the Novy Kostel focal zone (Vogtland/ NW- Bohemia)- comparison of the swarms of 1994, 1997 and 2000, *Journal of Geodynamics*. 35, 145-156.
- Polat, O., Haessler, H., Cisternas, A., Philip, H., Eyidogan, H., Aktar, et al. (2002a), The Izmit (Kocaeli) Turkish earthquake of August 17, 1999: Previous seismicity, aftershocks and seismotectonics, *Bulletin of the Seismological Society of America*. 92, 361-375.
- Polat, O., Haessler, H., Cisternas, A., Philip, H., & Eyidogan, H. (2002b), Analysis and interpretation of the aftershock sequence of the August 17, 1999, Izmit (Turkey) earthquake, *Journal of Seismology*. 6, 287-306.
- Polat, O., Gok, E. & Yilmaz, D. (2008). Earthquake hazard of the Aegean extension region (west Turkey). *Turkish Journal of Earth Sciences* 17, 593–614.

- Polat, O., Ceken, U., Uran, T., Gok, E., Yilmaz, N., Beyhan, N., et al. (2009). IzmirNet: A Strong-Motion Network in Metropolitan Izmir, Western Anatolia, Turkey. *Seismological Research Letters*. 80, 5, 831-838.
- Rivera, L., & Cisternas, A. (1990). Stress tensor and fault plane solution for a population of earthquakes, *Bulletin of the Seismological Society of America*. 80, 600-614.
- Ritter, J.R.R., Wagner, M., Bonjer, K.-P., & Schmidt, B. (2009). The 2005 Heidelberg and Speyer earthquakes and their relationship to active tectonics in the central Upper Rhine Graben, *Int. J. Earth. Sci.* 98, 697-705.
- Salomon-Calvi, W., & Kleinsorge, H. L. (1940). *Türkiyedeki zelzelere müteallik etüdler*. MTA Yayınları Seri B, No:5, Ankara.
- Saroglu, F., Emre, O., & Kuscu, I. (1992). *Turkish Active Faults Map*. Ankara, Turkey: Report of Directorate of Mineral Research and Exploration.
- Schindler, C., & Pfister, M. (Eds). (1997). *Active Tectonics of Northwestern Anatolia: The MARMARA Poly-Project*. Zurich, Switzerland.
- Sellami, S., Pavoni, N., Mayer-Rosa, D., Mueller, S., Eyidogan, H., Aktar, M., et al. (1997). Seismicity and Seismotectonics of the bursa Region. In C. Schindler, & M. Pfister (Eds.). *Active Tectonics of Northwestern Anatolia-The Marmara Poly-Project* (449-486). Hochschulverlag AG an der ETH Zurich-Swiss.
- Sengor, A.M.C., Satir, M., & Akkok, R. (1984). Timing of tectonic events in the Menderes Massif, western Turkey: implications for tectonic evolution and evidence for Pan-African basement in Turkey. *Tectonics* 3, 693-707.

- Sengor A.M.C., Görür N. & Şaroğlu F., (1985). Strike-slip faulting and related basin formation in zones of tectonic escape: Turkey as a case study, in: Biddle K.T., Christie-Blick N. (Eds.), *Strike-slip Faulting and Basin Formation. Soc. Econ. Paleontol. Mineral. Sp. Pub.*, 37, pp. 227–264.
- SESAME, (2004). *Guidelines for the implementation of the H/V spectral ratio technique on ambient vibrations: measurements, processing and interpretation*, 62 pp., <http://sesame-fp5.obs.ujfgrenoble.fr/Delivrables/Del-D23>
- Somerville, P.G., Smith, N.F., Graves, R.W., & Abrahamson, N.A. (1997). Modification of empirical ground motions attenuation relations to include the amplitude and duration effects of rupture directivity. *Seism. Res. Lett.* 68 (1), 199-222.
- Snoke, J.A. (2003). FOCMEC: FOCal MECHANism determinations. *Int Handb Eng. Seismol* 81B, 29-30.
- Sozbulir, H., Uzel, B., Sumer, O., Inci, U., Ersoy, Y. Kocer, T., Demirtas, R., & Ozkaymak, C. (2008). Evidence for a kinematically linked E-W trending Izmir Fault and NE-trending Seferihisar Fault: Kinematic and paleoseismological studies carried out on active faults forming the Izmir Bay, Western Anatolia. *Geological Bulletin of Turkey* 51 (2), 91-114 (in Turkish with English abstract).
- Sozbulir, H., Sari, B., Uzel, B., Sumer, O., & Akkiraz, S. (2010). Tectonic implications of transtensional supradetachment basin development in an extension-parallel transfer zone: the Kocacay Basin, western Anatolia, Turkey. *Basin Research*. doi: 10.1111/j.1365-2117.2010.00496.x.
- Straub, C. (1996), *Recent crustal deformation and strain accumulation in the Marmara Sea Region, NW Anatolia, inferred from GPS measurements*, *Mitteil. Inst. Geod. and Photogramm. Zurich-Swiss*, 56 p.

- Suzuki, T., Adachi, Y., & Tanaka, M. (1995). Application of Microtremor Measurements to the Estimation of Earthquake Ground Motions in Kushiro City during the Kushiro-Oki Earthquake of 15 January 1993. *Earthquake Eng. Struct. Dyn.* 24, 595–613.
- Tan, O. & Taymaz, T. (2001). Source parameters of November 6, 1992 Doganbey (Izmir) earthquake (Mw=6.0) obtained from inversion of teleseismic body-waveforms. *4th International Turkish Geology Symposium, 24–28 September 2001, Çukurova University, Adana, Turkey. Çukurova University Press, Adana*, p. 171. Abstract volume.
- Taymaz, T., Jackson, J.A. & McKenzie, D. (1991). Active tectonics of the north and central Aegean Sea. *Geophysical Journal International* 106, 433–490.
- Taymaz, T., Yilmaz, Y., Dilek, Y. (2007). The geodynamics of the Aegean and Anatolia: introduction. *London Geological Society Special Publications* 291, 1-16, doi: 10.1144/SP291.1.
- Tan, O., Tapirdamaz, C., & Yoruk, A. (2008). The earthquake catalogues for Turkey. *Turkish Journal of Earth Science* 17, 405–418.
- Theodulidis, N. P. & Bard, P. Y. (1995). Horizontal to Vertical Spectral Ratio and Geological Conditions: an Analysis of Strong Motion Data from Greece and Taiwan (SMART-1). *Soil Dyn. Earthquake Eng.* 14, 177–197.
- Topal, T., Doyuran, V., Karahanoglu, N., Toprak, V., Suzen, M.L., & Yesilnacar, E. (2003). Microzonation for earthquake hazard: Yenisehir settlement, Bursa, Turkey, *Engineering Geology.* 70, 93-108.
- TUIK. (2009), *Country population statistics for the year of 2008*. Turkish Statistical Institute, Primary Ministry of Turkish Republic, Ankara.

- Türkelli, N., Kalafat, D. & Gündoğdu, O. (1994). Field observations and focal mechanism solution of November 6, 1992 İzmir (Doğanbey). *Jeofizik 9 (10)*, 343–348.
- Ucer, B., Eyidogan, H., Gurbuz, C., Barka, A., & Baris, S. (1997). Seismic investigation of the Marmara region, In C. Shindler, & M. Pfister (Eds.). *Active Tectonics of Northwestern Anatolia-The Marmara Poly-Project* (89-100). Hochschulverlag AG an der ETH Zurich-Swiss.
- Ulusay, R., E. Tuncay, H. Sonmez, & C. Gokceoglu (2004). An attenuation relationship based on Turkish strong motion data and isoacceleration map of Turkey. *Engineering Geology 74*, 265–291.
- Uzel, B. & Sözbilir, H. (2005a). First record of Quaternary pull-apart basin in western Anatolia: the Cumaovası basin, İzmir Turkey. *International Earth Sciences Colloquium on the Aegen Region, İzmir, Abstracts*, p. 119.
- Uzel, B. & Sözbilir, H. (2005b). Batı Anadolu’ daki transtansiyonel ortama ait yapısal veriler: Kuvaterner yaşlı Cumaovası havzasından bir örnek (Structural evidences for transtensional tectonic setting in western Anatolia: An example from Quaternary Cumaovası Basin). *Geological Congress of Turkey, Ankara, Abstracts*, 52–53.
- Uzel, B. & Sözbilir., H. (2008). A First Record of a Strike-slip Basin in Western Anatolia and Its Tectonic Implication: The Cumaovası Basin. *Turkish Journal of Earth Sciences (Turkish J. Earth Sci.)*, Vol. 17, 2008, 559-591
- Uzel, B., Sozbilir, H., & Ozkaymak, C. (2010). Neotectonic evolution of an actively growing superimposed basin in western Anatolia: The inner bay of İzmir, Turkey. *Turkish J. Earth Sci.* doi: 10.3906/yer.0910.11.

- Yaltirak, C. (2002). Tectonic evolution of the Marmara Sea and its surroundings, *Marine Geology*. 190, 493-529.
- Yaltirak, C, & Alpar, B. (2002). Evolution of the middle strand of North Anatolian Fault and shallow seismic investigation of the southeastern Marmara Sea (Gemlik Bay), *Marine Geology*.190, 307-327.
- Yilmazer, M. (2003). *Online determination of earthquake source parameters using a new software zSacWin*, MSc Thesis, University of Istanbul, Istanbul-Turkey, 47 p (in Turkish).
- Wessel, P., & Smith, W.H.F. (1995). New version of the Generic Mapping Tools (GMT). *EOS Transactions* 76, 329.
- Westaway, R. (1990). Block rotation in western Turkey: 1. Observational evidence. *Journal of Geophysical Research* 95, 19857– 19884.
- Wiemer, S. (2001), A software package to analyze seismicity: ZMAP, *Seismological Research Letters*.72, 373-382.